Electronic Supplementary Material (ESI) for Photochemical & Photobiological Sciences.
This journal is © The Royal Society of Chemistry and Owner Societies 2016

Electronic Supplementary Information (ESI)

Monomolecular Pyrenol-Derivatives as Multi-Emissive Probes for Orthogonal Reactivities

Björn Finkler[a], Iris Riemann[b], Michael Vester[a], Andreas Grüter[a], Frank Stracke[b], Gregor Jung[a]*

[a] Biophysical Chemistry, Saarland University, Campus B2 2, 66123 Saarbrücken, Germany.

[b] Fraunhofer-IBMT, Ensheimer Straße 48, 66386 St. Ingbert, Germany.

Table of contents

Experimental Details

NMR Spectra

Compound **5** in acetone-d6

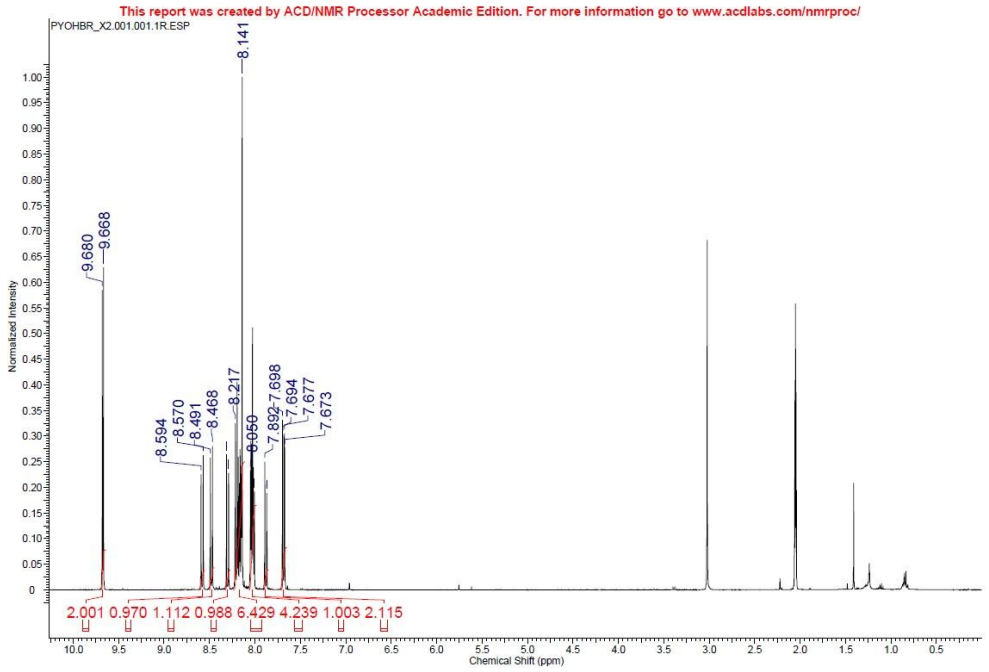

Figure S1: ^{1}H-NMR of compound **5**.

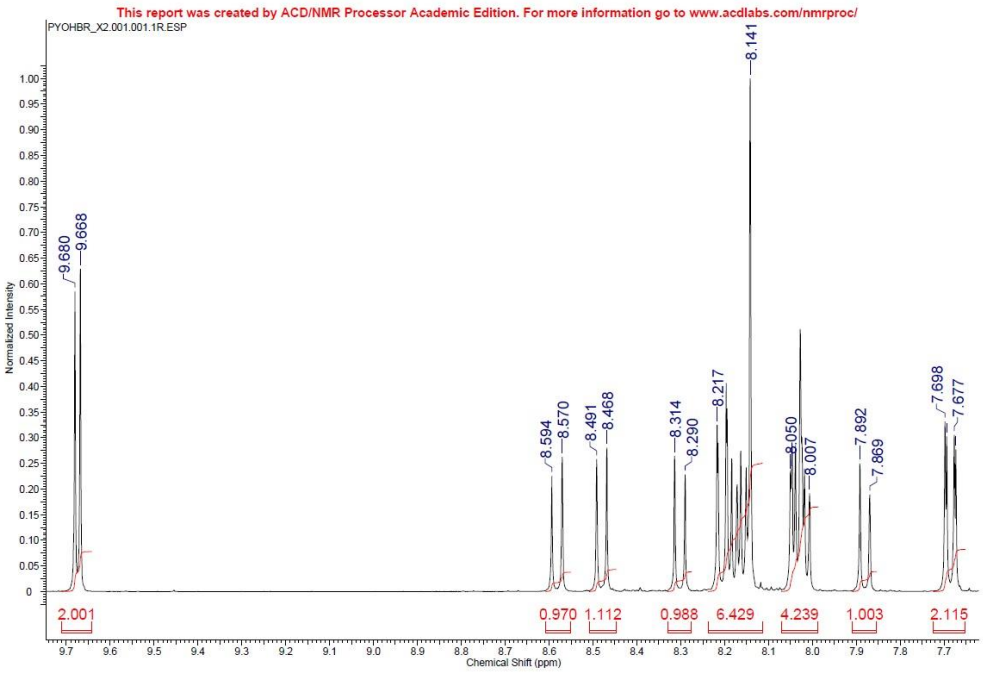

Figure S2: ^{1}H-NMR of compound **5**.

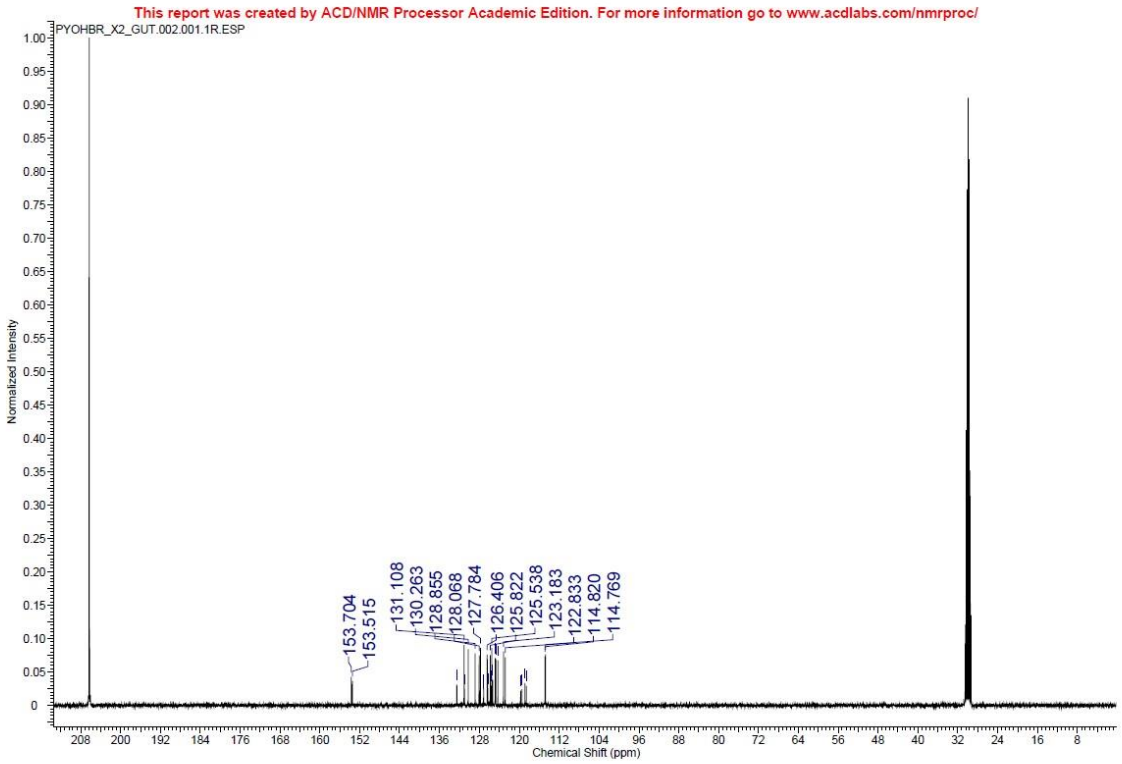

Figure S3: ^{13}C-NMR of compound **5**.

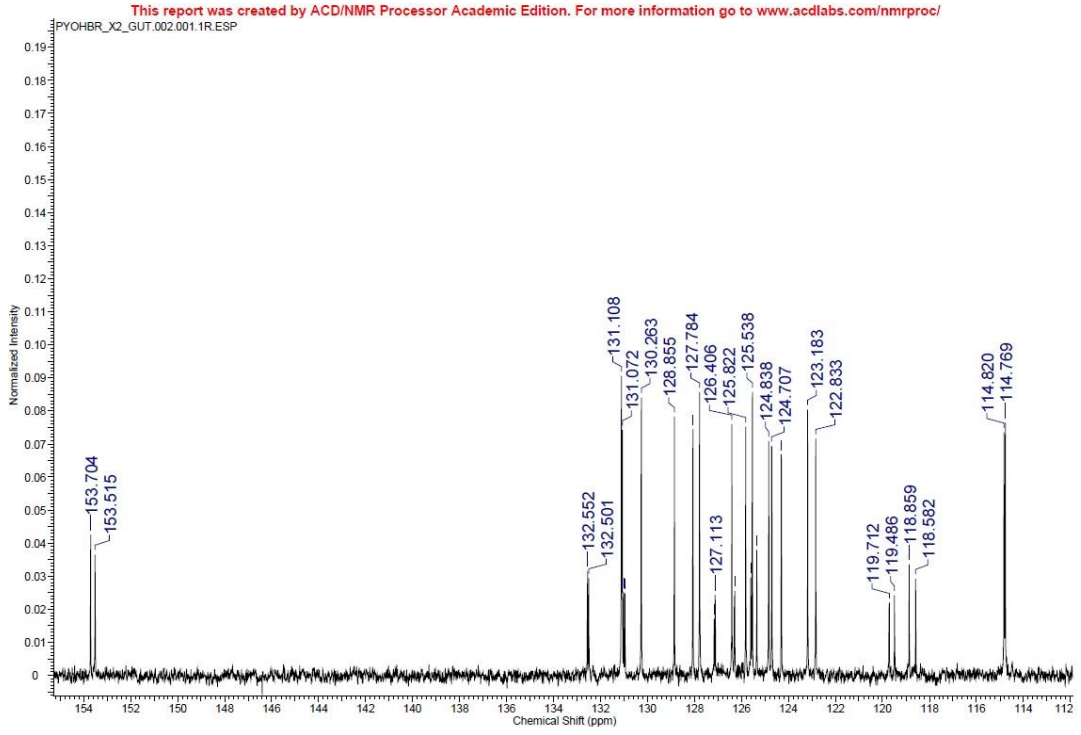

Figure S4: ^{13}C-NMR of compound **5**.

Compound **6** in acetone-d6

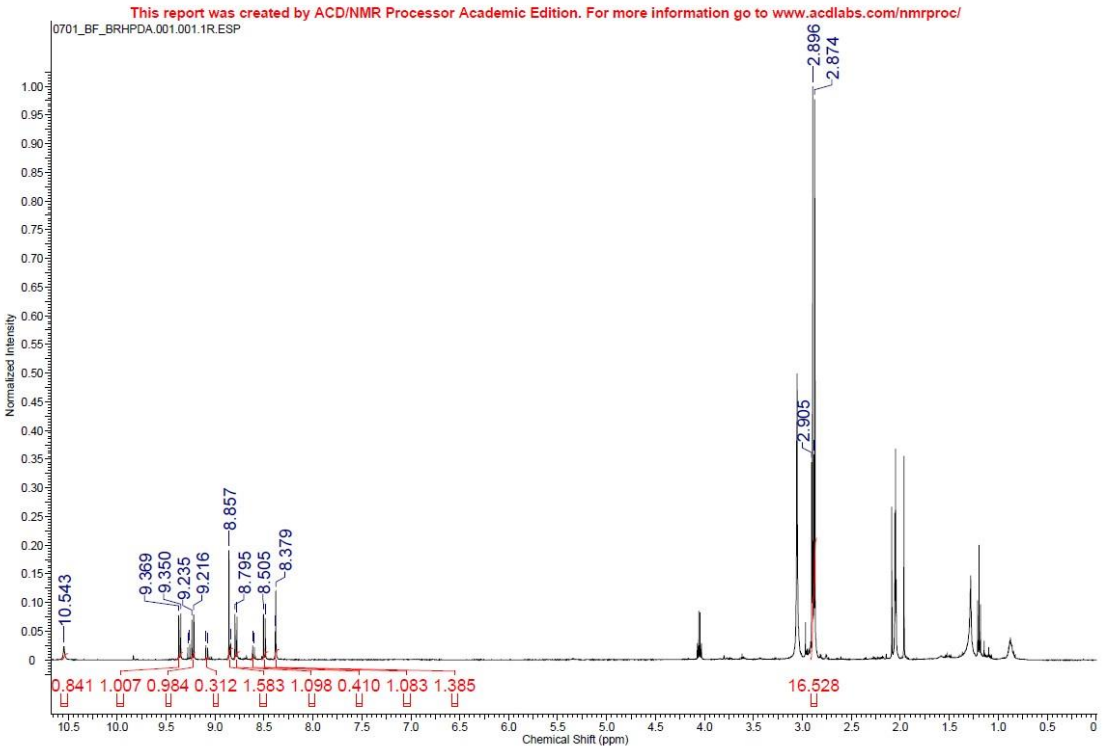

Figure S5: ^{1}H-NMR of compound **6**.

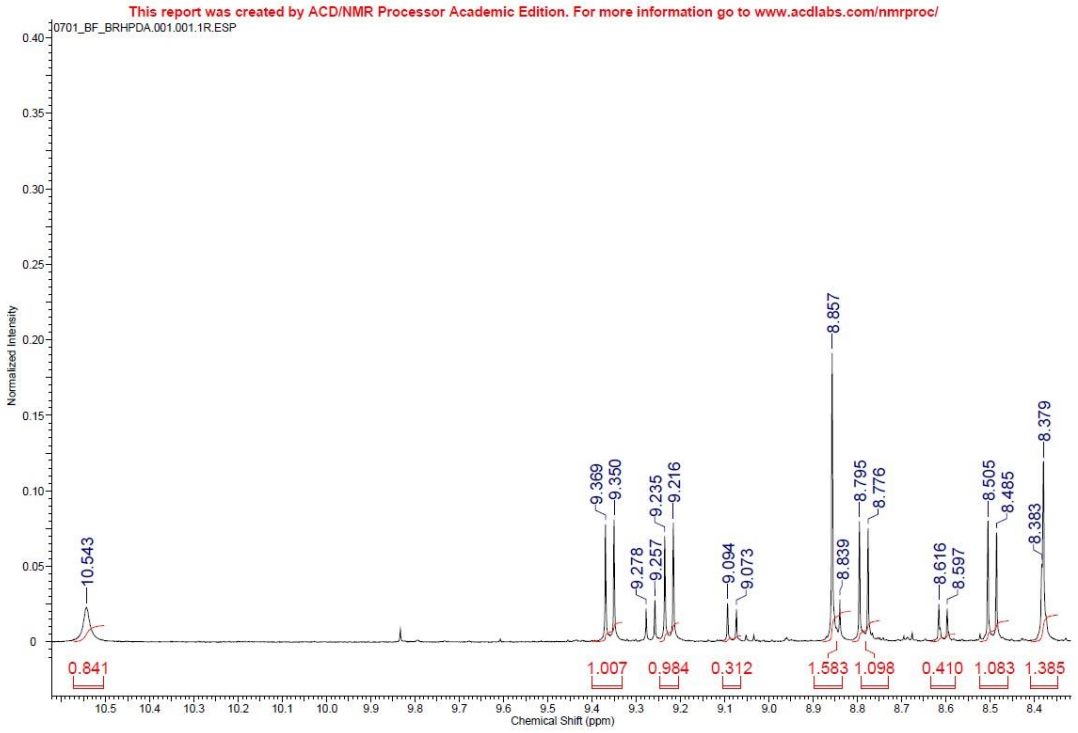

Figure S6: ^{1}H-NMR of compound **6**.

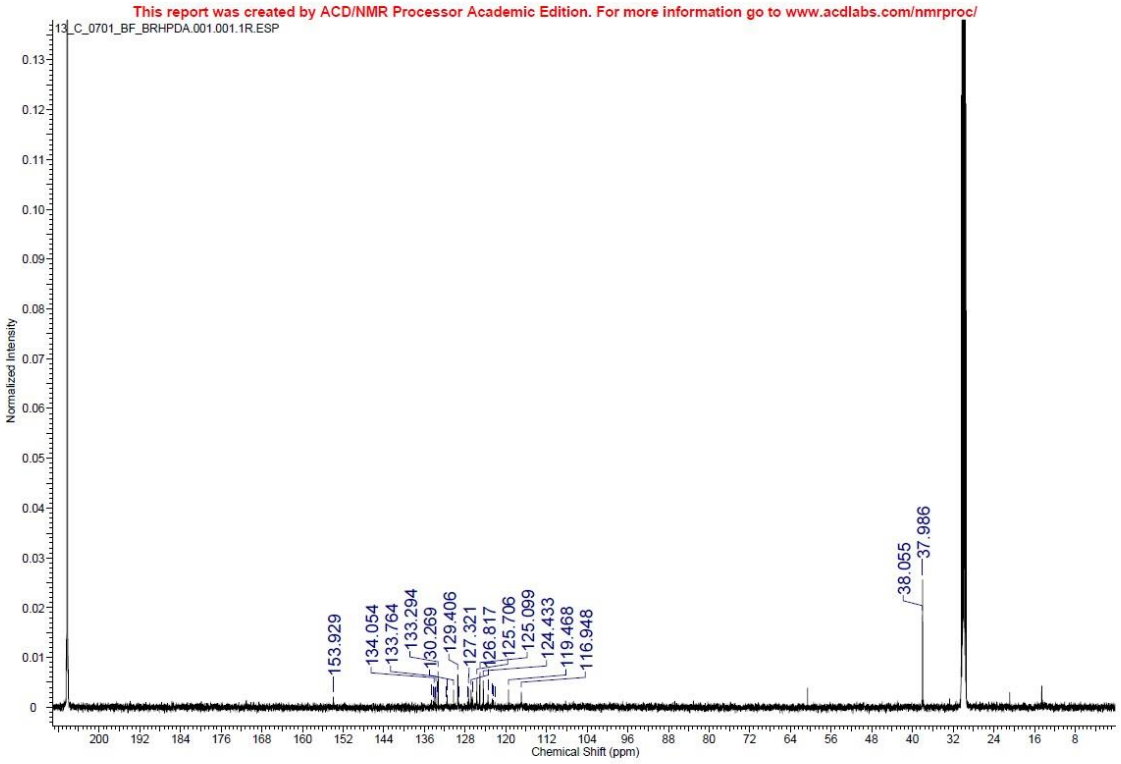

Figure S7: ^{13}C-NMR of compound **6**.

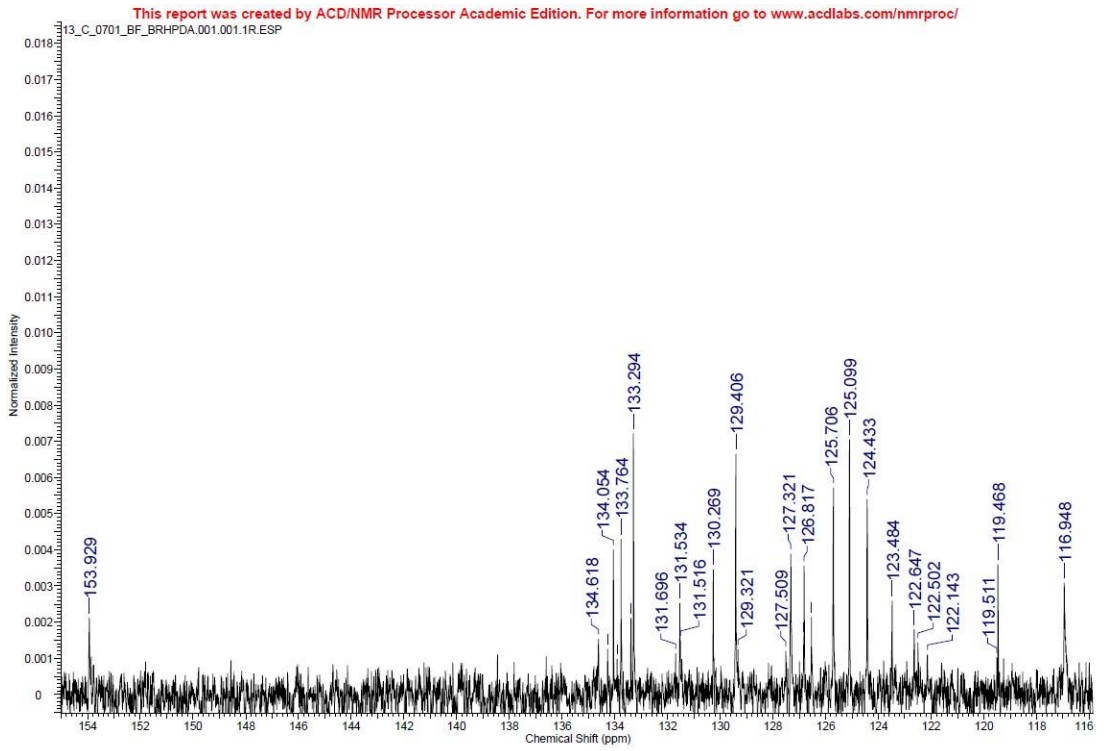

Figure S8: ^{13}C-NMR of compound **6**.

Compound **7** in chloroform-d

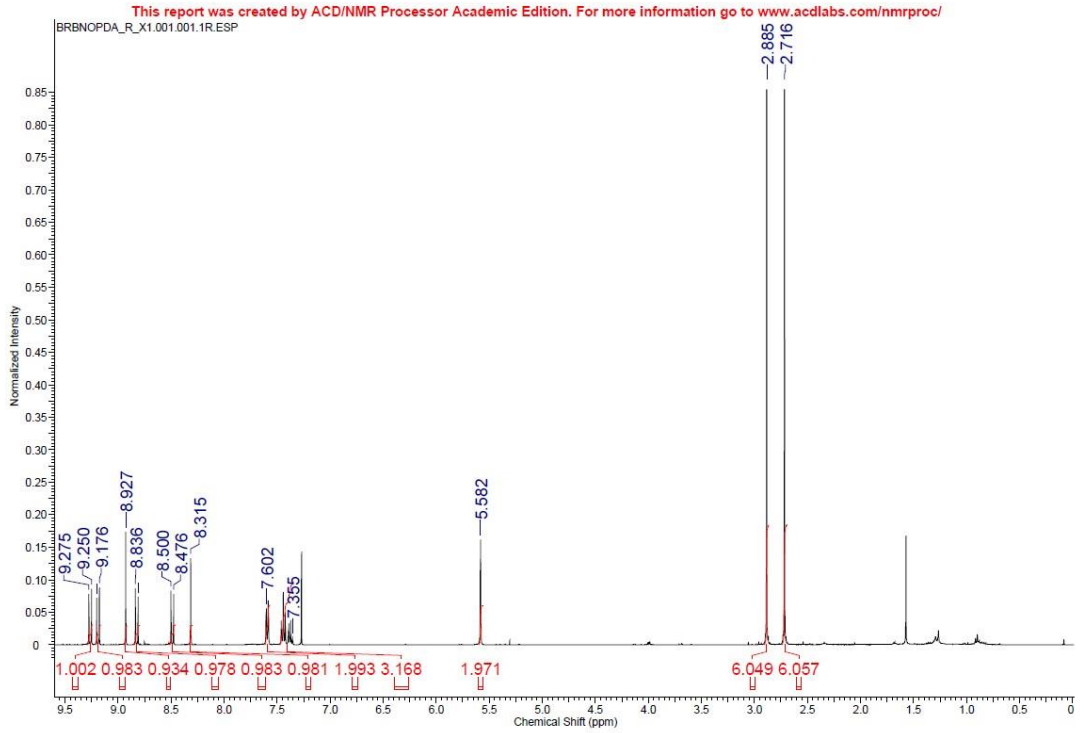

Figure S9: ^{1}H-NMR of compound **7**.

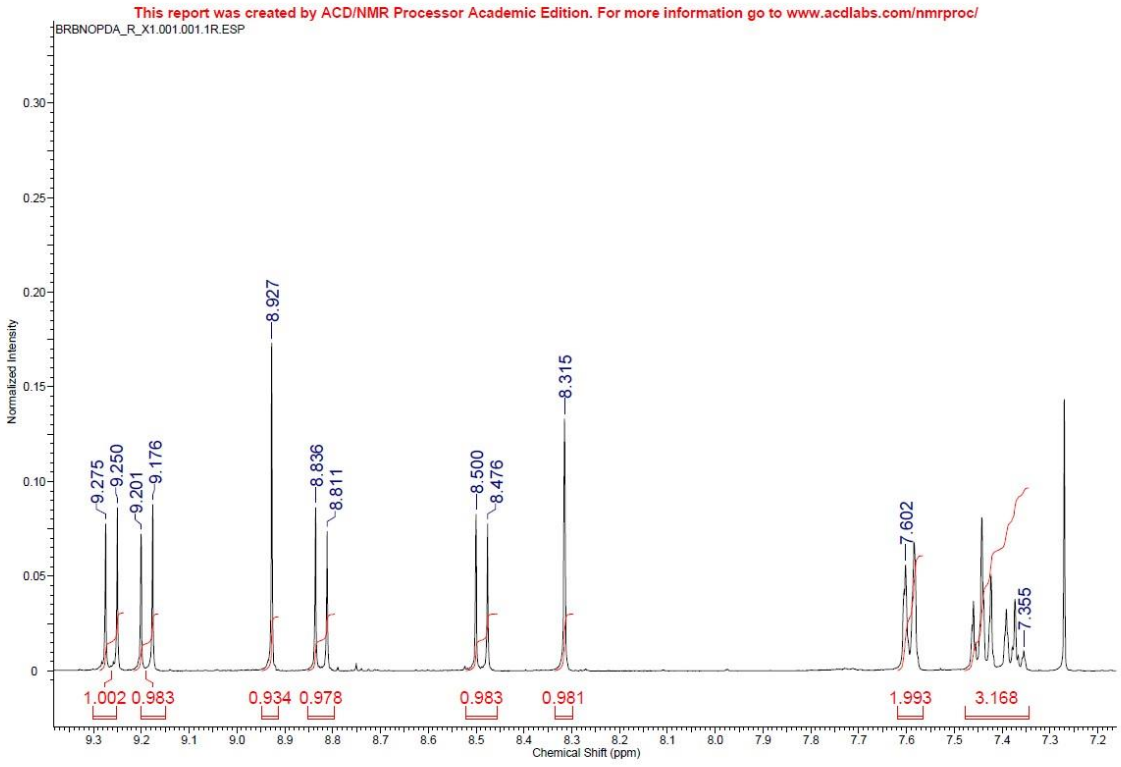

Figure S10: ^{1}H-NMR of compound **7**.

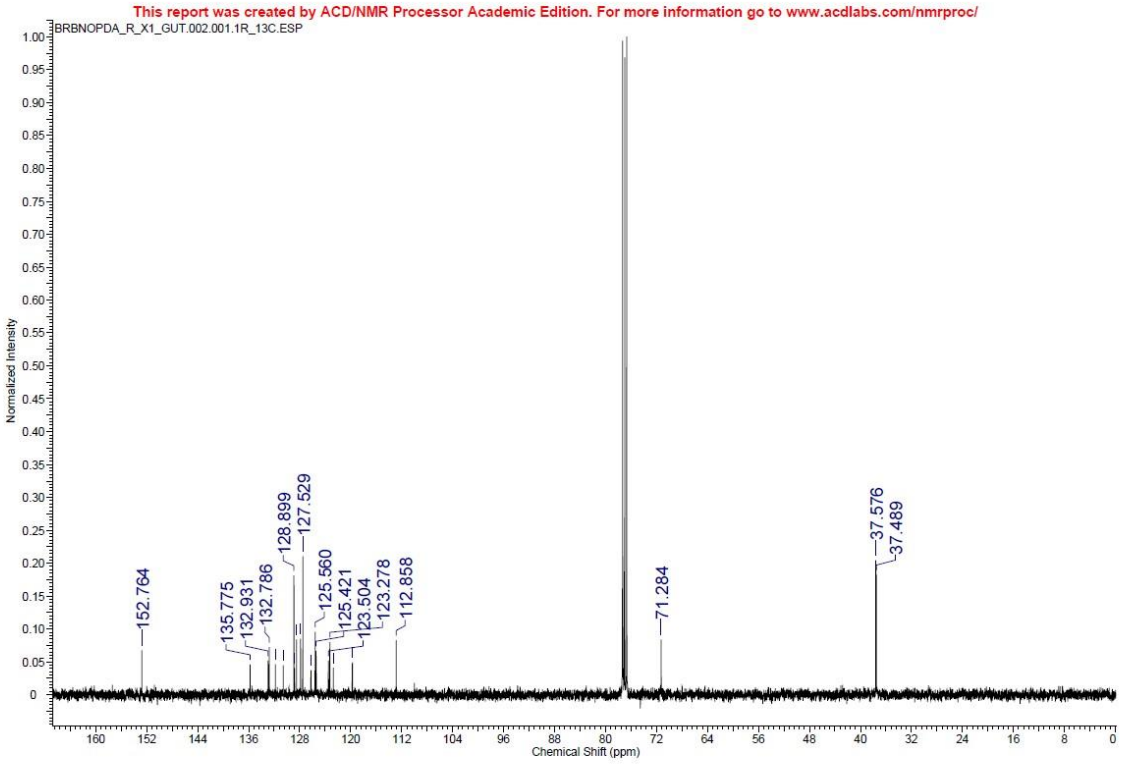

Figure S11: ^{13}C-NMR of compound **7**.

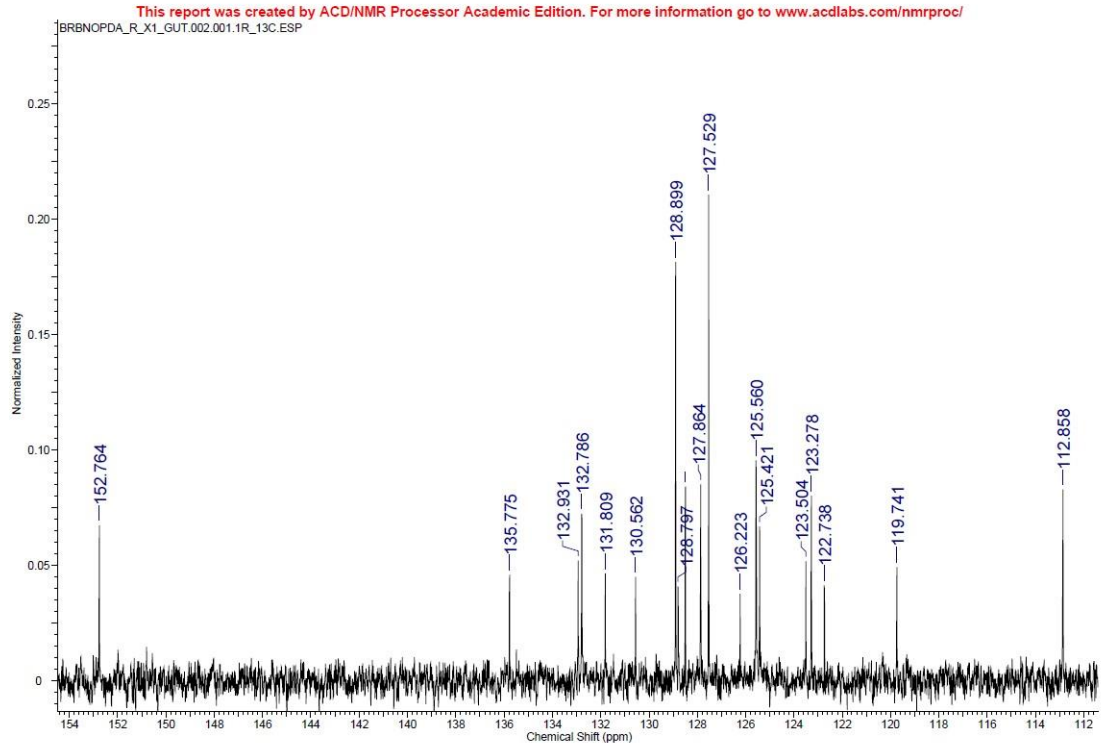

Figure S12: ^{13}C-NMR of compound **7**.

Compound **8** in chloroform-d

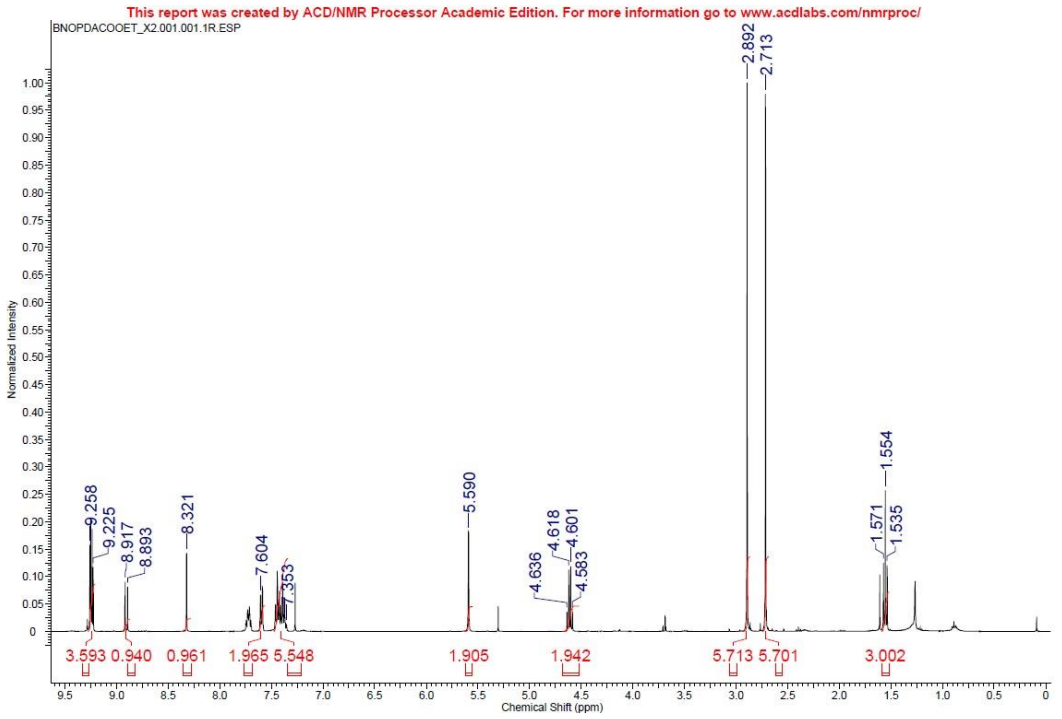

Figure S13: ^{1}H-NMR of compound **8**.

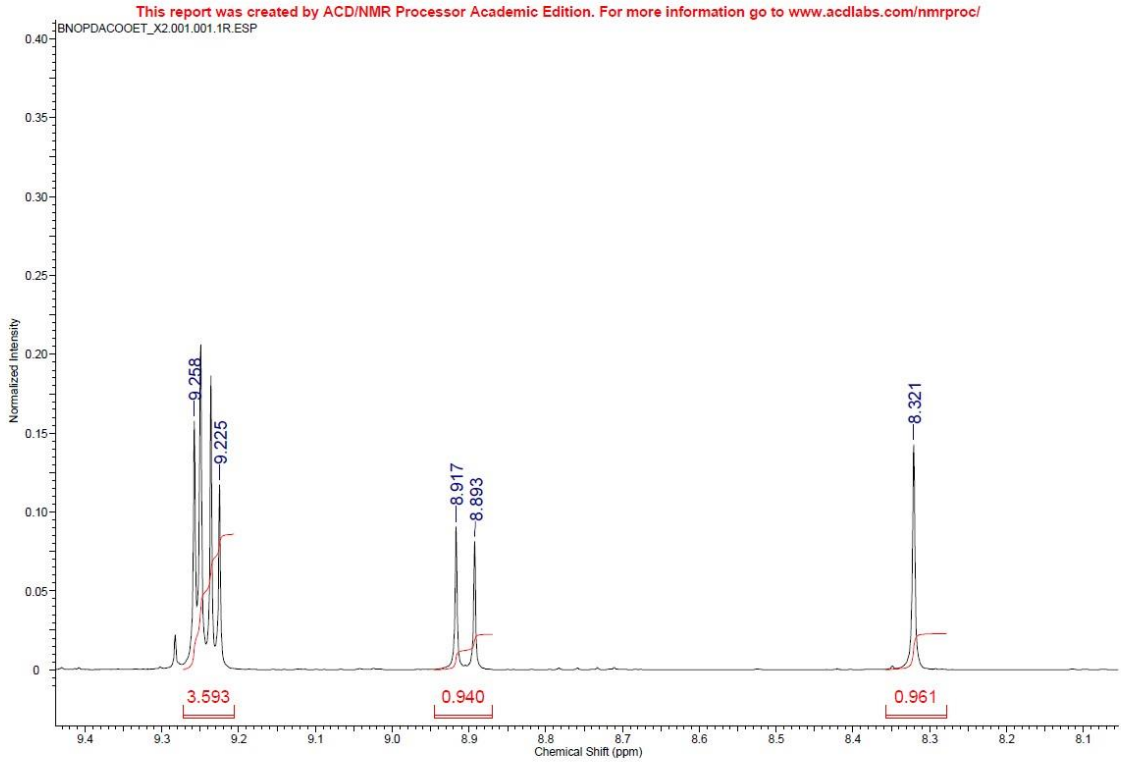

Figure S14: ^{1}H-NMR of compound **8**.

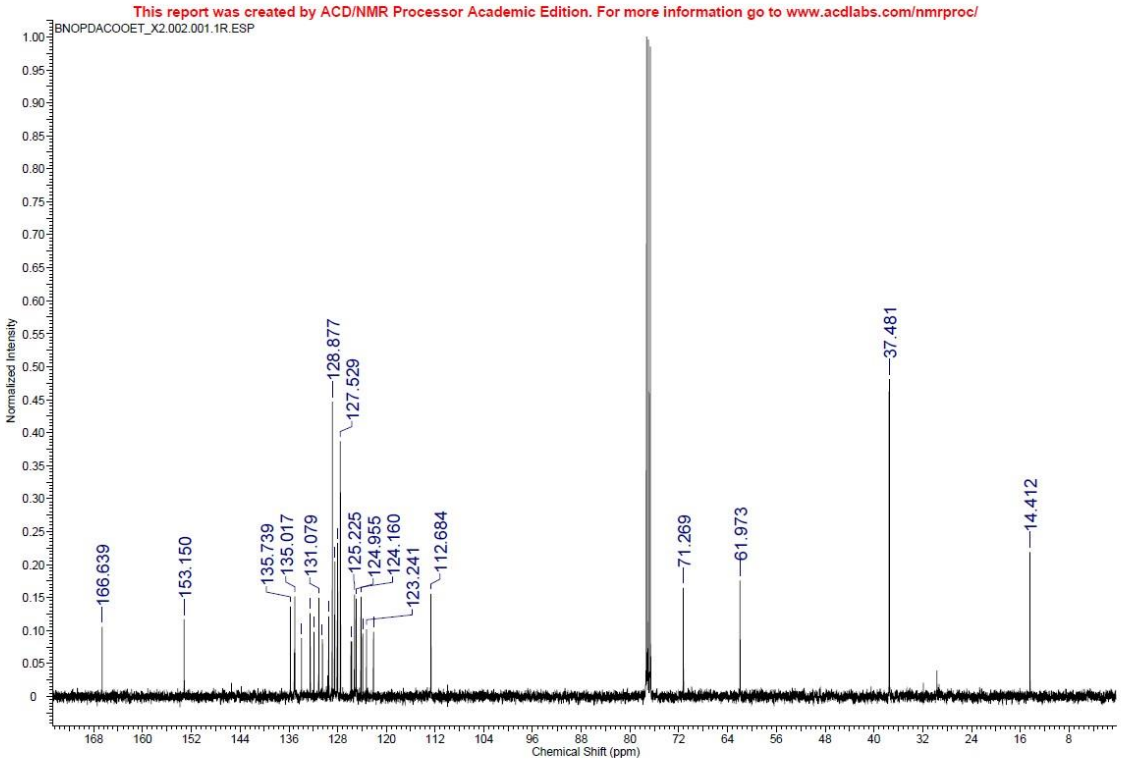

Figure S15: ^{13}C-NMR of compound **8**.

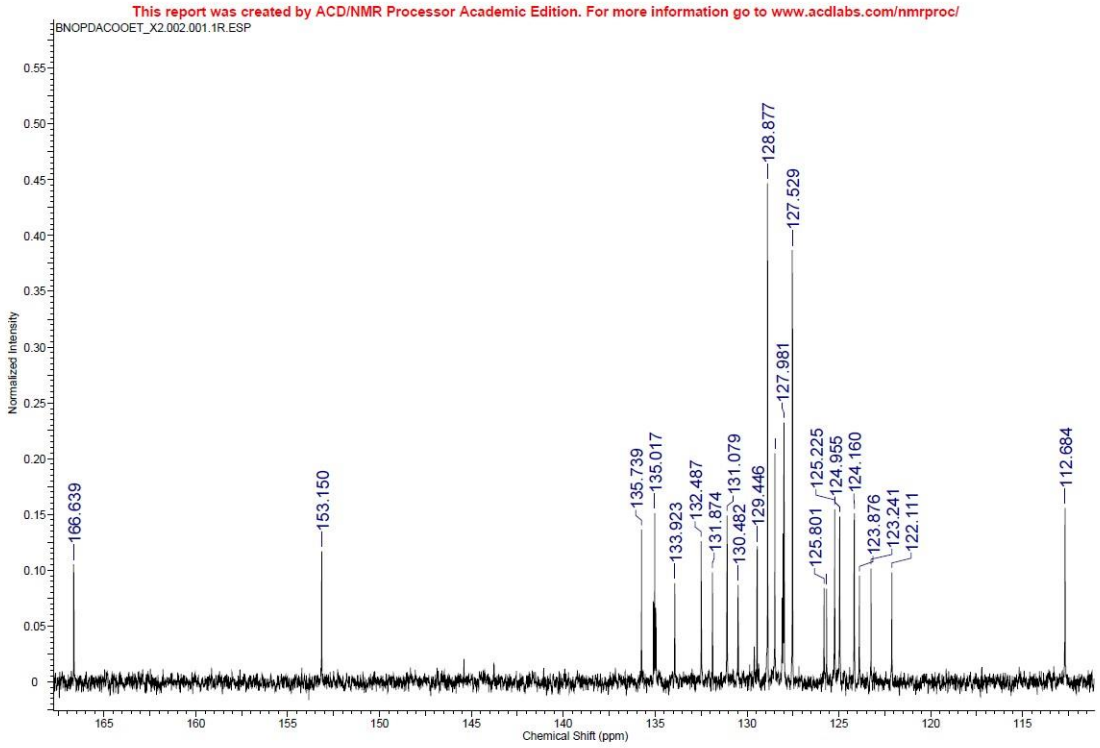

Figure S16: ^{13}C-NMR of compound **8**.

Compound **2** in acetone-d6

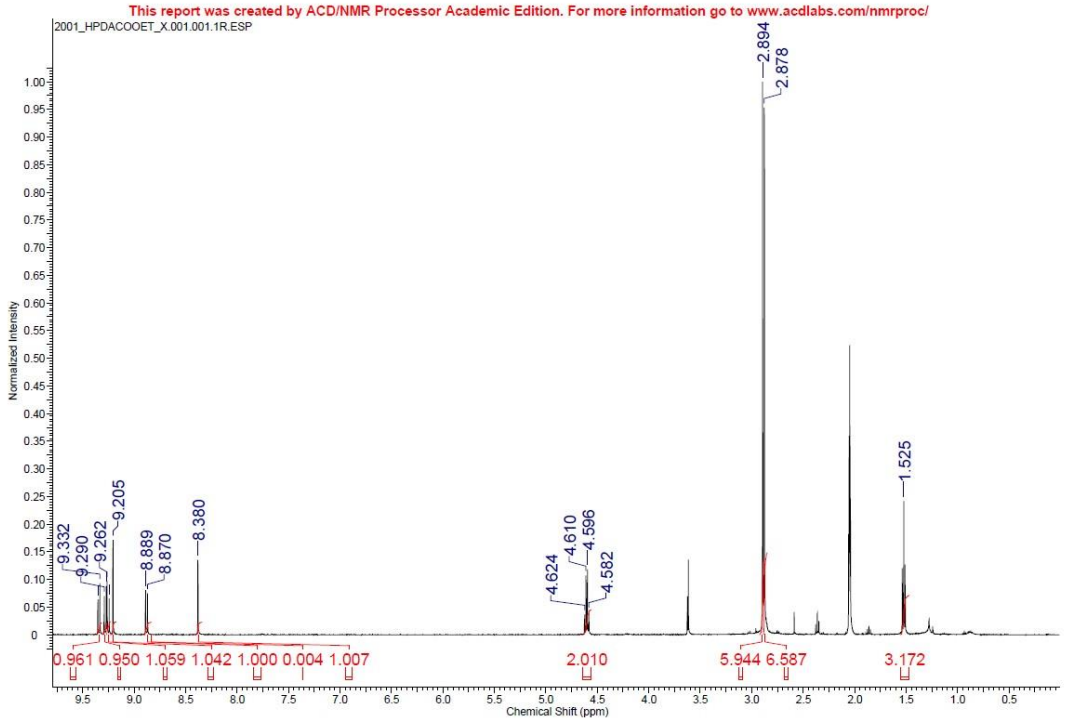

Figure S17: ^{1}H-NMR of compound **2**.

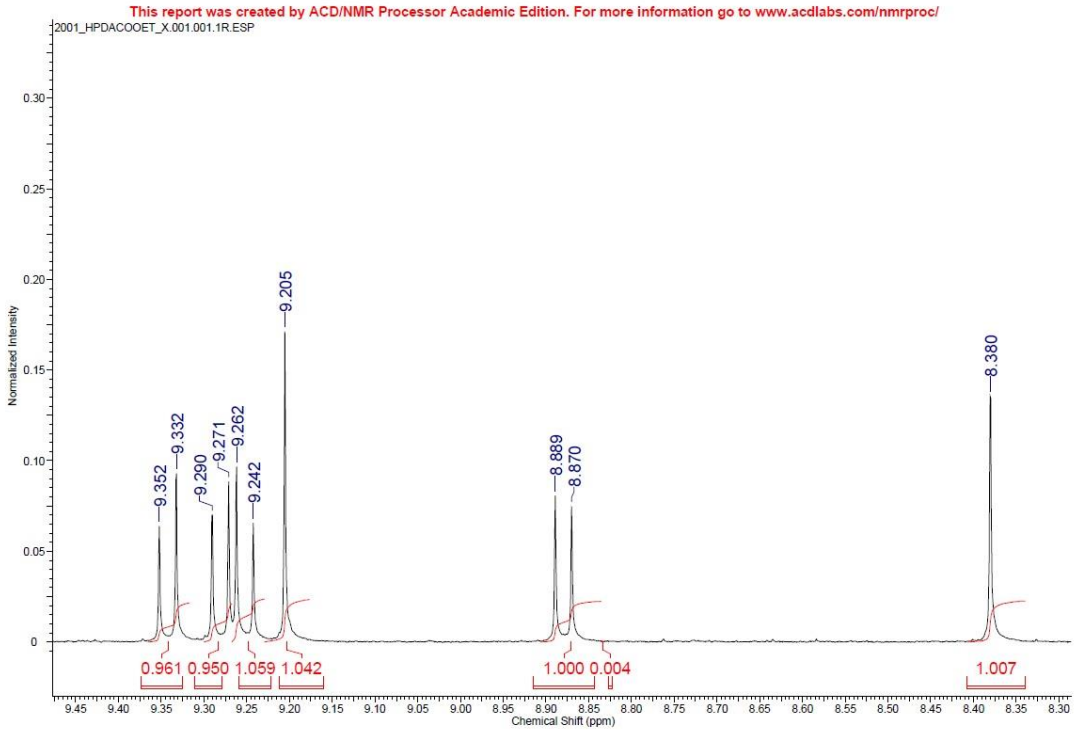

Figure S18: ^{1}H-NMR of compound **2**.

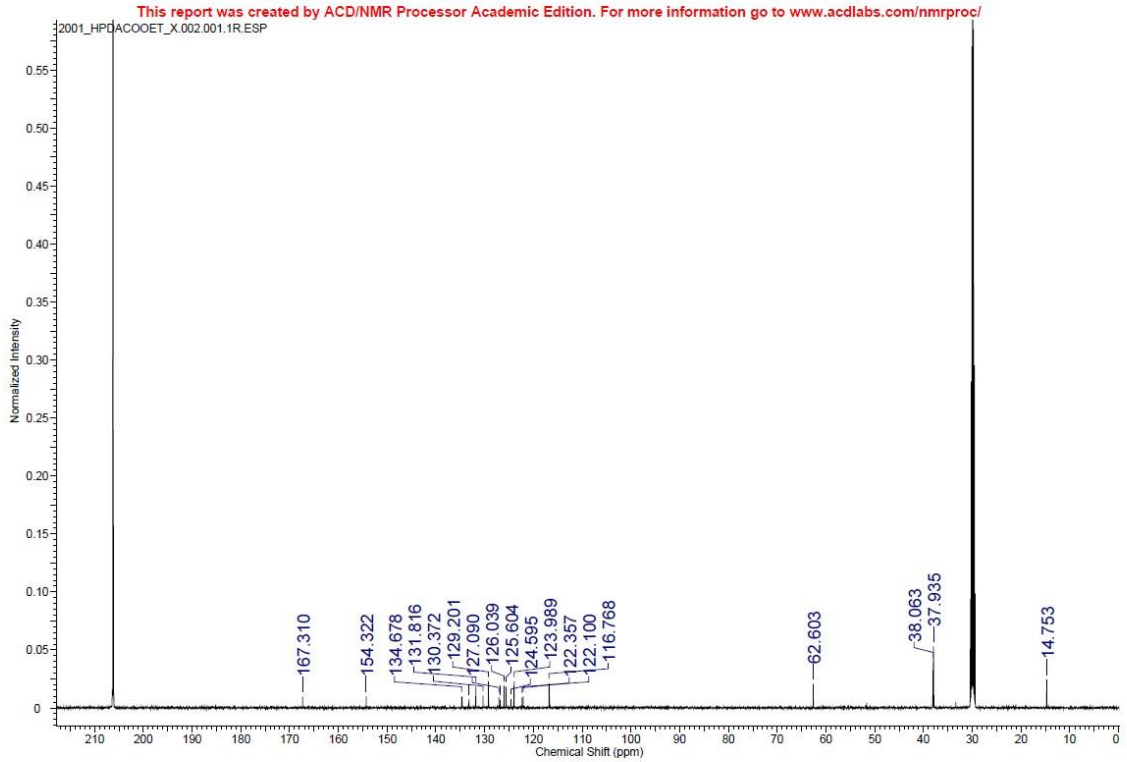

Figure S19: ^{13}C-NMR of compound **2**.

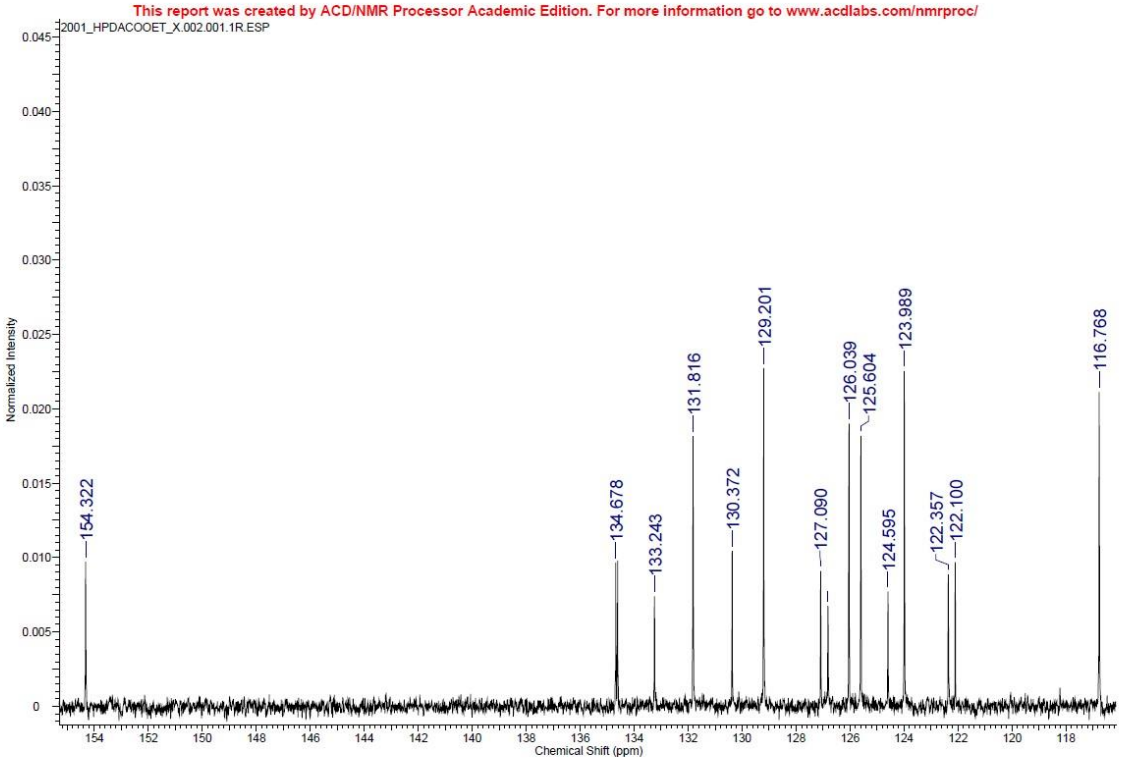

Figure S20: ^{13}C-NMR of compound **2**.

Compound **4** in acetone-d6

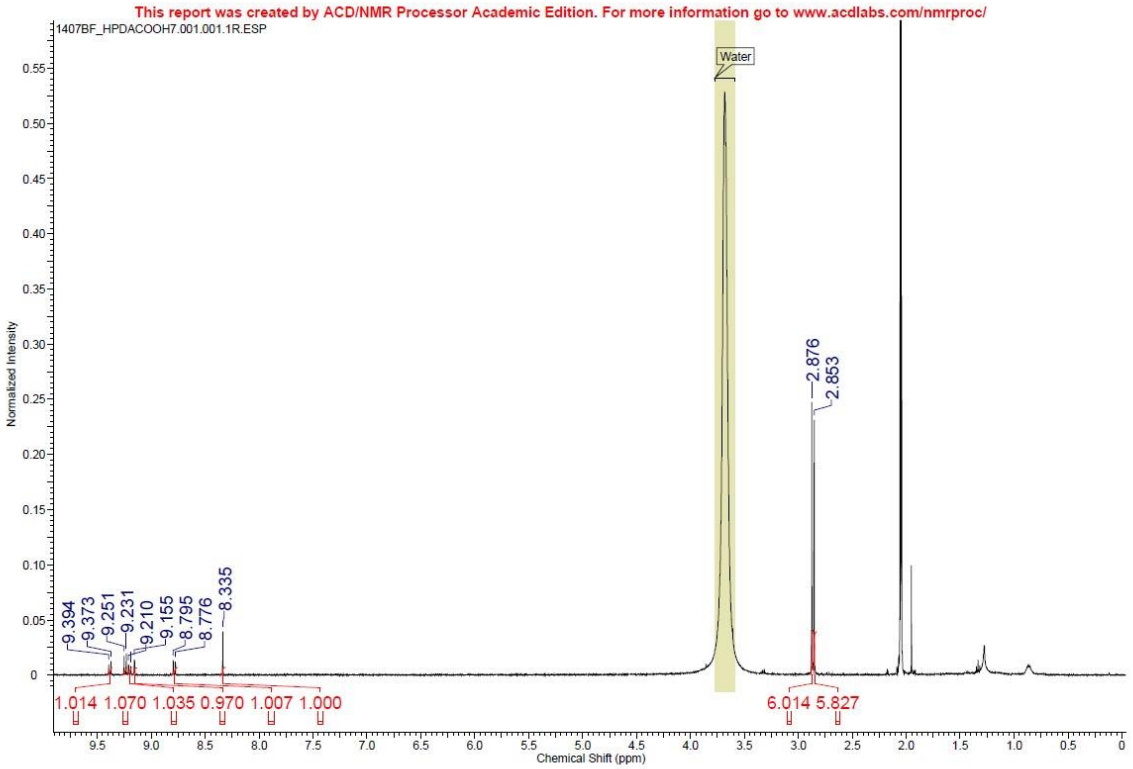

Figure S21: ^{1}H-NMR of compound **4**.

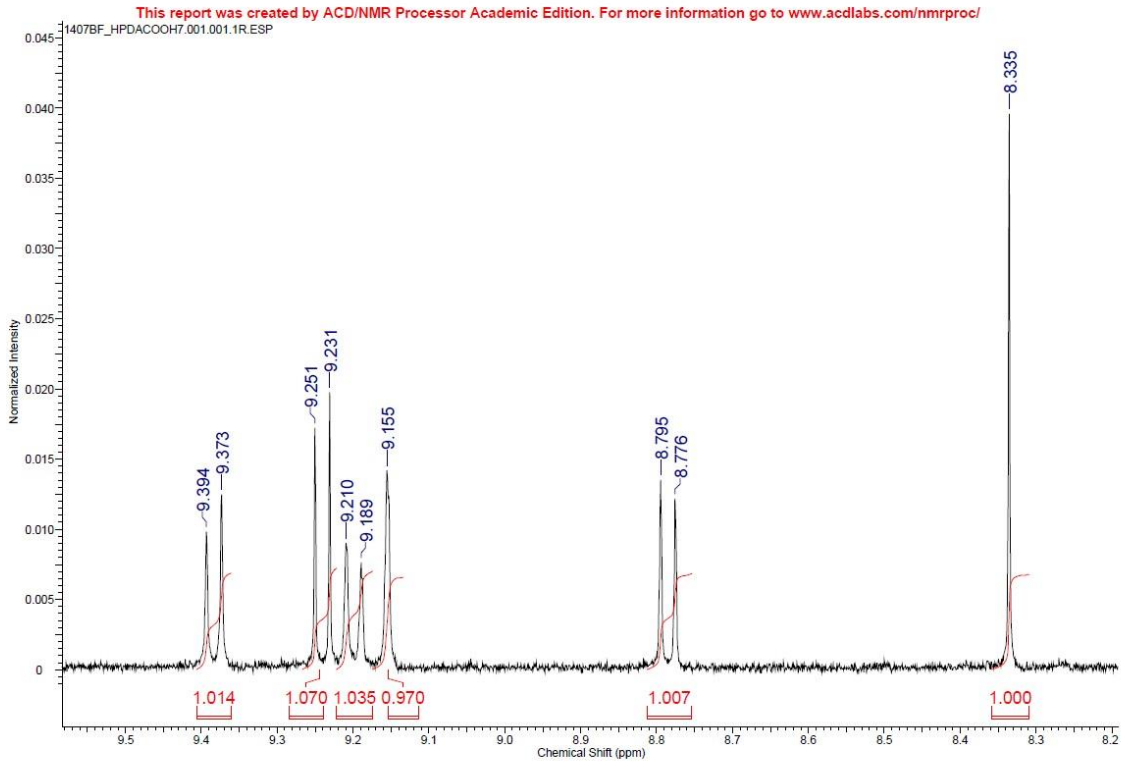

Figure S22: ^{1}H-NMR of compound **4**.

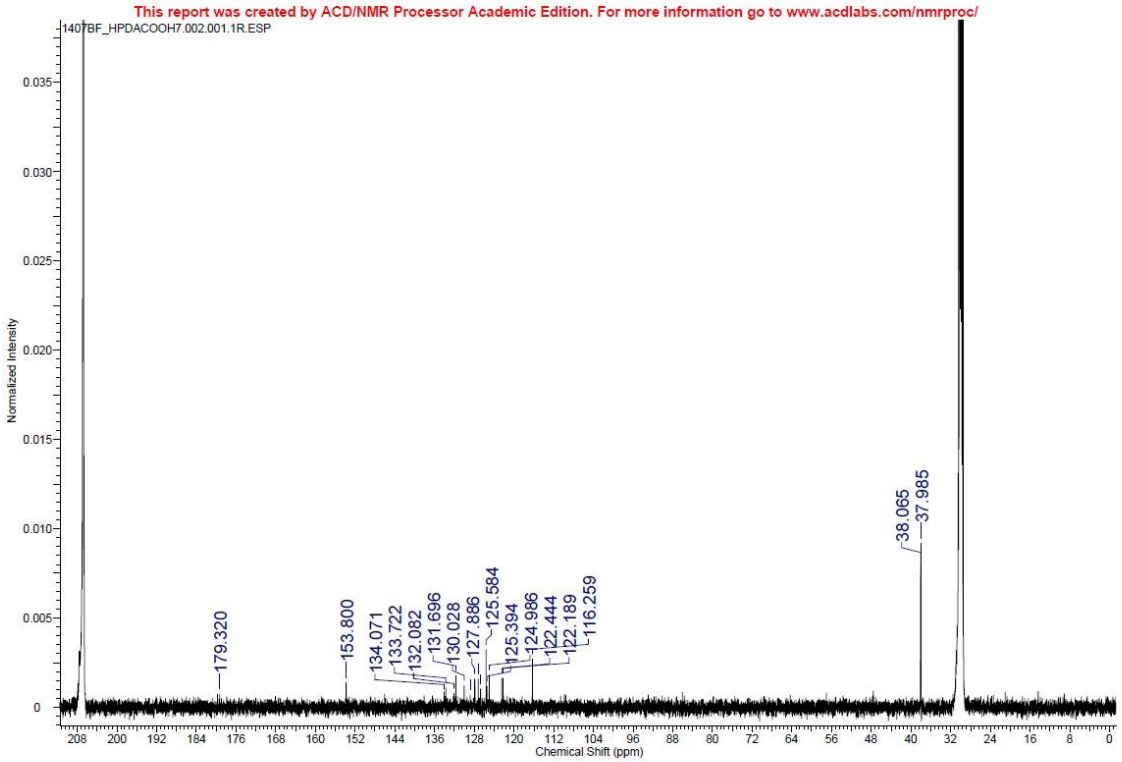

Figure S23: ^{13}C-NMR of compound **4**.

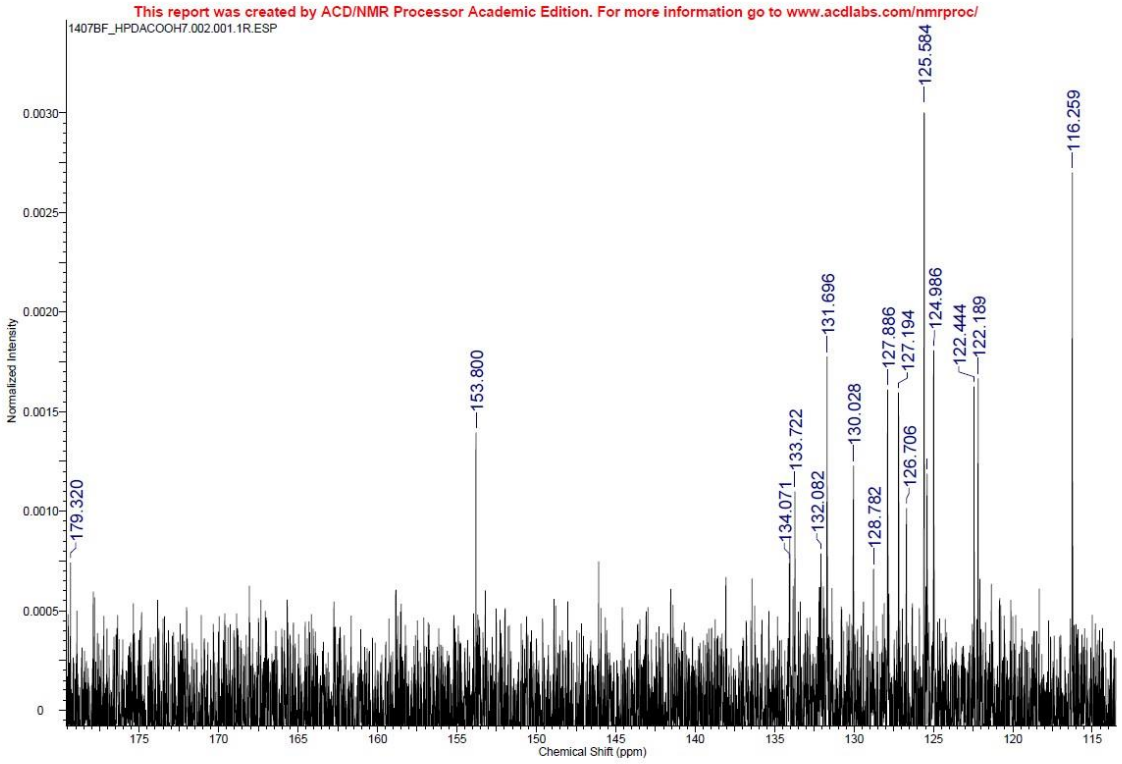

Figure S24: ^{13}C-NMR of compound **4**.

Compound **1** in methanol d4

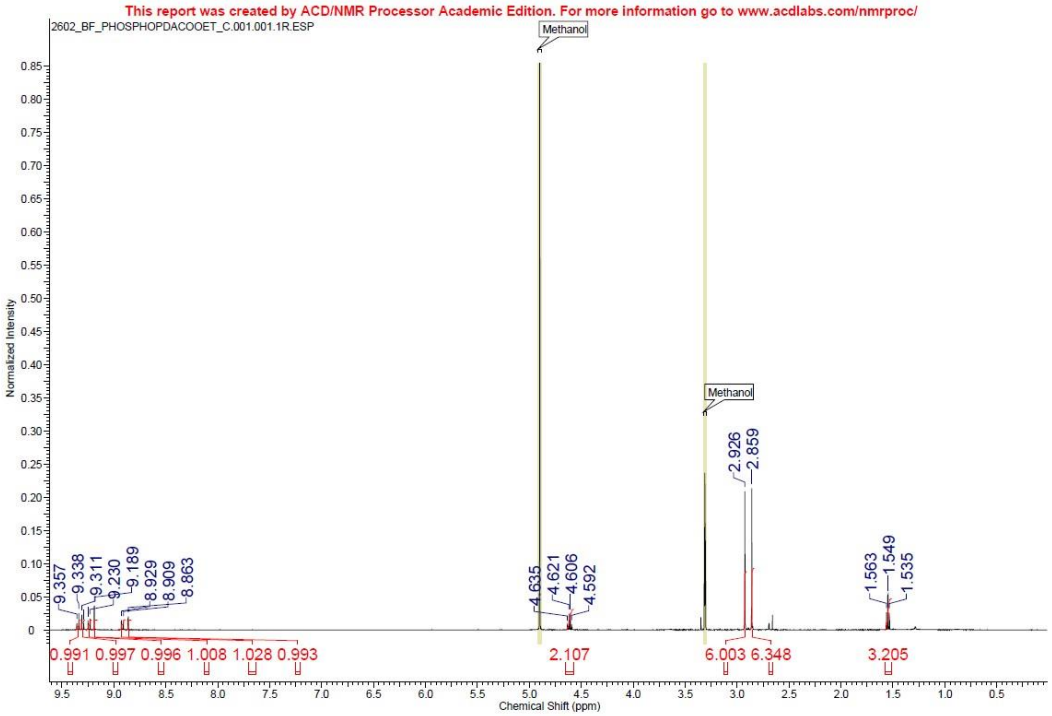

Figure S25: ^{1}H-NMR of compound **1**.

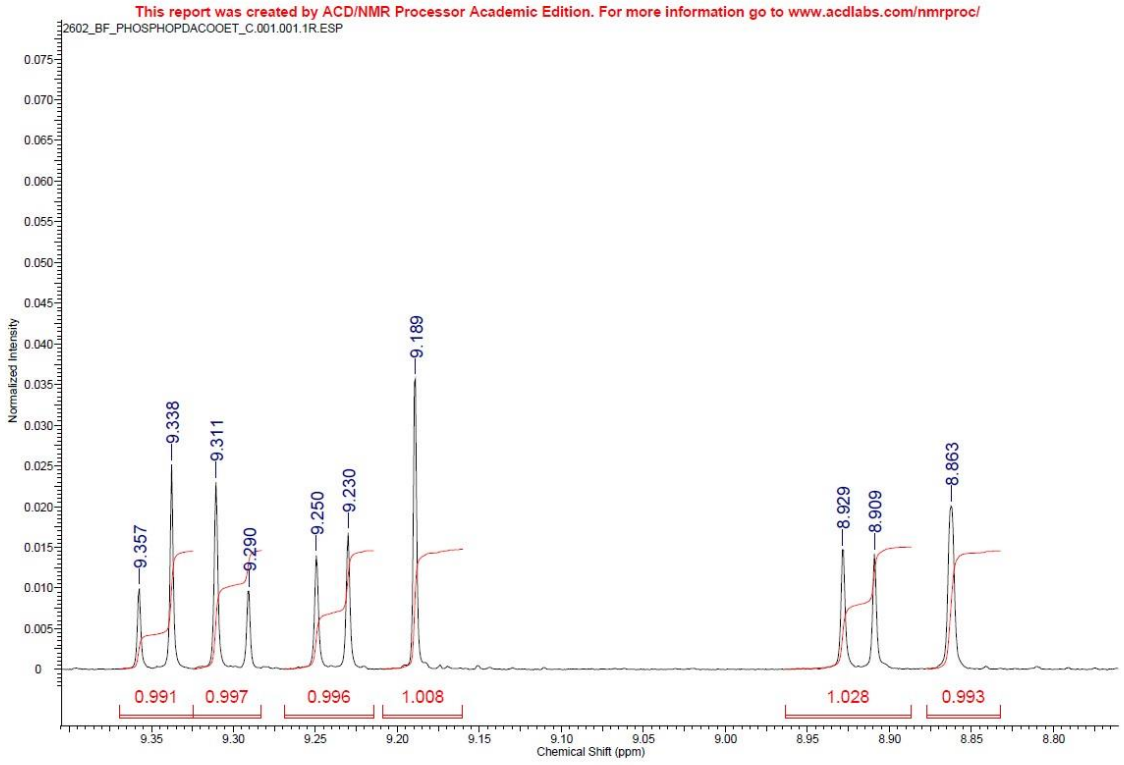

Figure S26: ^{1}H-NMR of compound **1**.

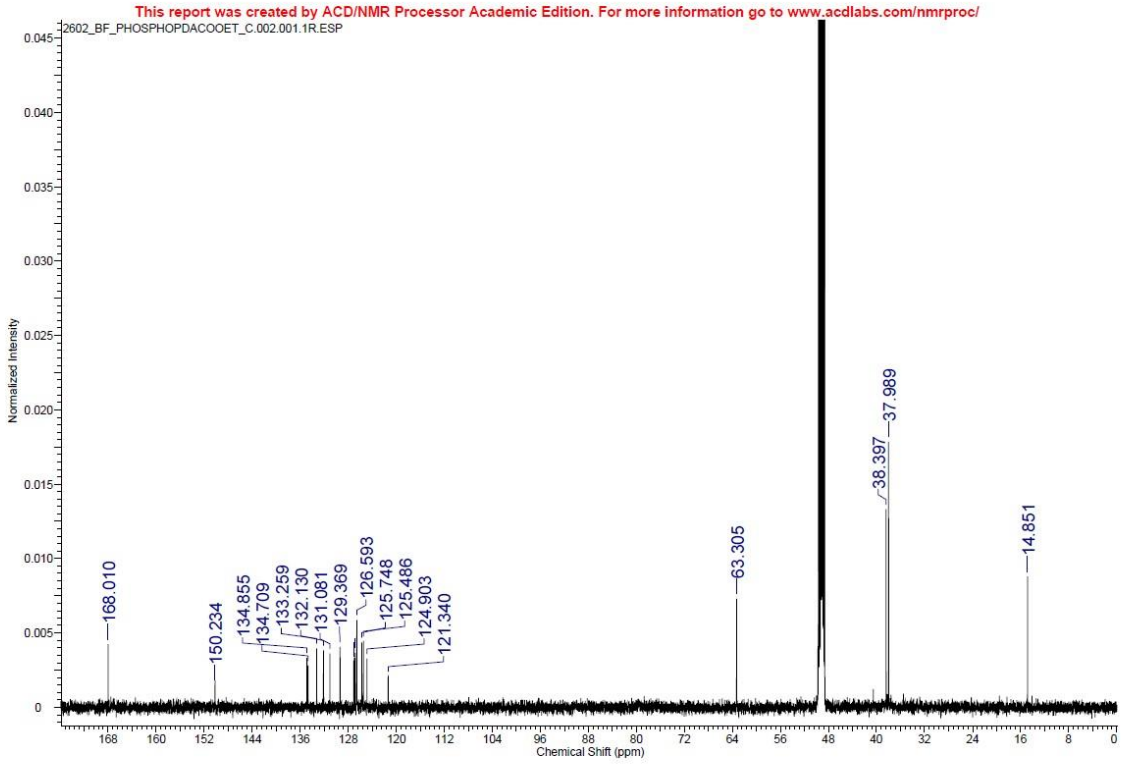

Figure S27: ^{13}C-NMR of compound **1**.

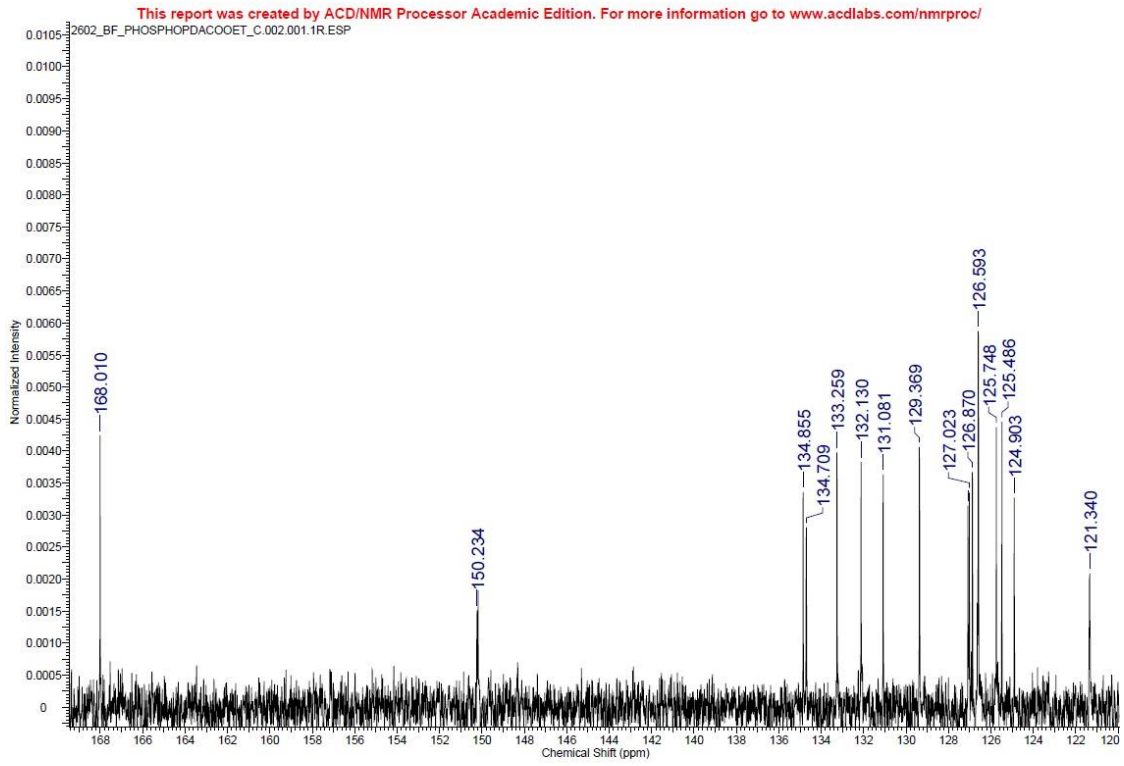

Figure S28: ^{13}C-NMR of compound **1**.

Compound **3** in methanol d4

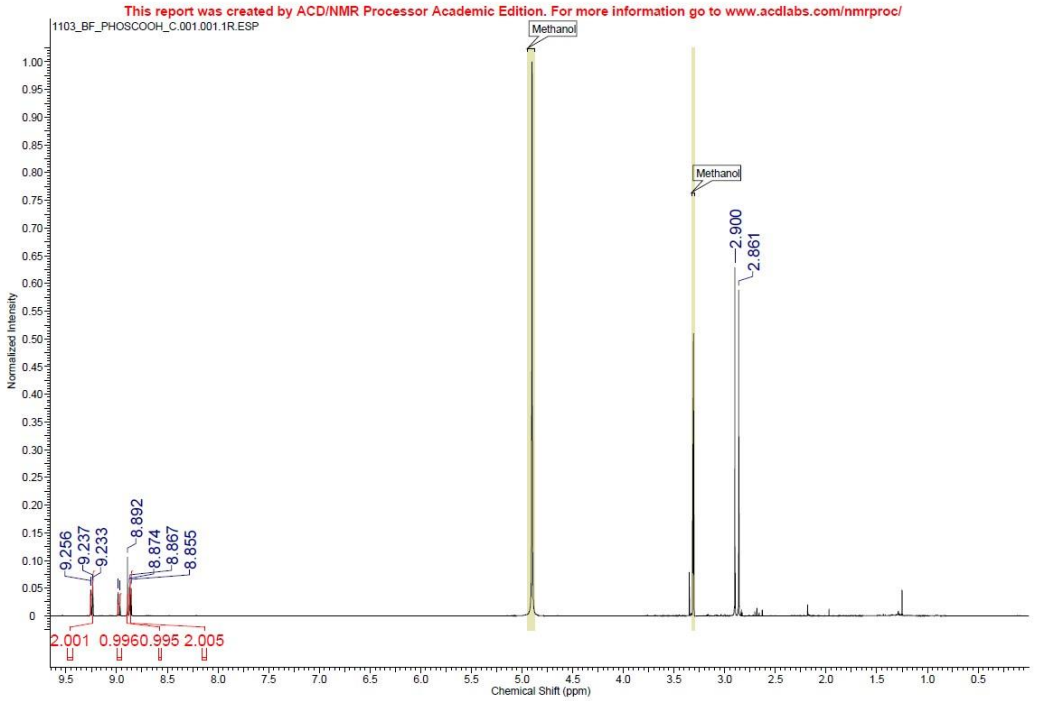

Figure S29: ^{1}H-NMR of compound **3**.

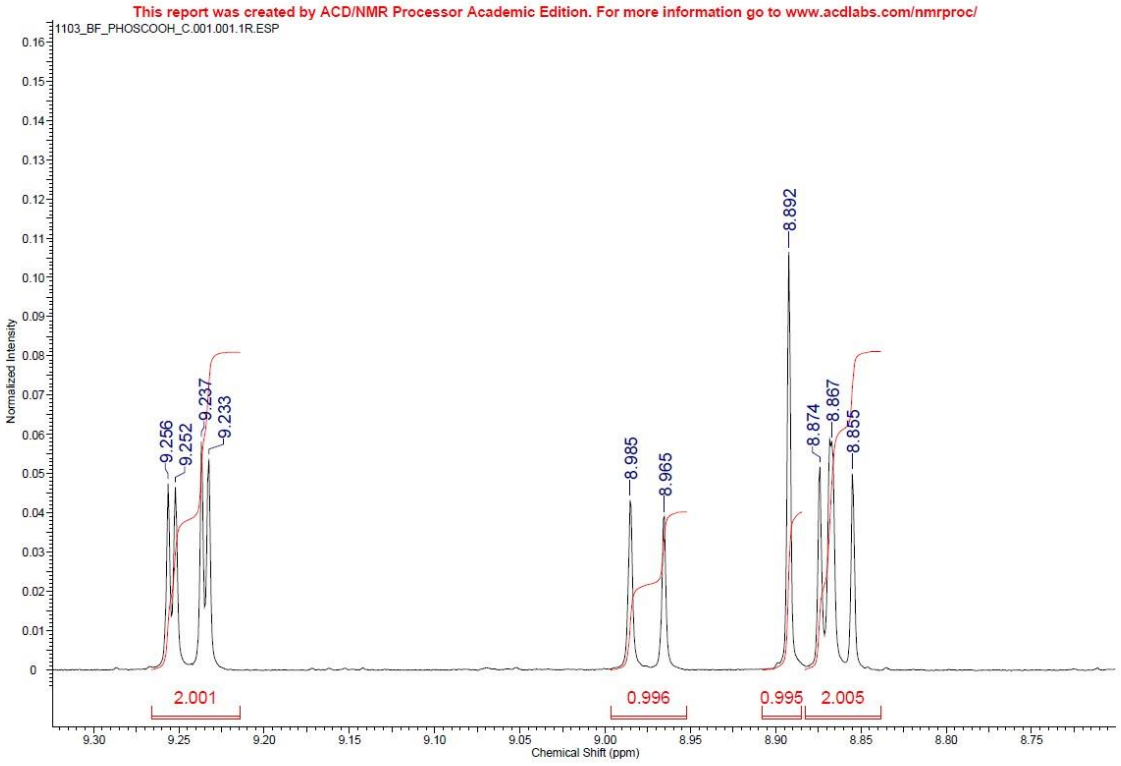

Figure S30: ^{1}H-NMR of compound **3**.

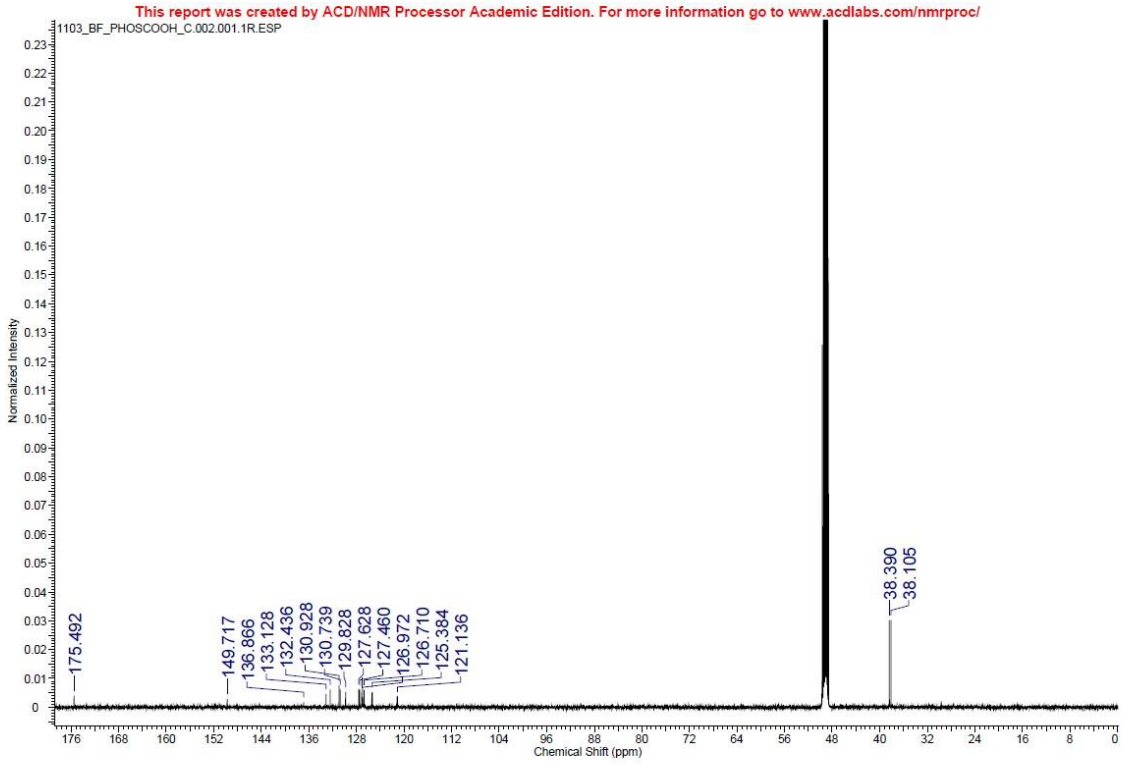

Figure S31: ^{13}C-NMR of compound **3**.

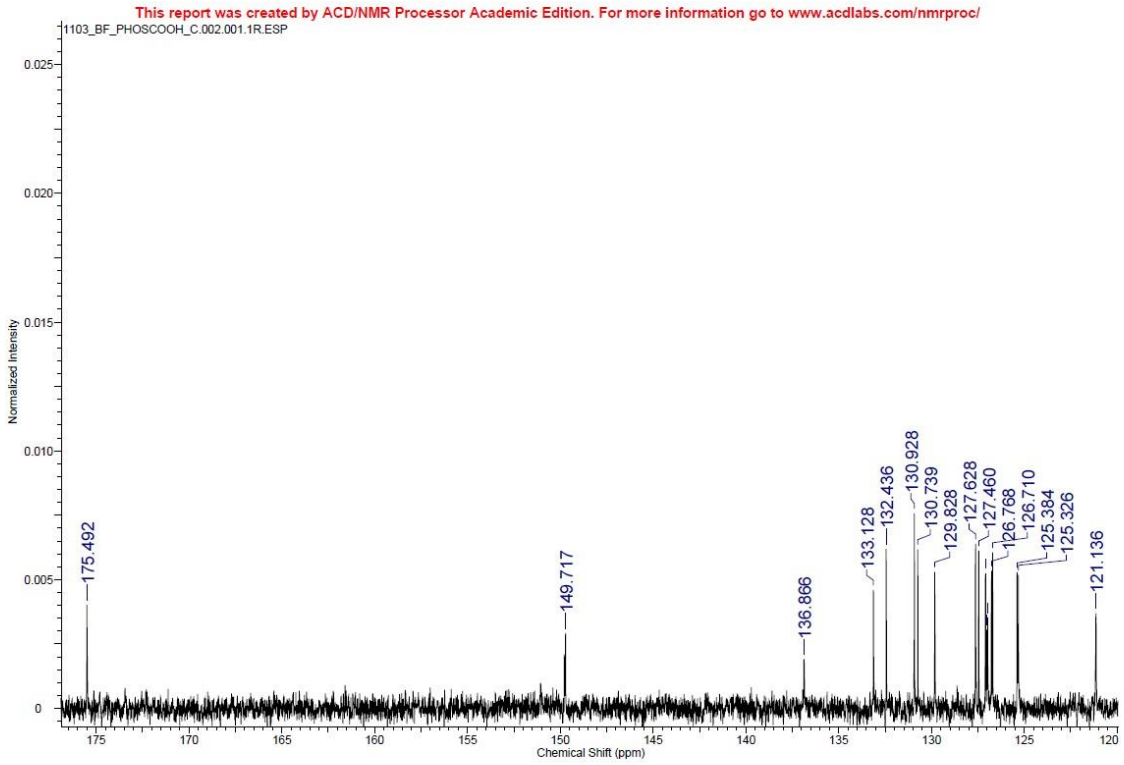

Figure S32: ^{13}C-NMR of compound **3**.

Crystallographic data

Crystallographic data for compound **7**

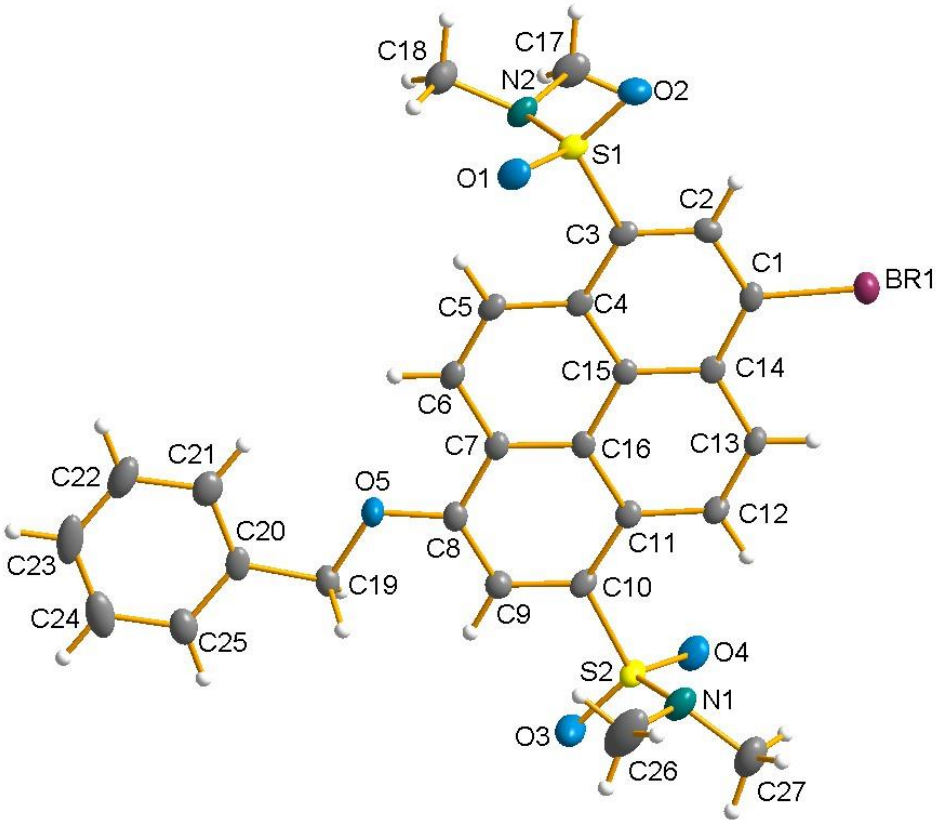

Figure S33: Crystallographic structure of compound **7**.

Table S1: Crystal data and structure refinement for compound **7**.

Identification code	sh3536	
Empirical formula	C27 H25 Br N2 O5 S2	
Formula weight	601.52	
Temperature	162(2) K	
Wavelength	0.71073 Å	
Crystal system	Triclinic	
Space group	P-1	
Unit cell dimensions	a = 6.9628(9) Å	α= 112.085(5)°.
	b = 14.1150(15) Å	β= 96.677(7)°.
	c = 14.1917(14) Å	γ = 97.399(7)°.
Volume	1260.9(2) $Å^3$	
Z	2	
Density (calculated)	1.584 Mg/m^3	
Absorption coefficient	1.839 mm^{-1}	
F(000)	616	
Crystal size	0.484 x 0.102 x 0.081 mm^3	
Theta range for data collection	1.574 to 27.102°.	
Index ranges	-8<=h<=8, -18<=k<=18, -18<=l<=18	
Reflections collected	19111	
Independent reflections	5417 [R(int) = 0.0582]	
Completeness to theta = 25.242°	98.3 %	
Absorption correction	Semi-empirical from equivalents	
Max. and min. transmission	0.7455 and 0.5915	
Refinement method	Full-matrix least-squares on F^2	
Data / restraints / parameters	5417 / 315 / 338	
Goodness-of-fit on F^2	1.057	
Final R indices [I>2sigma(I)]	R1 = 0.0488, wR2 = 0.1173	
R indices (all data)	R1 = 0.0712, wR2 = 0.1295	
Extinction coefficient	n/a	
Largest diff. peak and hole	0.910 and -1.206 e.$Å^{-3}$	

Table S2: Atomic coordinates (x 10^4) and equivalent isotropic displacement parameters ($Å^2$x 10^3) for compound **7**. U(eq) is defined as one third of the trace of the orthogonalized U^{ij} tensor.

	x	y	z	U(eq)
Br(1)	4169(1)	7306(1)	10772(1)	24(1)
S(1)	3156(1)	9181(1)	8048(1)	19(1)
S(2)	2531(1)	2060(1)	6121(1)	21(1)
N(1)	554(5)	1956(2)	6620(2)	28(1)
N(2)	5083(5)	9356(2)	7536(2)	25(1)
O(1)	1449(4)	9002(2)	7286(2)	26(1)
O(2)	3284(4)	9972(2)	9057(2)	27(1)
O(3)	2325(5)	1267(2)	5107(2)	36(1)
O(4)	4179(4)	2157(2)	6877(2)	27(1)
O(5)	2160(4)	4156(2)	3872(2)	24(1)
C(1)	3702(5)	7165(3)	9381(2)	17(1)
C(2)	3668(5)	8056(2)	9203(2)	18(1)
C(3)	3344(5)	8000(2)	8202(3)	17(1)
C(4)	3089(5)	7049(2)	7340(2)	16(1)
C(5)	2841(5)	6962(3)	6290(3)	19(1)
C(6)	2630(5)	6032(2)	5491(3)	19(1)
C(7)	2618(5)	5091(2)	5657(2)	17(1)
C(8)	2375(5)	4123(3)	4821(2)	19(1)
C(9)	2356(5)	3217(3)	4991(3)	19(1)
C(10)	2568(5)	3268(2)	5995(3)	18(1)
C(11)	2834(5)	4210(2)	6864(2)	17(1)
C(12)	3084(5)	4299(2)	7918(2)	19(1)
C(13)	3363(5)	5231(2)	8715(2)	18(1)
C(14)	3404(5)	6182(2)	8567(2)	16(1)
C(15)	3114(5)	6128(2)	7531(2)	15(1)
C(16)	2848(5)	5137(2)	6681(2)	15(1)
C(17)	6982(6)	9703(3)	8246(3)	31(1)
C(18)	4925(7)	9803(3)	6758(3)	34(1)
C(19)	1984(5)	3202(3)	2996(2)	19(1)
C(20)	1710(5)	3414(3)	2029(2)	20(1)
C(21)	1855(6)	4405(3)	2042(3)	26(1)
C(22)	1598(6)	4536(3)	1108(3)	34(1)
C(23)	1230(6)	3696(4)	184(3)	37(1)

C(24)	1106(6)	2705(4)	166(3)	36(1)
C(25)	1333(6)	2564(3)	1084(3)	26(1)
C(26)	-1312(7)	1777(4)	5915(4)	55(1)
C(27)	486(7)	1287(3)	7194(3)	39(1)

Mass spectra

Table S3: Data from mass spectroscopic analysis.

Dye/ scanmode	Formula	$[M-H]^-$/ $[M+H]^+$ calculated	$[M-H]^-$/ $[M+H]^+$ found	Deviation / ppm	*comment*
5 **ES$^-$**	C16H9BrO	294.975852	294.97555	-1.02	Br-79
		295.979207	295.97893	-0.94	"; C-13
		296.973806	296.97352	-0.96	Br-81
		297.977161	297.9769	-0.88	"; C-13
6 **ES$^-$**	C20H19BrN2O5S2	508.984052	508.98384	-0.42	Br-79; S-32
		509.987407	509.98762	0.42	"; C-13
		510.982006	510.9816	-0.80	Br-81; S-32
		511.985361	511.98536	-0.002	"; C-13
		512.977802	512.97863	1.61	Br-81; S-34
7 **ES$^+$**	C27H25BrN2O5S2	623.028043	623.02891	1.39	Br-79; S-32; Na+ adduct
		624.031398	624.03232	1.48	"; C-13
		625.025997	625.02684	1.35	Br-81; 2xS-32
		626.029352	626.03016	1.29	"; C-13
		627.021793	627.02257	1.24	"; 1xS-32; 1xS-34
8 **ES$^+$**	C30H30N2O7S2	617.138661	617.13953	1.41	2xS-32; Na+ adduct
		618.142016	618.14307	1.71	"; C-13
		619.134457	619.13535	1.44	1x-S-32; 1xS-34
2 **ES$^-$**	C23H24N2O7S2	503.09467	503.09282	-3.68	S-32
		504.098025	504.0971	-1.84	"; C-13
		505.090466	505.09014	-0.65	S-34
4 **ES$^-$**	C21H20N2O7S2	475.06337	475.06494	3.31	2x B-11
		476.066725	476.06773	2.11	2x B-11; C-13
		477.059166	477.05931	0.30	2x B-11; 2x C-13
1 **ES$^-$**	C23H25N2O10PS2	583.06155	583.06245	1.54	
		584.064905	584.06619	2.20	C-13
3 **ES$^-$**	C21H21N2O10PS2	555.03025	555.03196	3.08	
		556.033605	556.03549	3.39	C-13

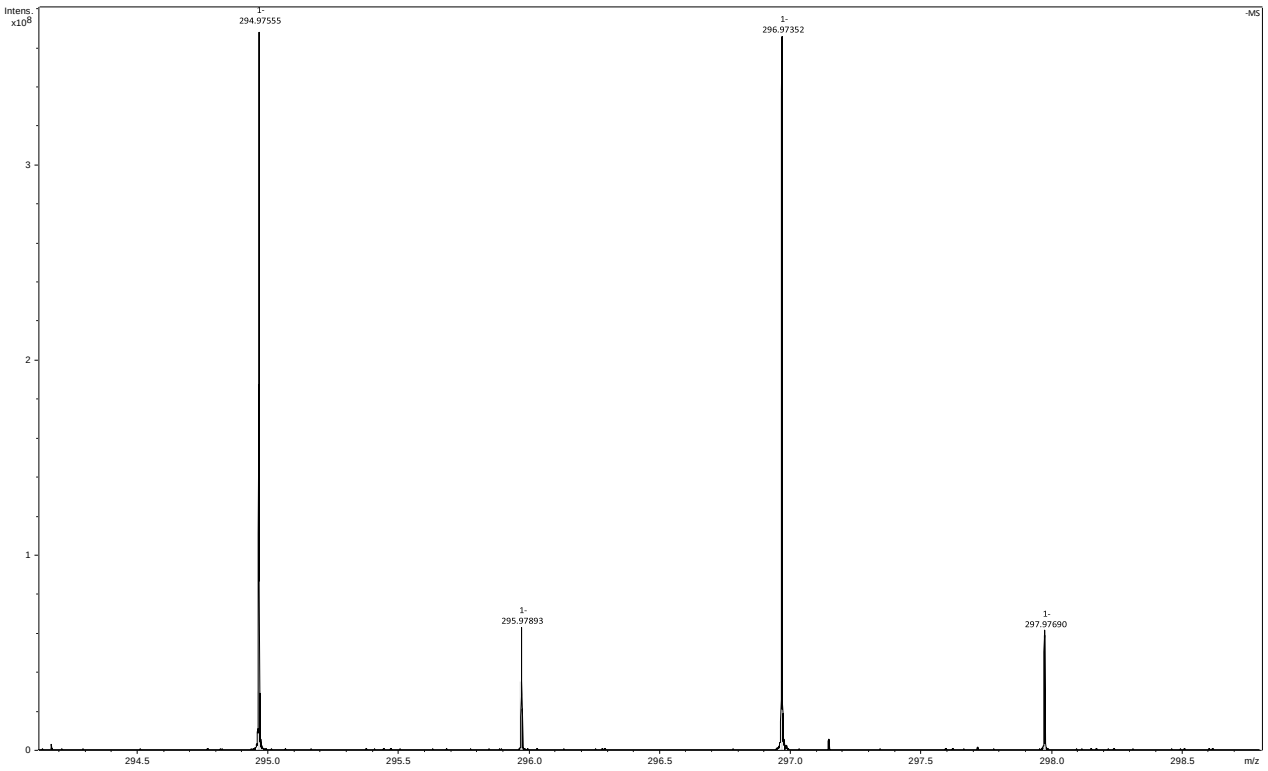

Figure S34: ES$^-$ Spectrum of compound **5**.

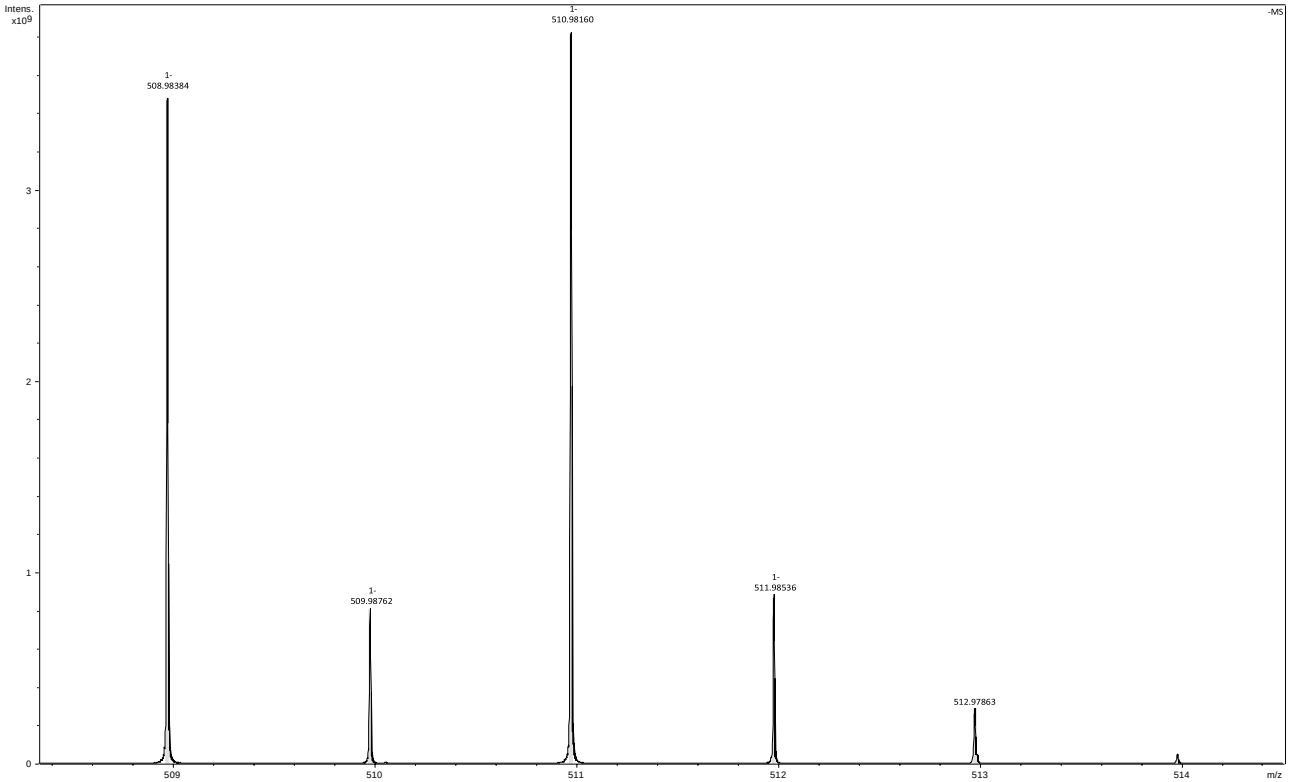

Figure S35: ES$^-$ Spectrum of compound **6**.

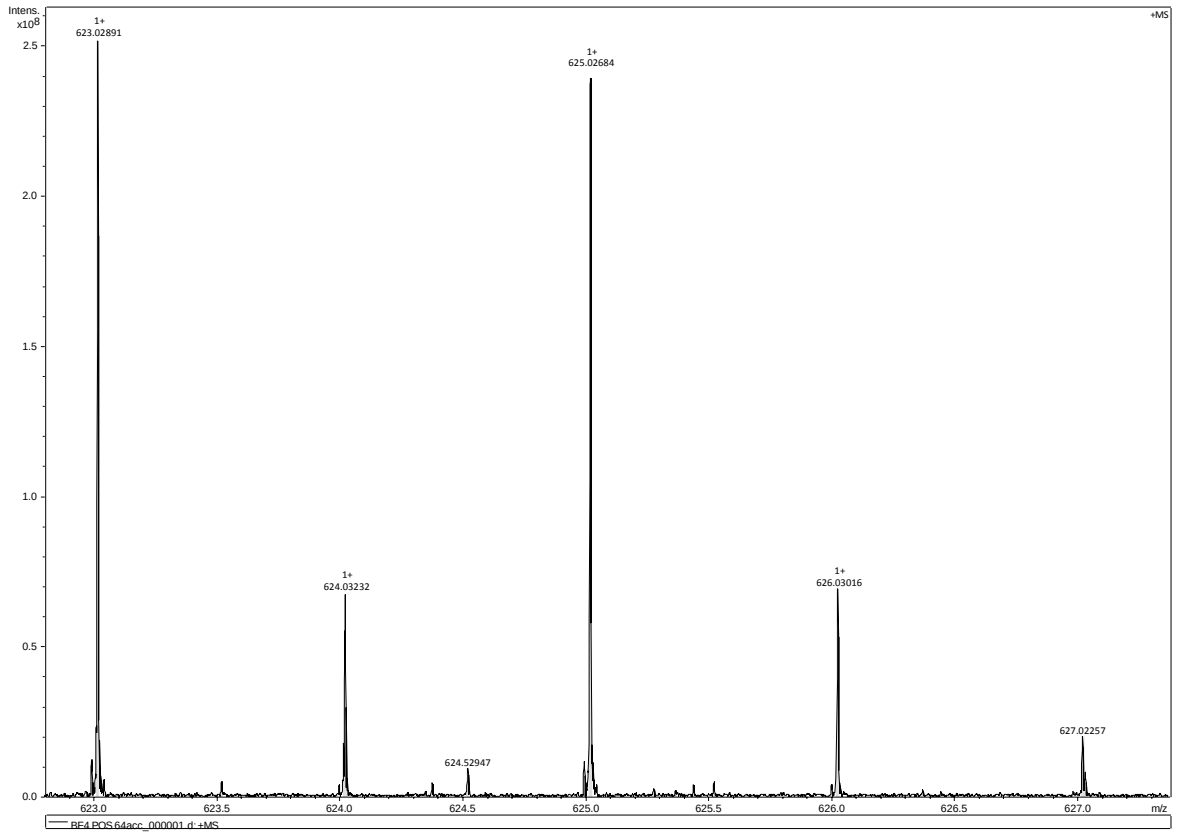

Figure S36: ES$^+$ Spectrum of compound **7**.

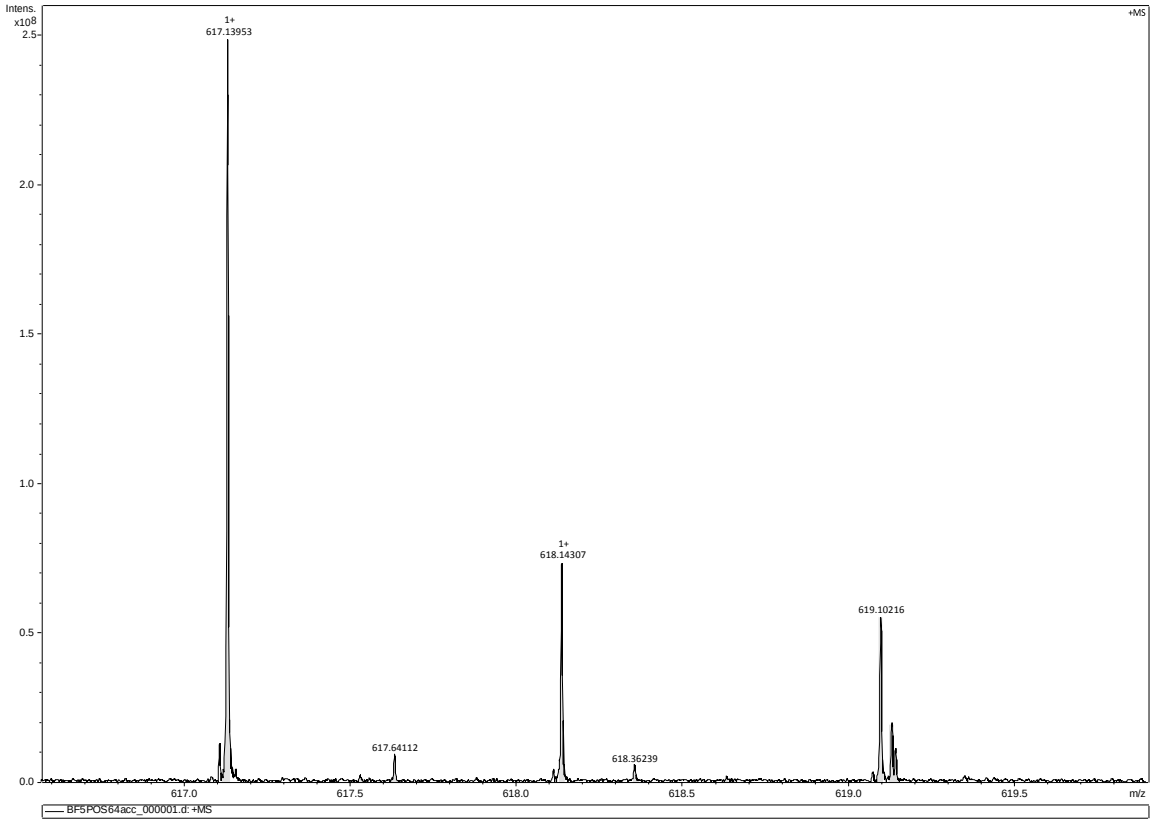

Figure S37: ES$^+$ Spectrum of compound **8**.

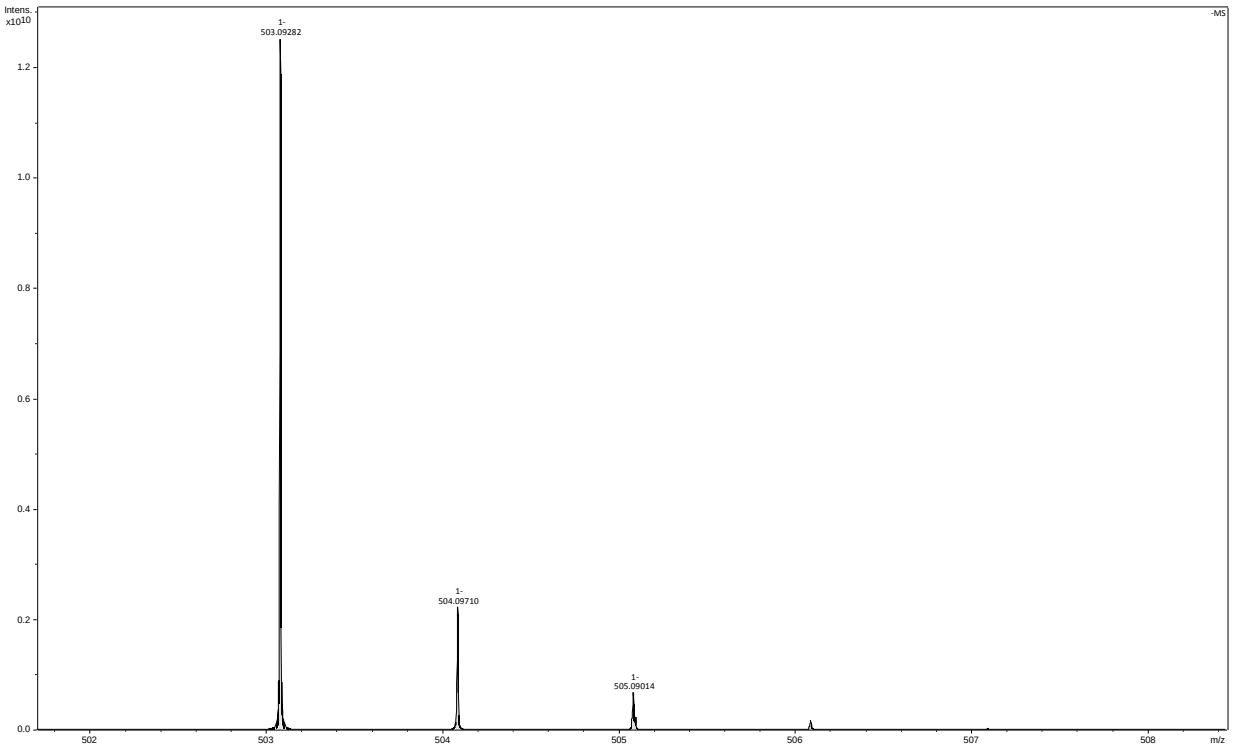

Figure S38: ES$^-$ Spectrum of compound **2**.

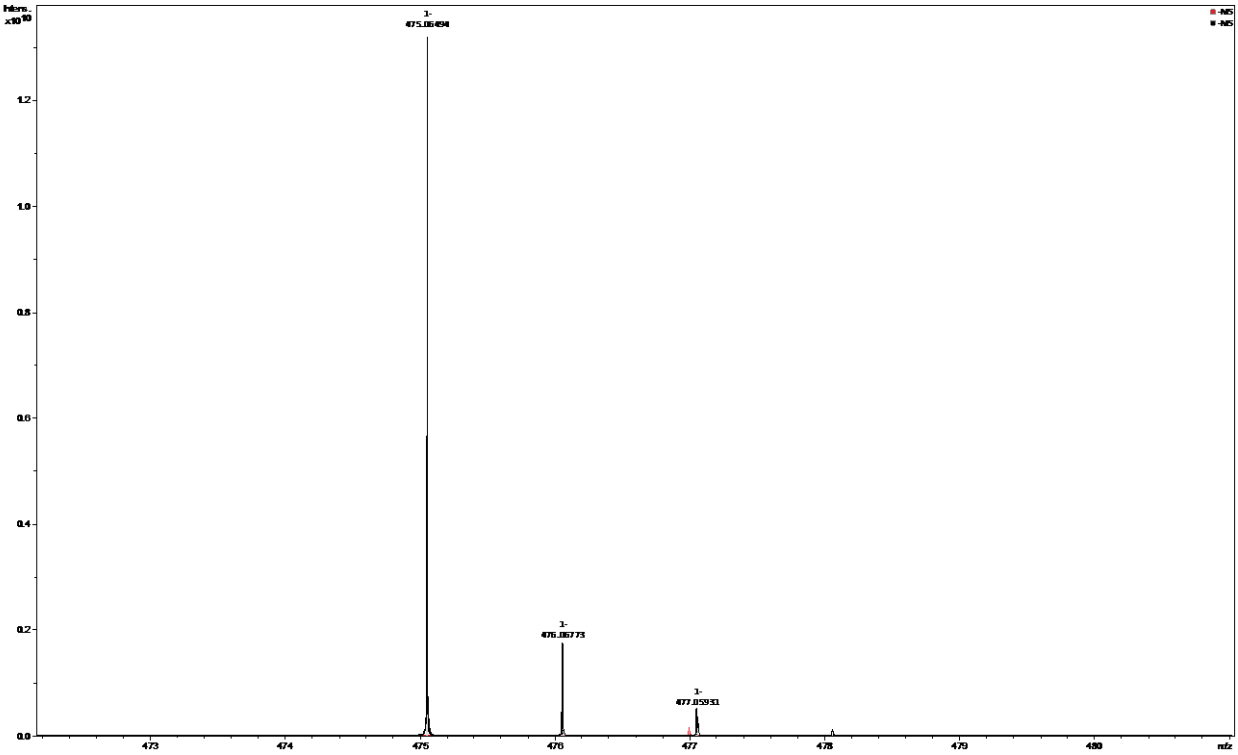

Figure S39: ES$^-$ Spectrum of compound **4**.

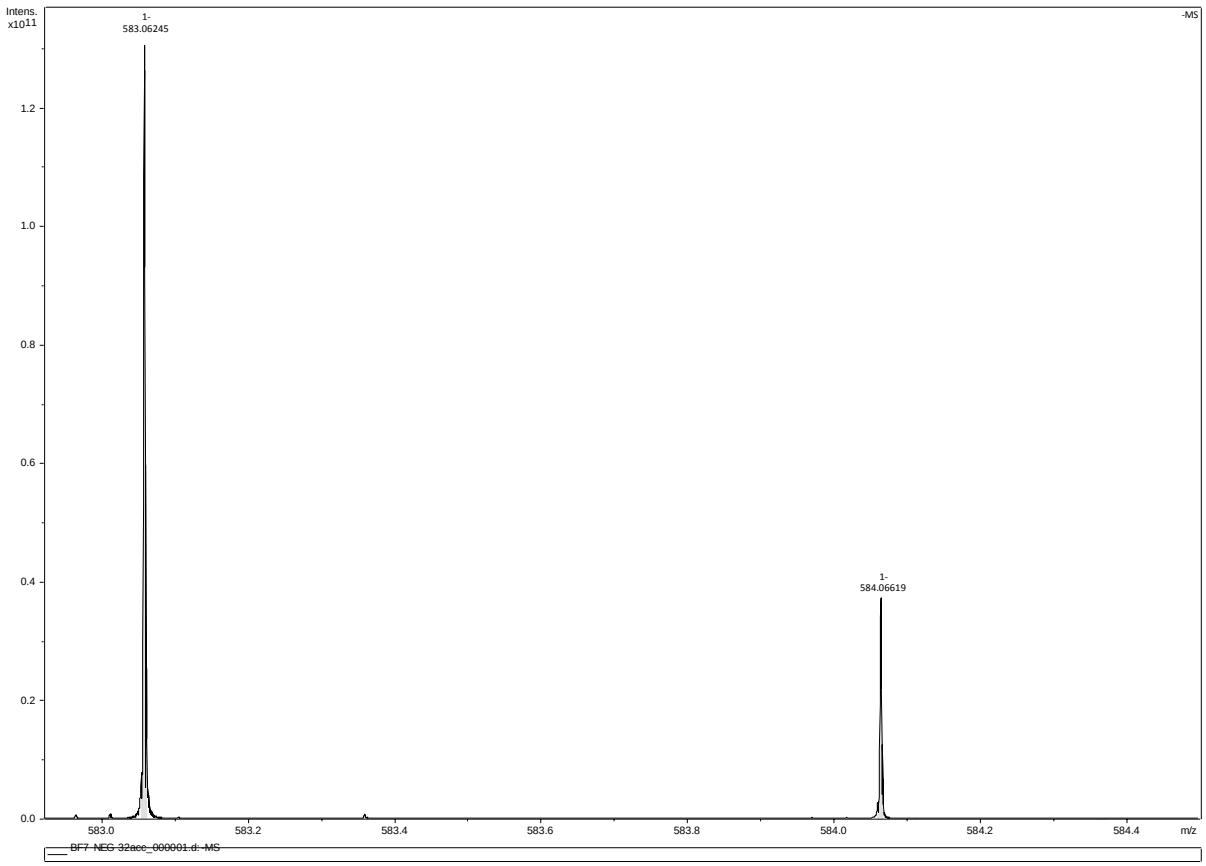

Figure S40: ES$^-$ Spectrum of compound **1**.

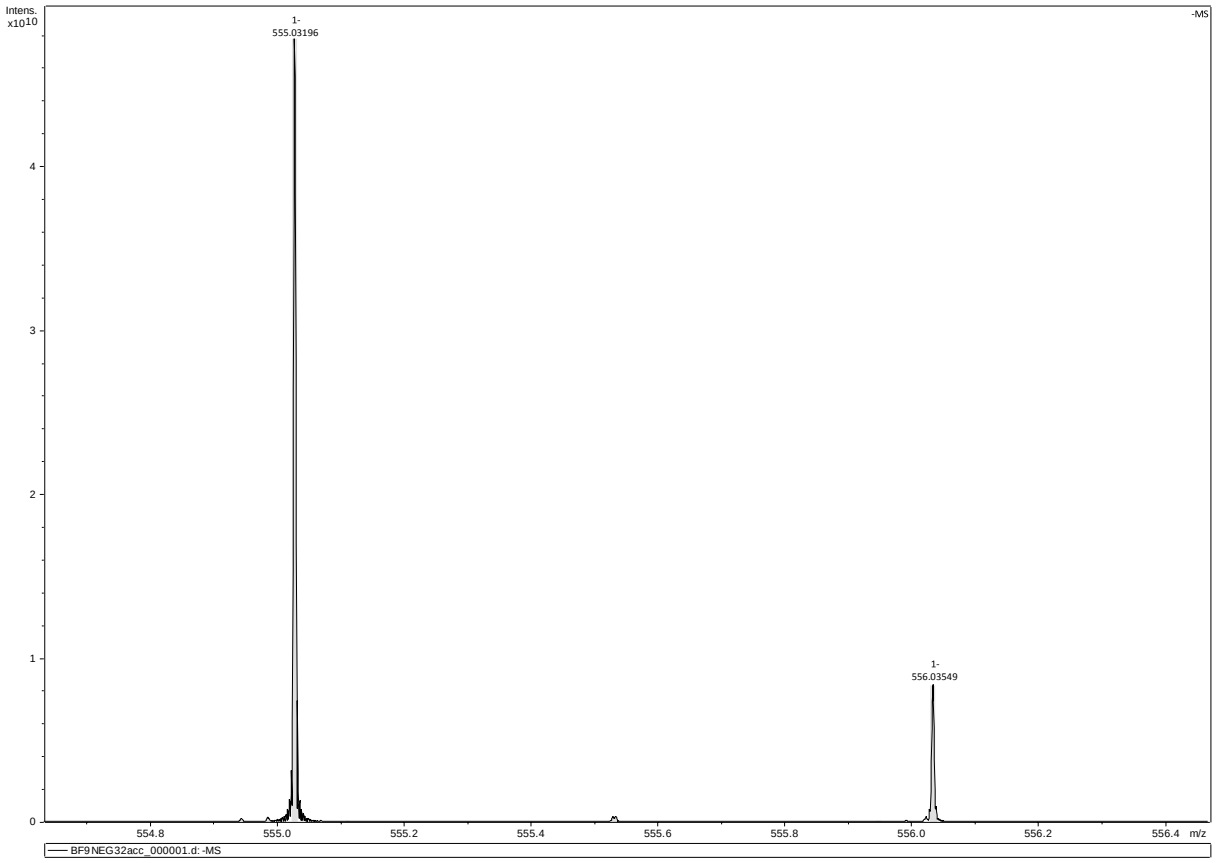

Figure S41: ES$^-$ Spectrum of compound **3**.

Fluorescence spectra

Compound **1**

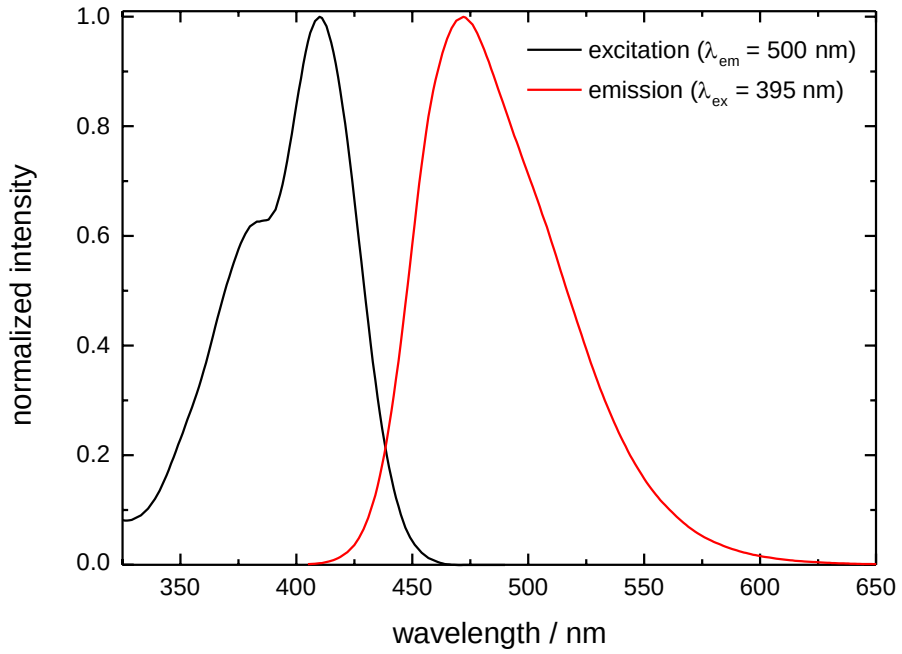

Figure S42: Fluorescence spectra of compound **1** in H_2O at pH = 8.

Compound **2**

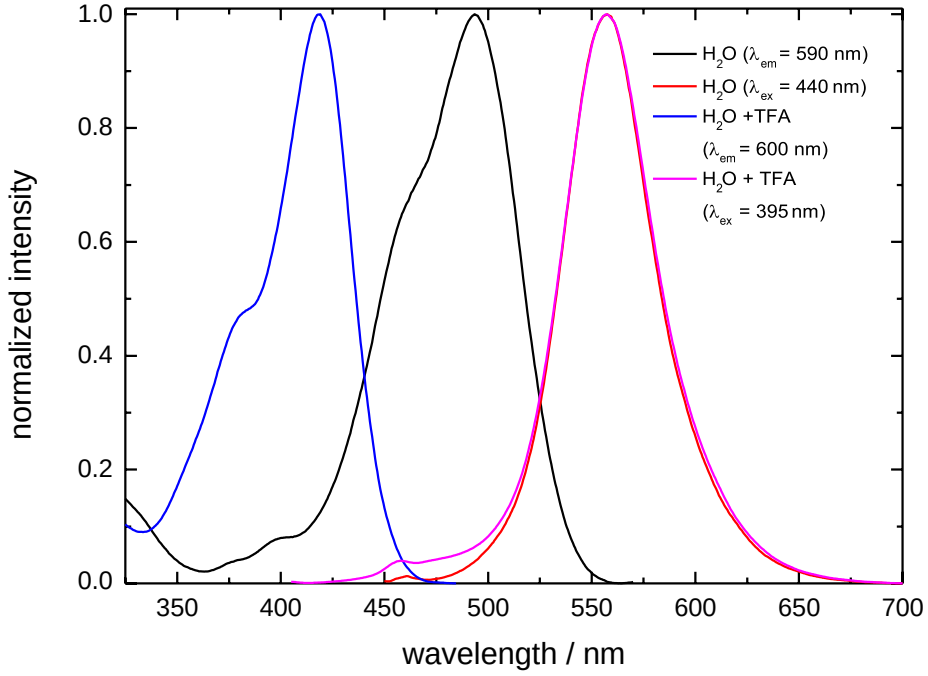

Figure S43: Fluorescence spectra of compound **2** in H_2O.

Compound **3**

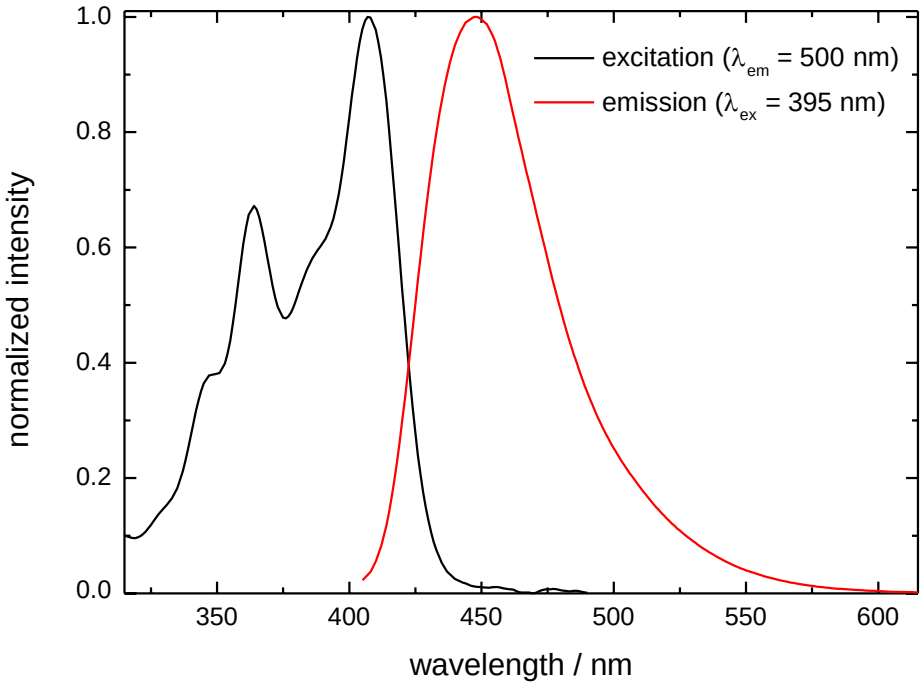

Figure S44: Fluorescence spectra of compound **3** in H_2O at pH = 8.

Compound **4**

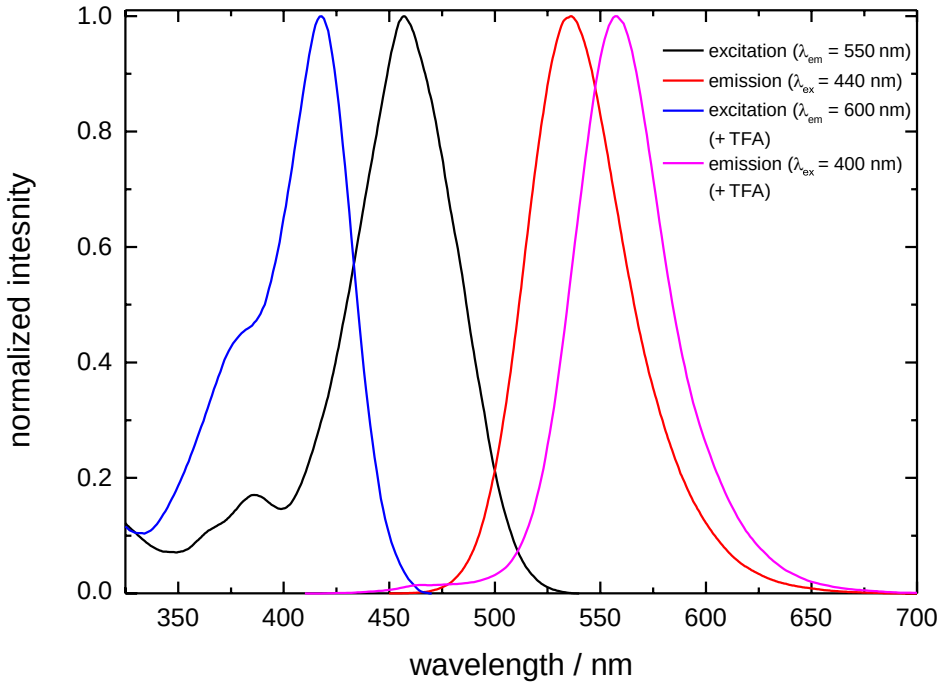

Figure S45: Fluorescence spectra of compound **4** in H_2O.

Time-resolved fluorescence spectra

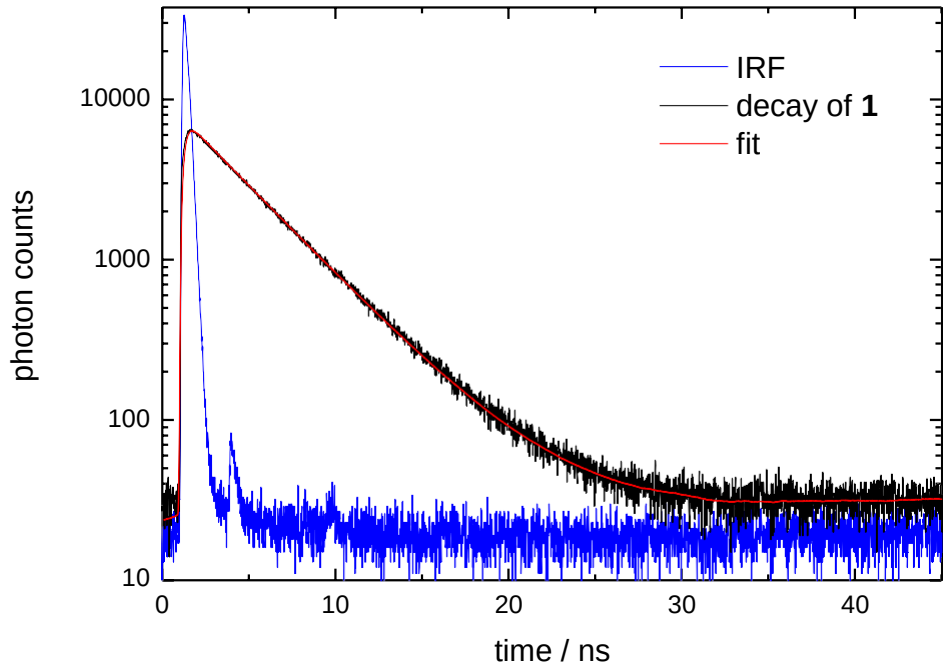

Figure S46: TCSPC histogram of compound **1** in H_2O at pH = 8; λ_{ex} = 405 nm; λ_{det} = 450 – 490 nm.

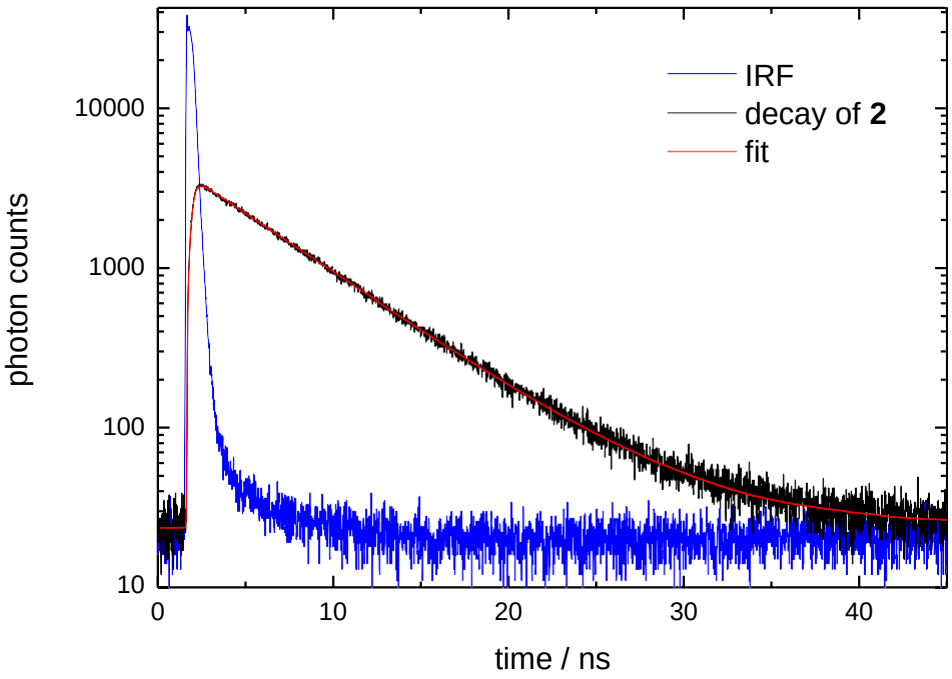

Figure S47: TCSPC histogram of compound **2** in H_2O at pH = 8; λ_{ex} = 470 nm; λ_{det} = 555 – 625 nm.

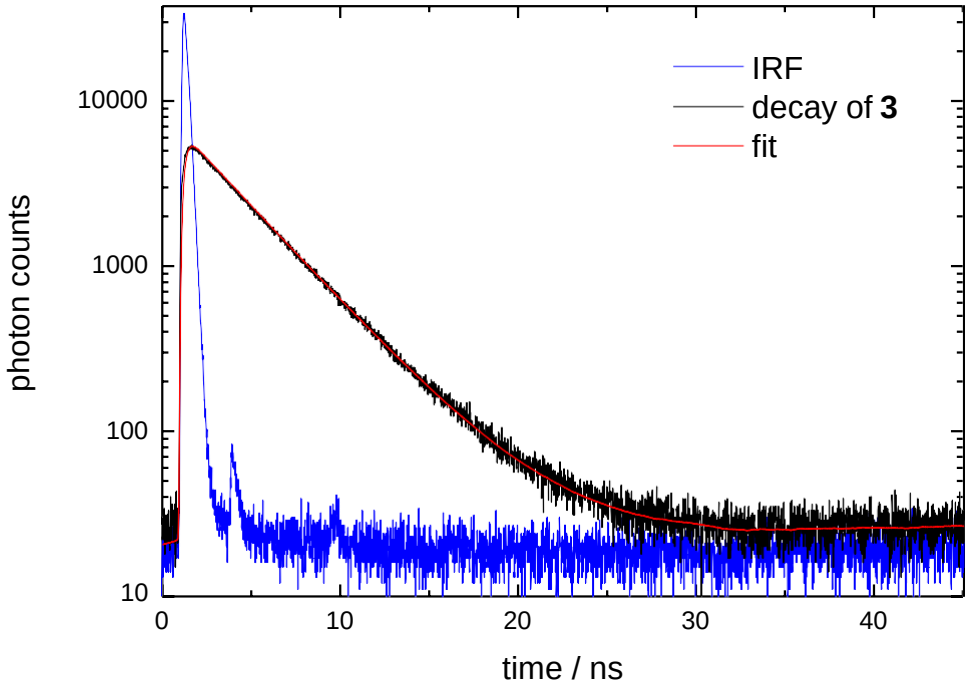

Figure S48: TCSPC histogram of compound **3** in H_2O at pH = 8; λ_{ex} = 405 nm; λ_{det} = 450 – 490 nm.

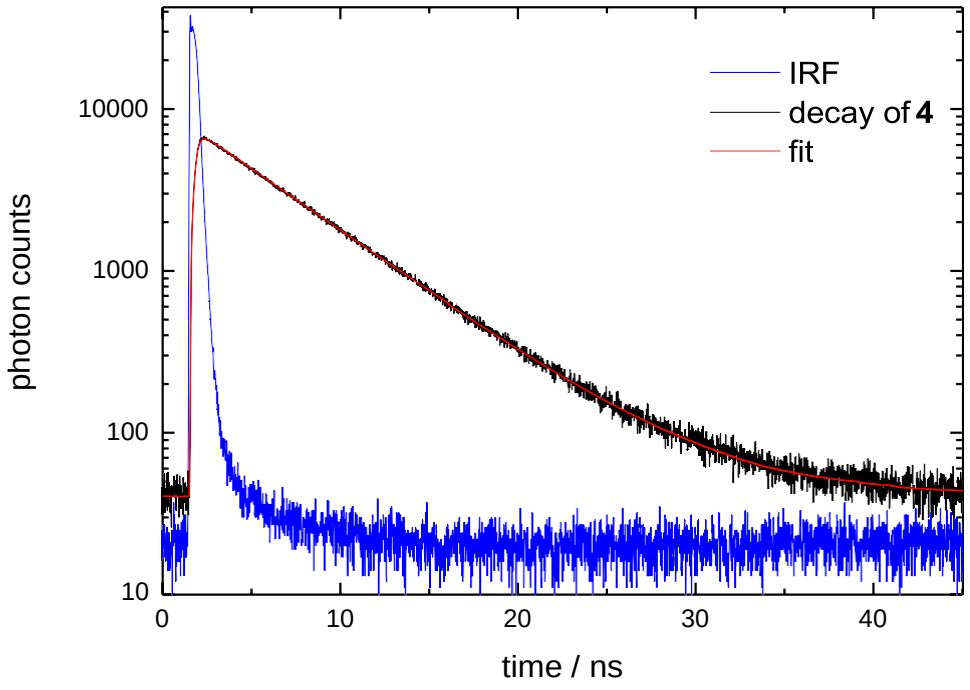

Figure S49: TCSPC histogram of compound **4** in H_2O at pH = 8; λ_{ex} = 470 nm; λ_{det} = 555 – 625 nm.

pK_a determination with absorption/fluorescence titration

Compound **2**

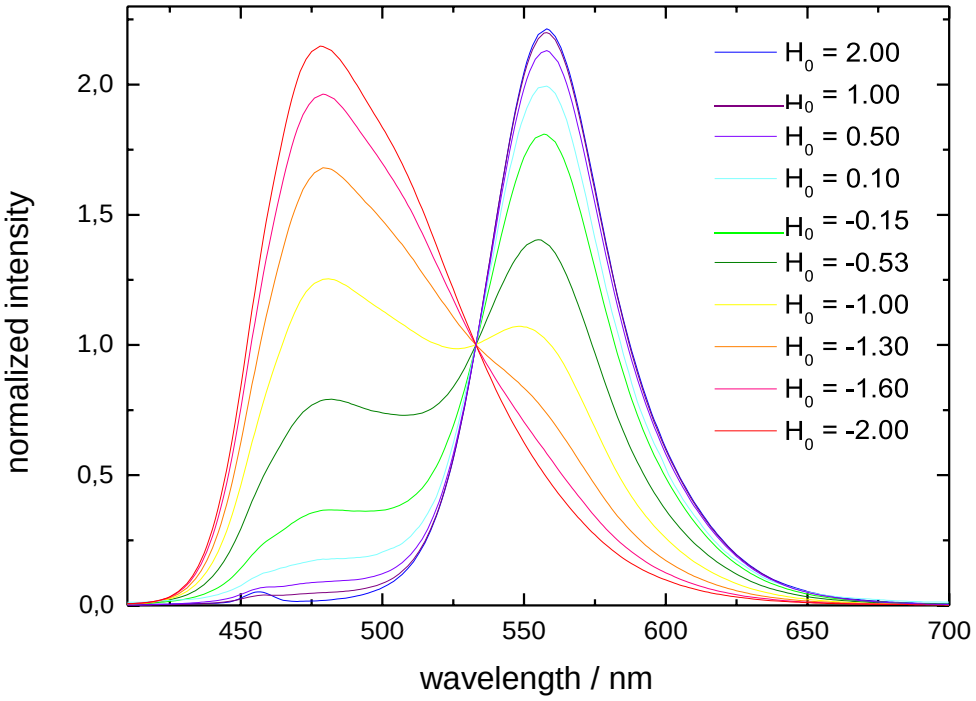

Figure S50: Fluorescence titration of compound **2** (λ_{ex} = 395 nm).

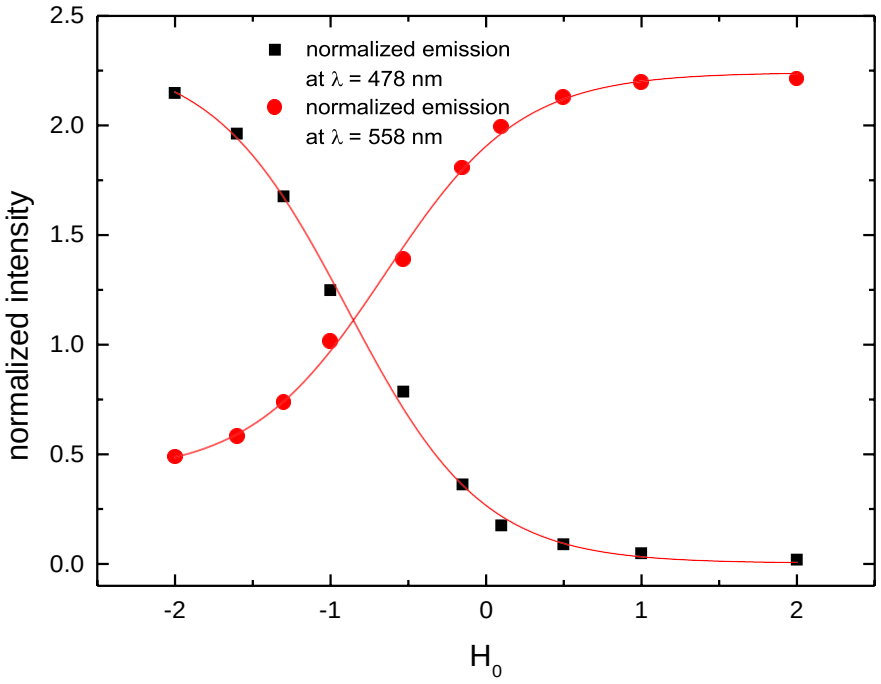

Figure S51: Fluorescence maxima of the ROH/RO^- forms of compound **2**.

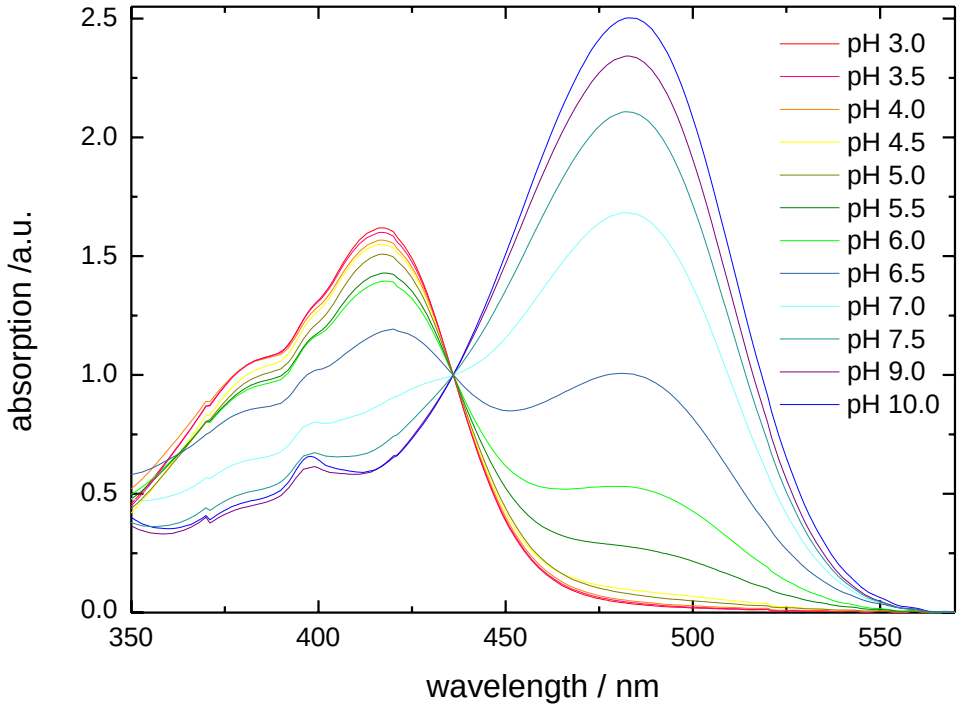

Figure S52: Absorption titration of compound **2**.

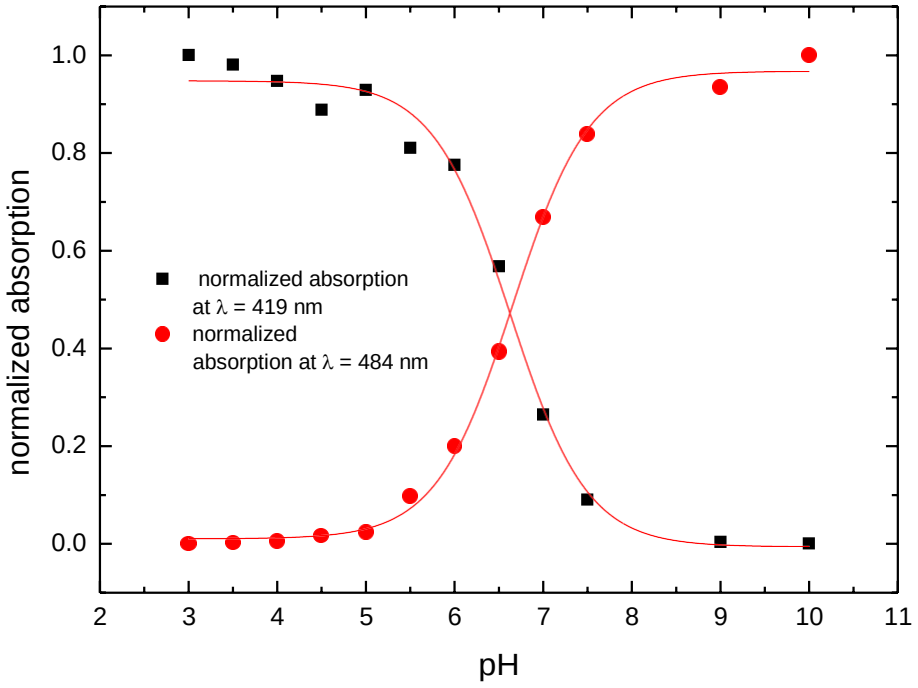

Figure S53: Absorption maxima of the ROH/RO^- forms of compound **2**.

Compound **4**

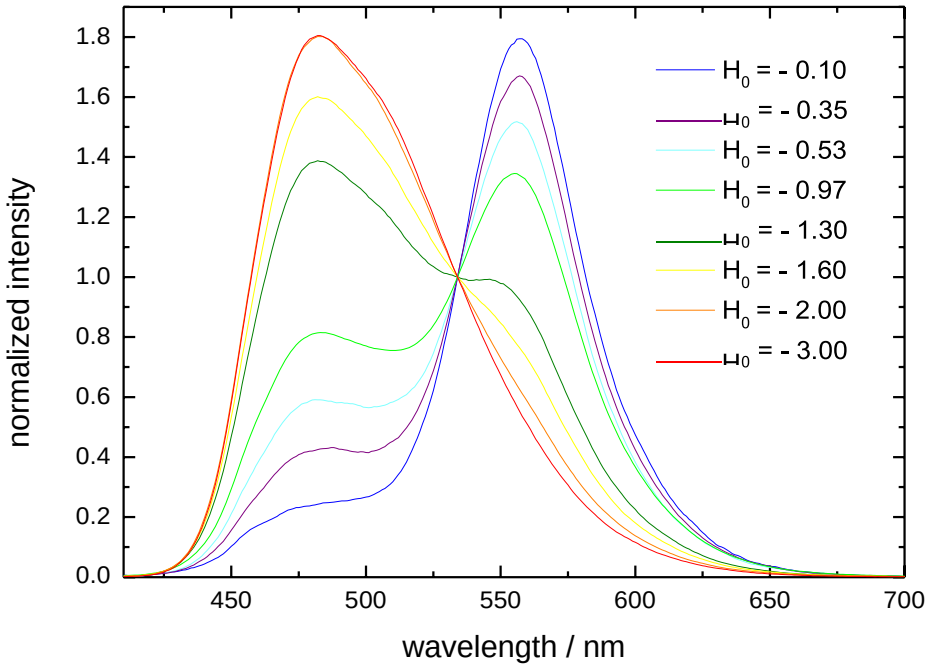

Figure S54: Fluorescence titration of the ROH function of compound **4** (λ_{ex} = 395 nm).

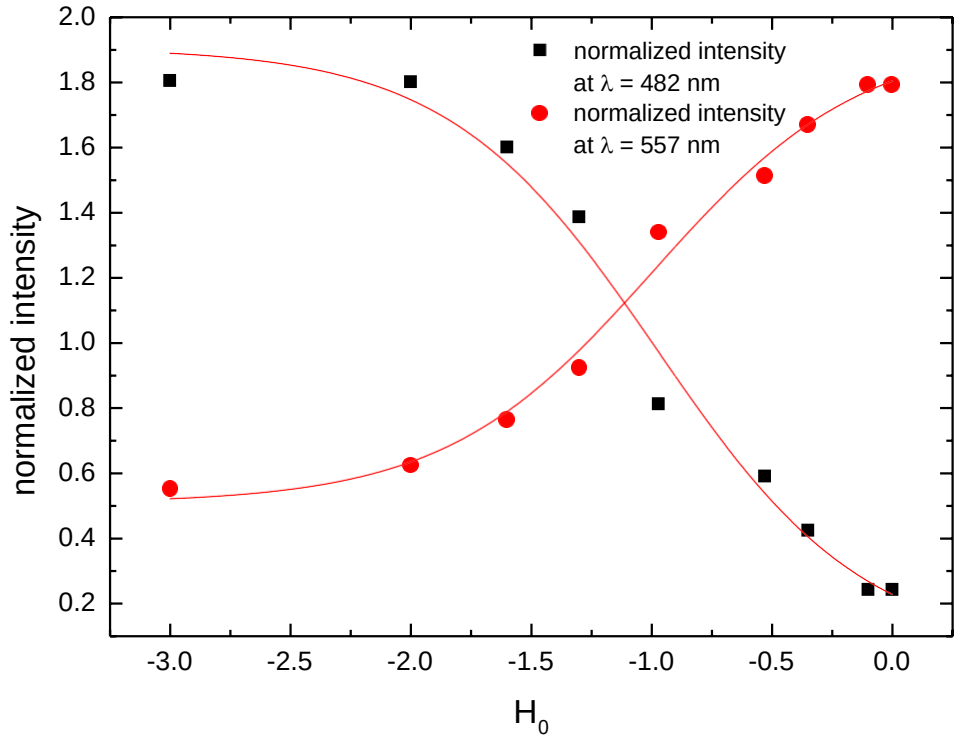

Figure S55: Fluorescence maxima of the ROH/RO^- forms of compound **4**.

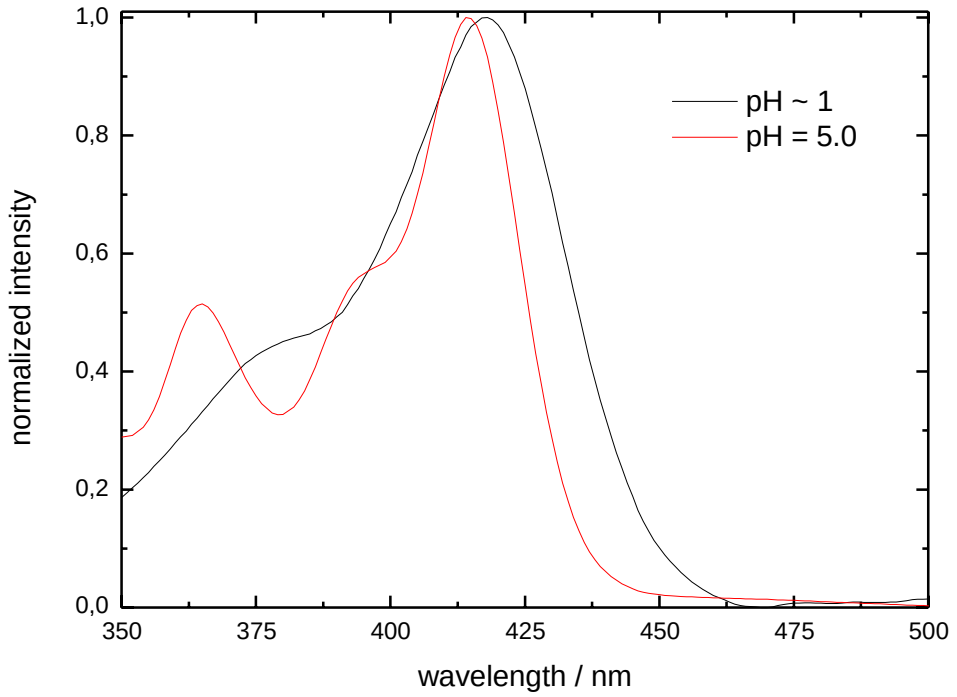

Figure S56: Fluorescence excitation spectra of compound **4** at different pH values (λ_{em} = 580 nm).

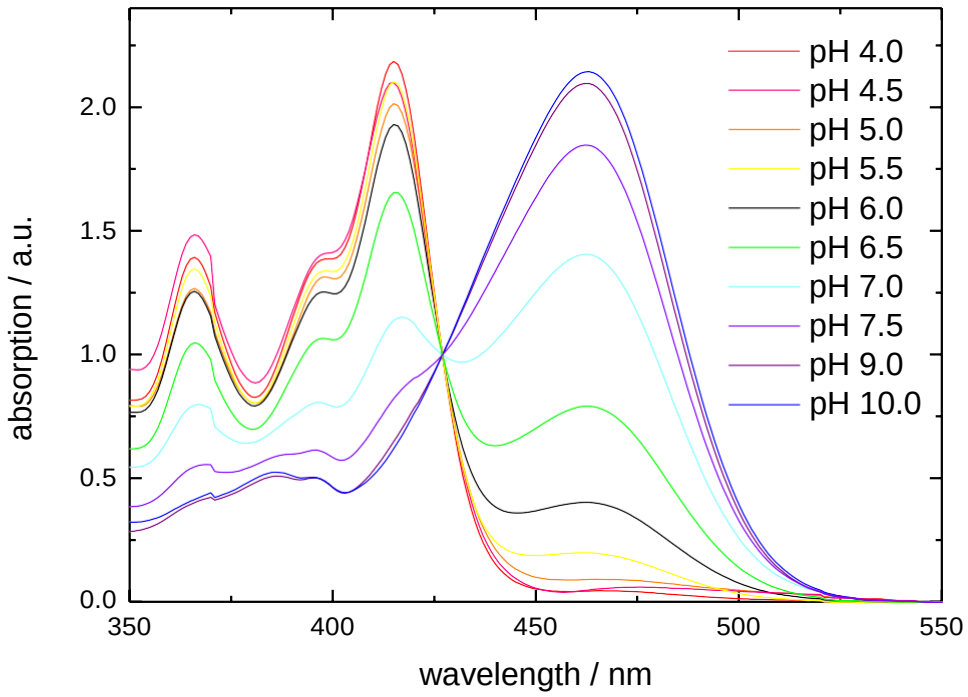

Figure S57: Absorption titration of the ROH function of compound **4**.

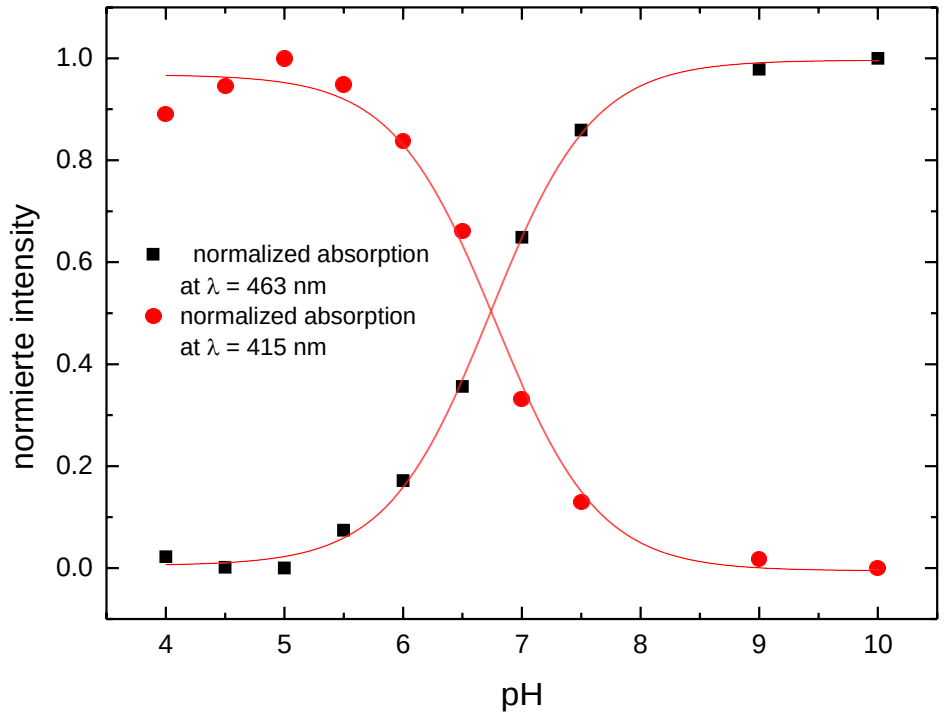

Figure S58: Absorption maxima of the ROH/RO$^-$ forms of compound **4**.

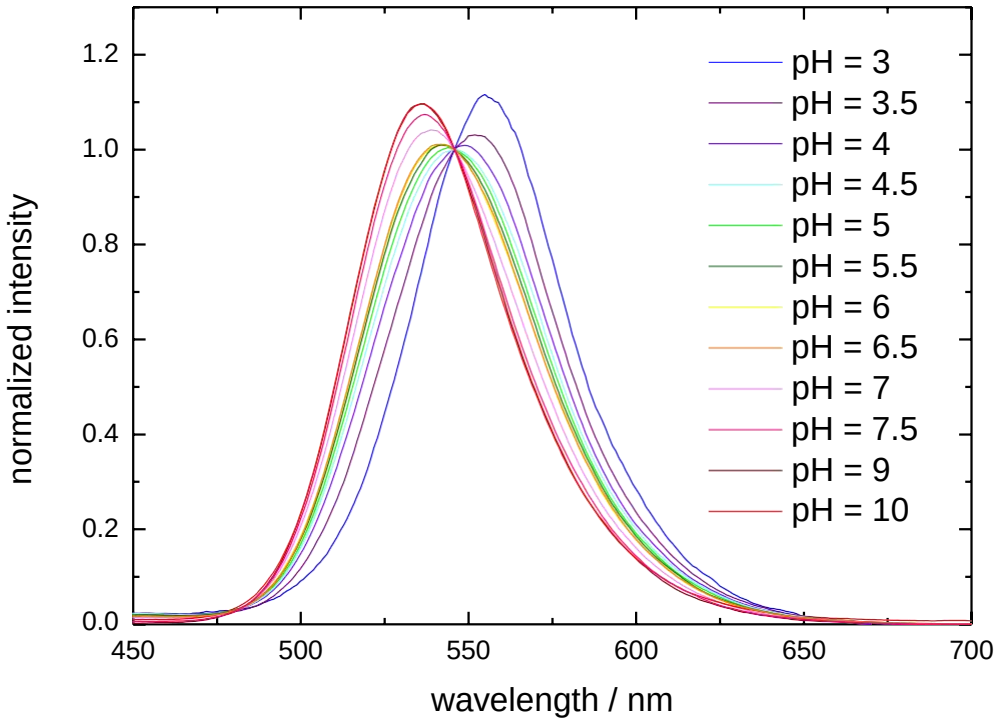

Figure S59: Fluorescence titration of the RCOOH function of compound **4** (λ_{ex} = 395 nm).

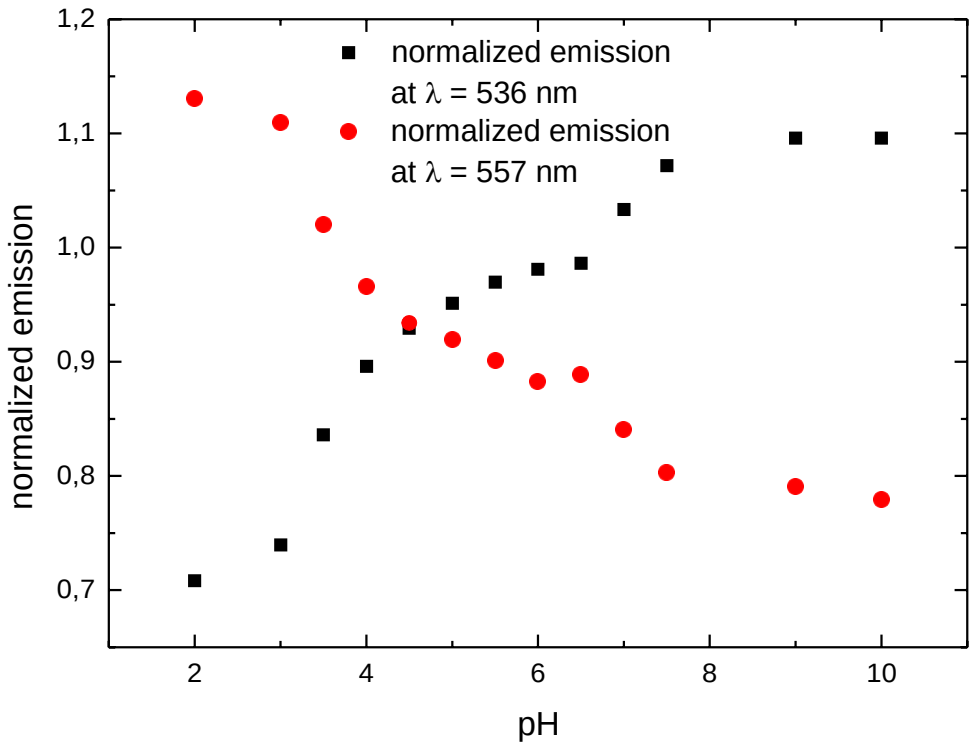

Figure S60: Fluorescence maxima of the RCOOH/RCOO$^-$ forms of compound **4**.

Table S4: Spectrophysical data of compounds **1**-**4**.

	1	**2**	**3**	**4**
$\lambda_{max,abs}$ [nm]	410	419[a]; 484[b]	407	418[c]; 415 [d]; 463[f]
$\lambda_{max,em}$ [nm]	472	478[a]; 558[b]	448	482[c]; 557[e]; 536[f]
pK$_a$ [i]	-	6.6	-	6.8 (R**OH**COO$^-$,); ~ 2.0 (RO$^-$**COOH**)
pK$_a$*	-	-0.4[g] -0.8[h]	-	4.5 (ROH**COOH**)[g]; -0.9 (R**OH**COOH)[h]
Φ	0.98	0.86[b]	1.00	0.85[f]
$\tau_{fl,\ RO^-}$ [ns]	3.89	5.81	3.73	5.58

[a] ROH; [b] RO$^-$; [c] ROHCOOH (**4a**); [d] ROHCOO$^-$ (**4d**); [e] RO$^-$COOH (**4b**); [f] RO$^-$COO$^-$ (**4c**); [g] determined via Förster cycle; [h] determined with fluorescence titration; [i] determined via absorption titration.

Structurally and electronically, the reaction products **2** and **4** bearing two sulfonamide groups are derivatives of the photoacid HPTA (N,N,N',N',N'',N''-hexamethyl-1,3,6-trisulfonamide).[1-6] The excited state acidity (pK$_a$*, Table S4) of **2**, evaluated by fluorescence titration,[7,8] lies in the range of that of HPTA (pK$_a$* = -0.4 *resp.* -1.0 (via Förster cycle))[32]. As

the ground state acidity is lower than that of HPTA, the enhancement of the acidity upon excitation (ΔpK_a) is higher by one logarithmic unit. Furthermore, the fluorescence emission of the corresponding base in aqueous solution is shifted bathochromically compared to that of HPTA. This finding is not in line with the trend we observed for different substituted HPTA derivatives.[2] Consequently, it can be concluded, that the connection between the photophysical properties and the substitution pattern is not only limited to the electron- withdrawing properties of one substituent. We assume that the electron withdrawing strength of a substituent is just one factor in a more complex process affecting the properties of the photoacids based on pyrene. The effect of different substitution patterns will be addressed in forthcoming publication.

pK_a determination with FCS

For comparison, the pK_a values of the photoacids **2** and **4** were determined with fluorescence correlation spectroscopy, according to the experimental procedure of Widengren et al.[9] A detailed description of the evaluation of pK_a can be found in the supporting information of our previous work[2]. The hydoxyl's pK_a of **2** was determined to be 6.2, which deviates slightly from the value determined by ratiometric titration (pK_a = 6.6). Compared to that, the values found for the hydroxyl's pK_a of **4** even less by just 0.2 logarithmic units (pK_a (titration) = 6.8; pK_a (FCS) = 6.6).

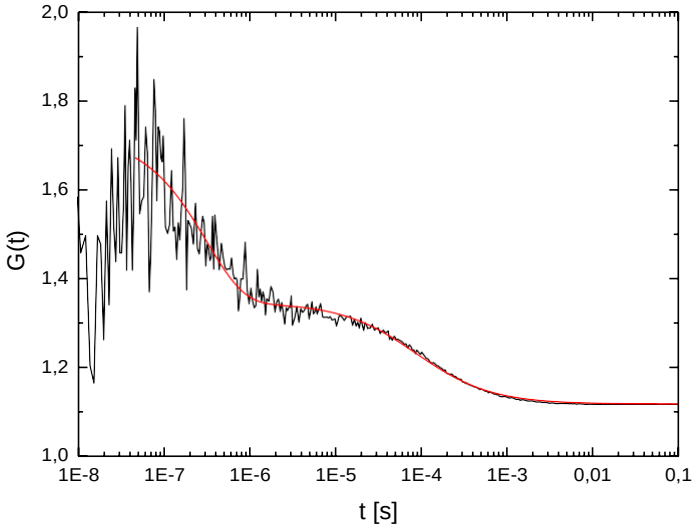

Figure S61: Normalized correlation function of **2**. Excitation was performed at λ = 488 nm with a laser intensity of 270 kW cm^{-2} in a 20 mM citrate-buffer at pH 6.0. Fluorescence was detected at λ_{det} = 540-600 nm. A pK_a of 6.2 is calculated as a mean value of three measurements.

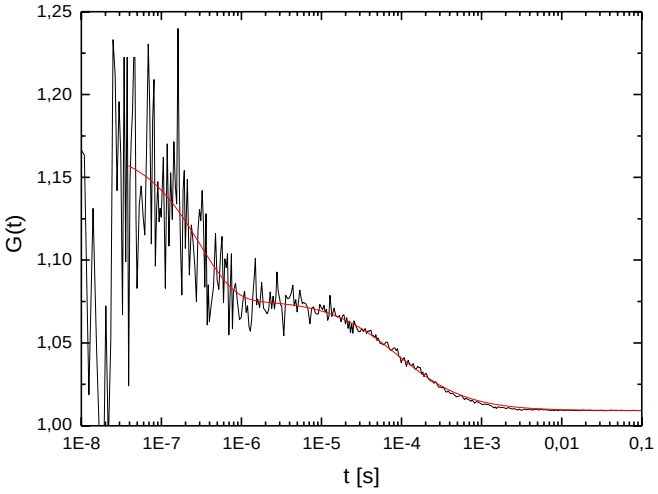

Figure S62: Normalized correlation function of **4**. Excitation was performed at λ = 488 nm with a laser intensity of 270 kW cm^{-2} in a 20 mM citrate-buffer at pH 6.5. Fluorescence was detected at λ_{det} = 540-600 nm. A pK_a of 6.6 is calculated as a mean value of three measurements.

Photostability

Photostability was evaluated by fluorescence correlation spectroscopy according the procedure reported by Hinkeldey *et al.*[2,10] Compared to the bleaching rates found for other pyrene based photoacids (ϕ_{bl} ~ 300 ppm), that of **2** and **4** (table 1 and 3 of the main manuscript, figure S63) are fivefold higher. As we have shown in that publication there is a distinct correlation of photostability and electron-withdrawing strength of the substituents at the aromatic core.[2] An explanation for the enhanced photobleaching rates might be that the carboxlic acid / ester are less electron-withdrawing than the sulfonamide/sulfonic ester groups of the derivatives we examined in our previous work. In contrast, the phosphorylated compounds **1** and **3** exhibit a much higher photostability (table S5, figure S63) in the range of that found for the above mentioned sulfonamide derivatives.[2] A possible reason is that the phosphate group has a stronger electron-withdrawing character (σ_p = 0.00)[11] than the deprotonated hydroxyl group (σ_p = -0.81).[11] Nevertheless, all examined compounds (**1**-**4**) show sufficient photostability for *in vivo* fluorescence measurements.

Table S5: Evaluation of bleaching rates.

	σ_{bl} / hν / cm²/kWs	σ_{bl} / cm²	ε / L/mol/cm	σ_{abs} / m²	σ_{abs} / A²	ϕ_{bl} / 1	ϕ_{bl} / ppm
R110	12.10	$4.93*10^{-25}$	77000	$2.94*10^{-20}$	2.94	$1.67*10^{-05}$	16
2, pH 11[a]	239	$9.74*10^{-24}$	24900	$9.52*10^{-21}$	0.95	$1.02*10^{-03}$	1022
4, pH 11[a]	221	$9.00*10^{-24}$	16200	$6.19*10^{-21}$	0.62	$1.45*10^{-03}$	1453
1, pH 11[b]	41	$2.01*10^{-24}$	19300	$7.38*10^{-21}$	0.74	$2.73*10^{-04}$	272
1, pH 11[a]	32	$1.57*10^{-24}$	19300	$7.38*10^{-21}$	0.74	$2.13*10^{-04}$	212
3, pH 7[b]	36	$1.77*10^{-24}$	14500	$5.54*10^{-21}$	0.55	$3.72*10^{-04}$	318
3, pH 3[b]	86	$4.22*10^{-24}$	14500	$5.54*10^{-21}$	0.55	$7.61*10^{-04}$	761
3, pH 3 [a]	85	$4.17*10^{-24}$	14500	$5.54*10^{-21}$	0.55	$7.53*10^{-04}$	752

λ_{exc} = 488 nm; hν = $4.07*10^{-22}$ kJ

λ_{exc} = 405 nm; hν = $4.91*10^{-22}$ kJ

[a] C-Apochromat, 63x/1.2 W Korr

[b] C-Apochromat, 40x/1.2 W Korr

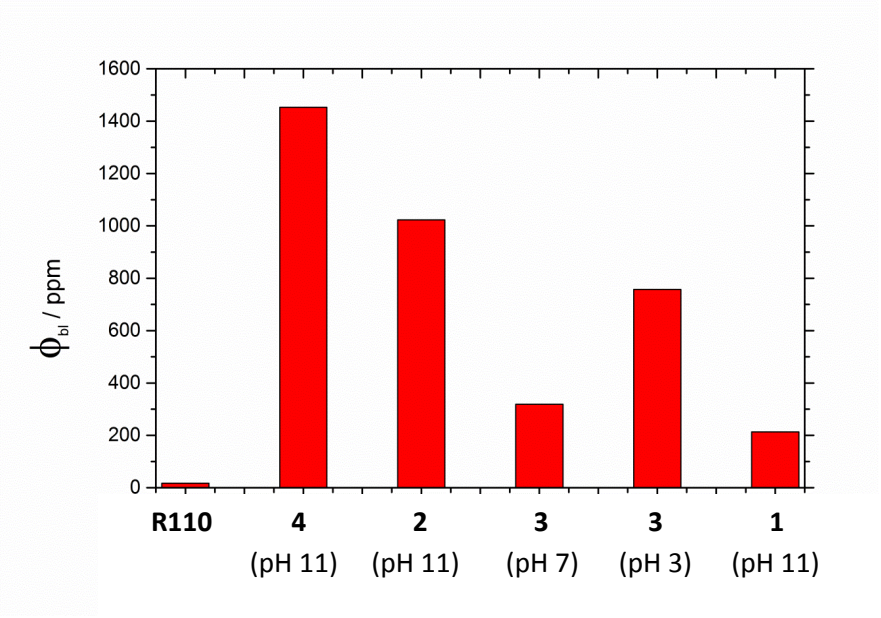

Figure S63: Photobleaching rates.

Enzyme Kinetics

Fluorescence intensity at the reaction end points were defined as 100 % conversion and used to calculate the amount of converted product at a time. Fluorescence intensity at the maximal emission wavelength of the substrate at the starting point was assumed to be adequate to the substrate start concentration. The remaining emission at the observed wavelength after complete reaction was nearly 0, and considered to be complete substrate conversion. Only values under 10% substrate consumption were taken into account for the determination of the initial velocity by linear regression of the conversion over time. Red indicated points were excluded from linear regression. If not otherwise stated, enzyme kinetics were determined by this method.

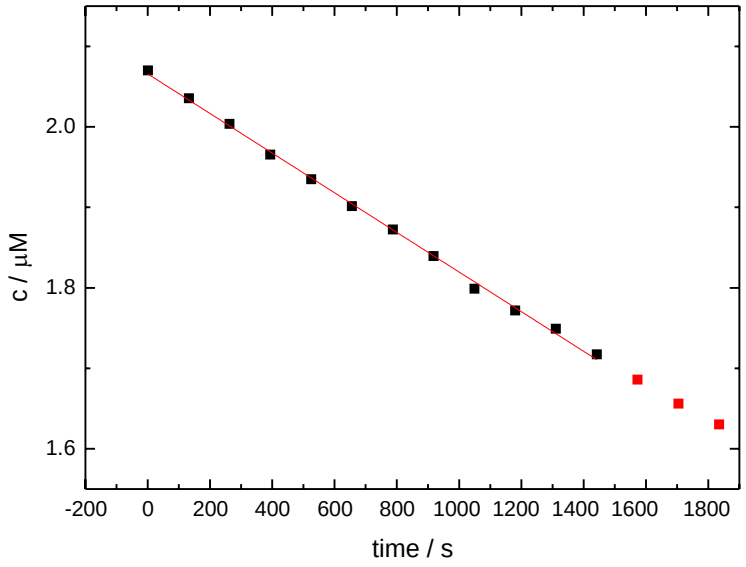

Figure S64: Concentration of substrate **1** over time.

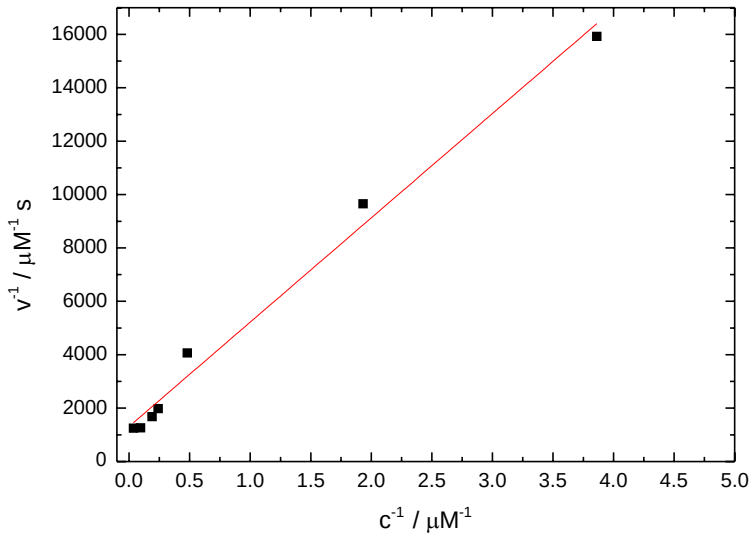

Figure S65: Reciprocal plot (Lineweaver-Burk) of initial velocity v of the hydrolysis of **1** versus different concentrations of substrate **1**.

Substrate **1** + AlP (turn-on detection)

For turn-on detection the evolution of the product (**2**) emission band was monitored. When the fluorescence emission was the same for an hour, the reaction was assumed to be complete (100% conversion), and the signal was used to calculate the concentration of the formed product over time.

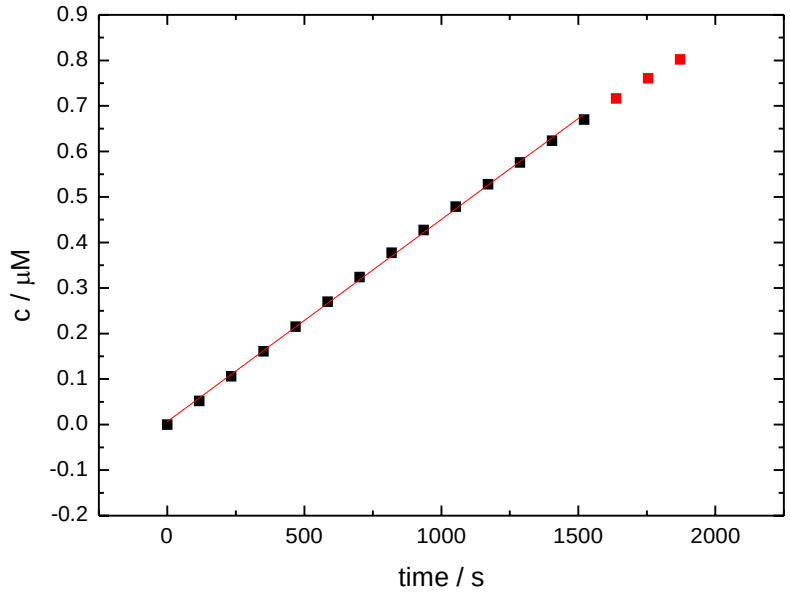

Figure S66: Formation of **2** by hydrolysis of substrate **1** over time.

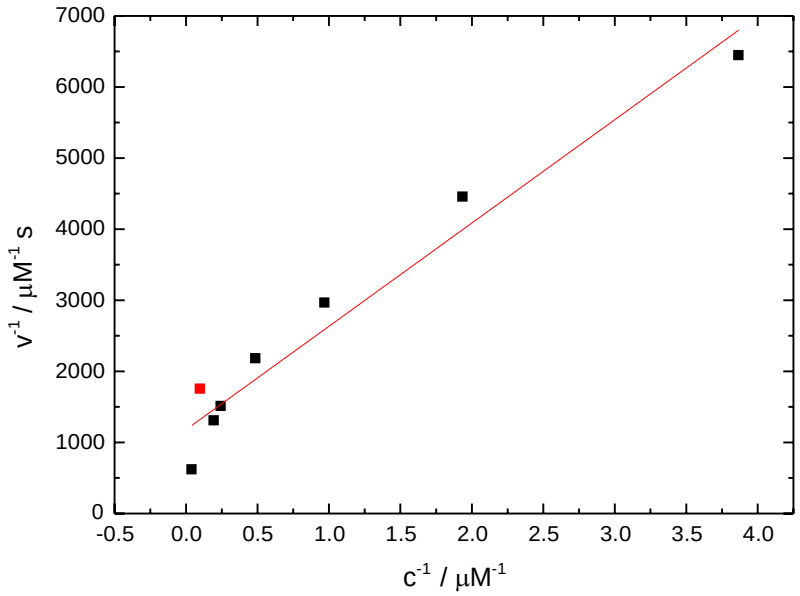

Figure S67: Reciprocal plot (Lineweaver-Burk) of initial velocity v of the hydrolysis of **1** versus different concentrations of substrate **1**, turn-on detection.

Compound **3** + AlP

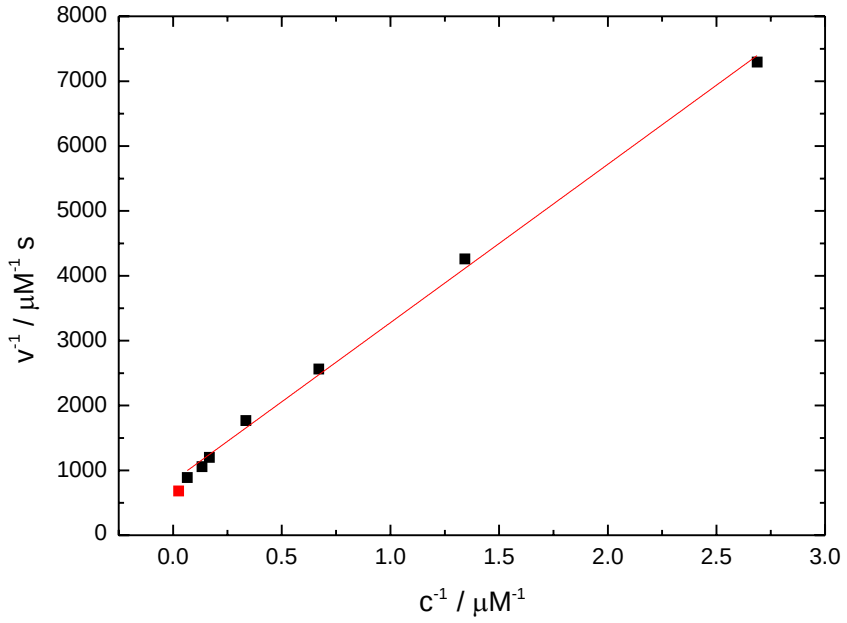

Figure S68: Reciprocal plot (Lineweaver-Burk) of initial velocity v of the hydrolysis of **3** versus different concentrations of substrate **3**.

4-Methylumbelliferyl phosphate + AlP (turn on detection)

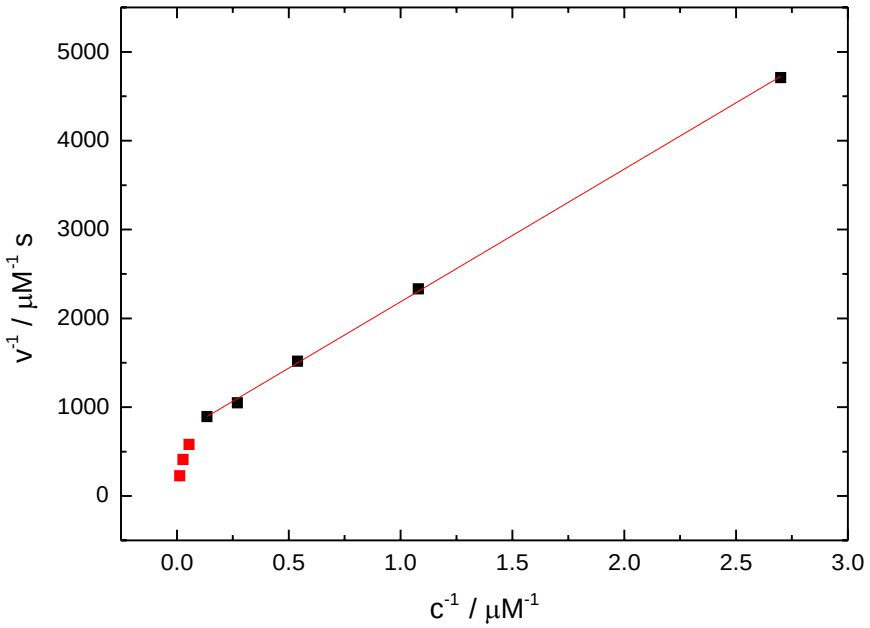

Figure S69: Reciprocal plot (Lineweaver-Burk) of initial velocity v of the hydrolysis of 4-MUP versus different concentrations of substrate 4-MUP.

Compound **1** + AP

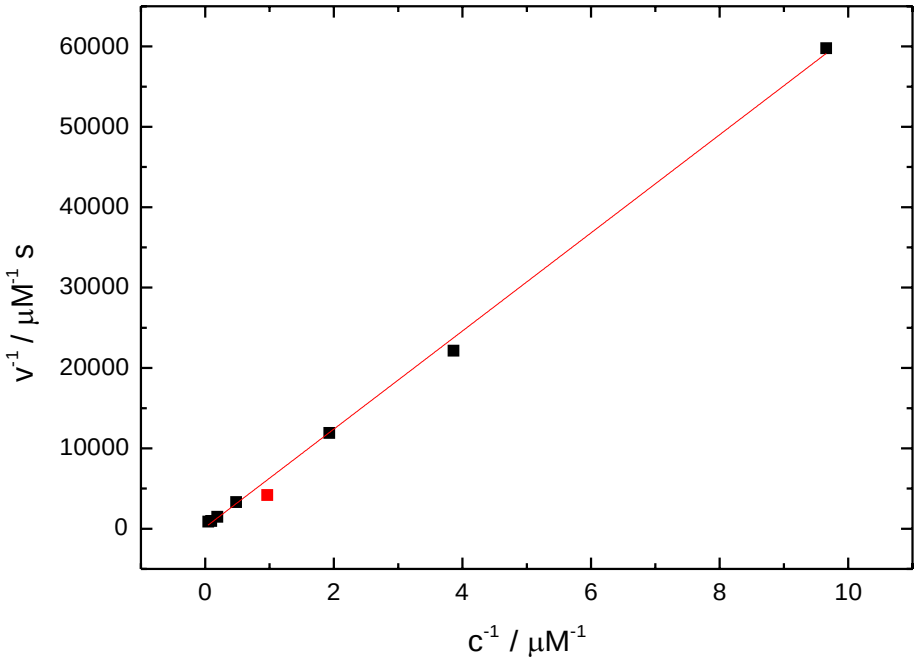

Figure S70: Reciprocal plot (Lineweaver-Burk) of initial velocity v of the hydrolysis of **1** versus different concentrations of substrate **1**.

Compound **3** + AP

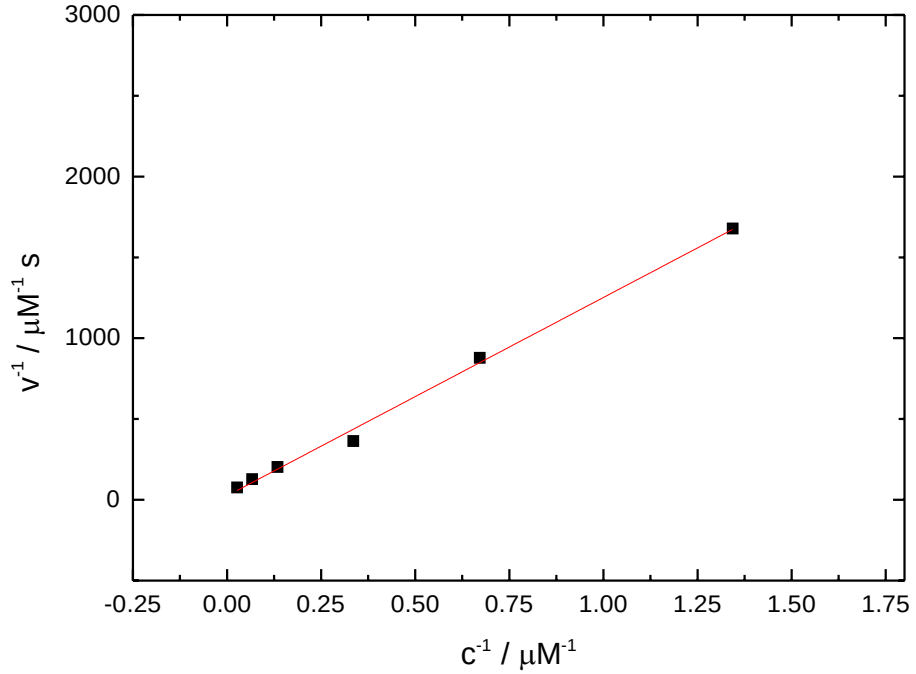

Figure S71: Reciprocal plot (Lineweaver-Burk) of initial velocity v of the hydrolysis of **3** versus different concentrations of substrate **3**.

Compound **2** + PLE

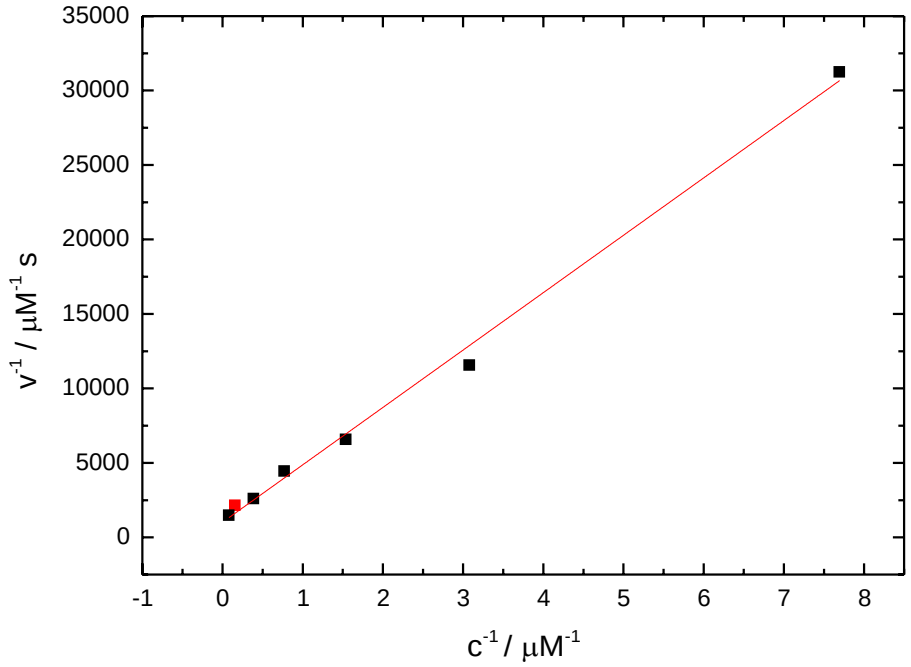

Figure S72: Reciprocal plot (Lineweaver-Burk) of initial velocity v of the hydrolysis of **2** versus different concentrations of substrate **2**.

4-Methylumbelliferyl butyrate + PLE (turn-on detection)

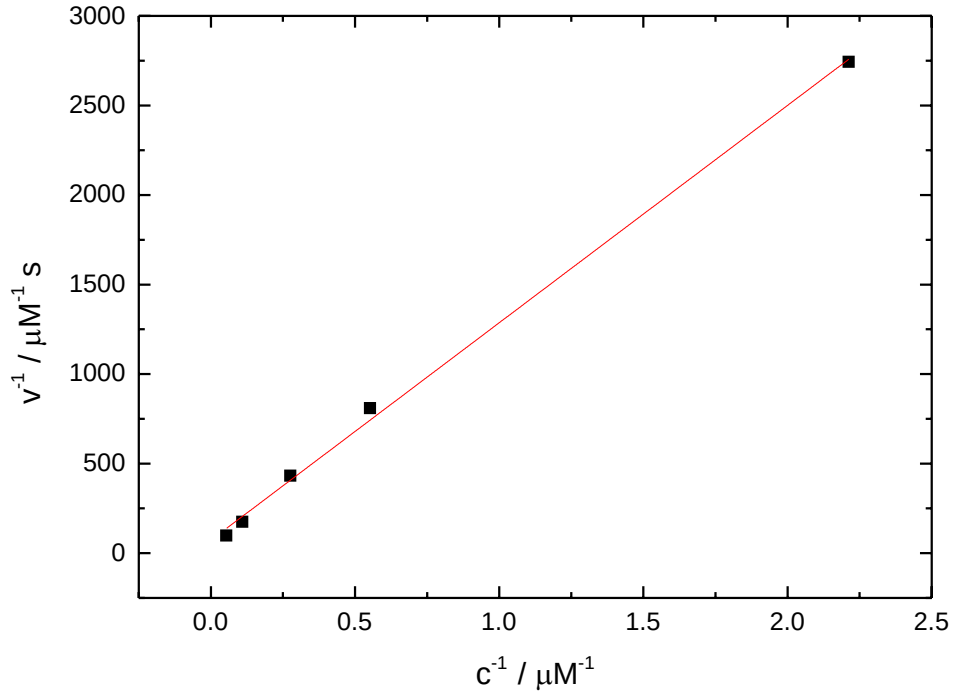

Figure-S73: Reciprocal plot (Lineweaver-Burk) of initial velocity v of the hydrolysis of 4-MUBu versus different concentrations of substrate 4-MUBu.

Table S6: Kinetic parameters for reactions of the dye system with different enzymes.

Compound	**1**	**3**	**4-MUP**	**1**	**3**	**2**	**4-MUBu**
Enzyme	**Alkaline Phosphatase**			**Acid Phosphatase**		**Porcine Liver Esterase**	
K_m [µM]	3.0	2.9	2.2	40.8	48.6	3.7	16.9
v_{max} [µM/s]	7.7×10^{-4}	1.2×10^{-3}	1.5×10^{-3}	6.7×10^{-2}	4.0×10^{-2}	9.5×10^{-4}	1.4×10^{-2}
k_{cat} [1/s]	2.1×10^{2}	3.3×10^{2}	39.2	2.4×10^{-2}	1.9	2.5×10^{-2}	9.7×10^{-2}
k_{cat}/K_m [1/M/s]	6.9×10^{8}	1.1×10^{8}	1.8×10^{7}	6.0×10^{2}	3.9×10^{4}	7.1×10^{3}	5.7×10^{3}

Live Cell application

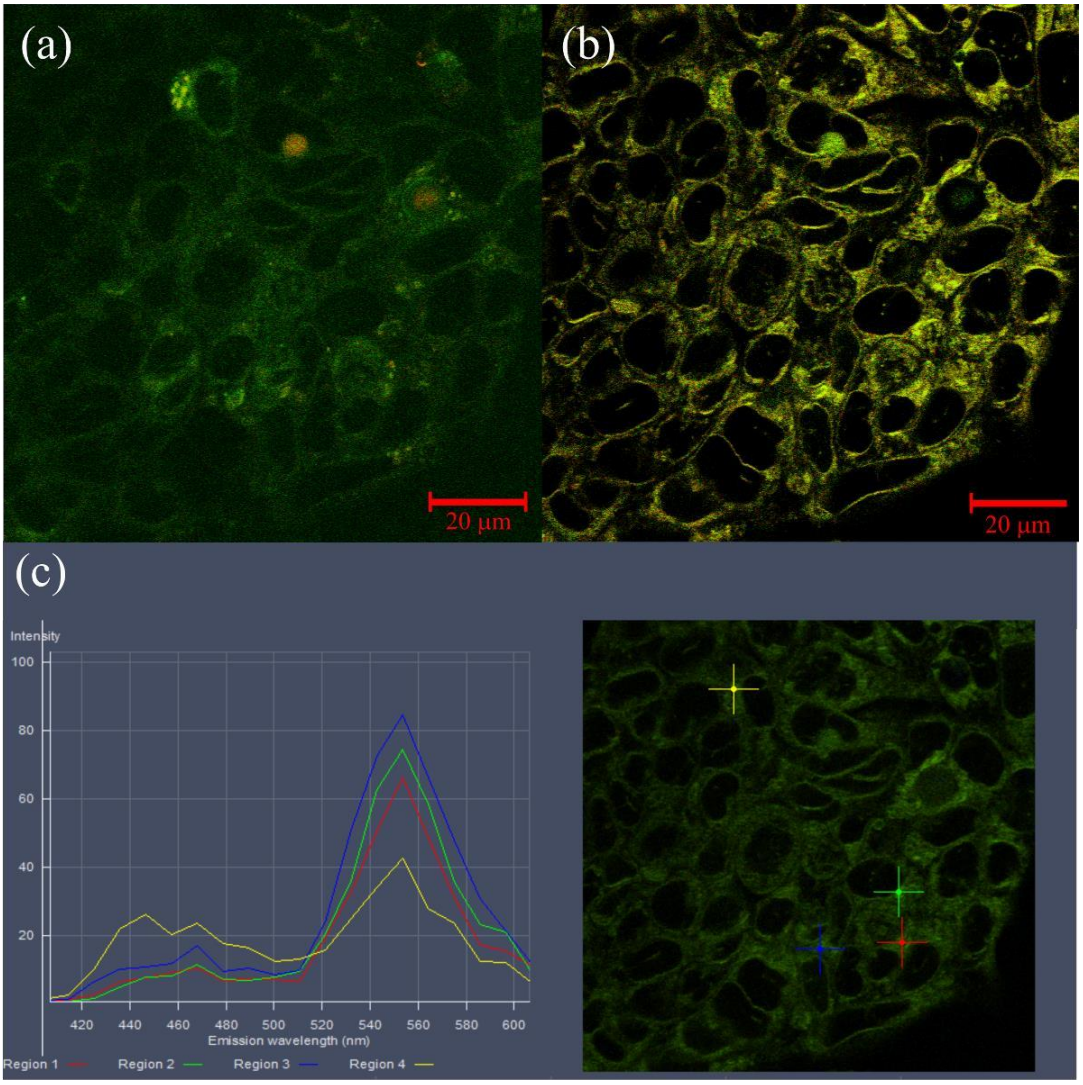

Figure S74: (a) T84 cells 3 hours after incubation, overlay, green channel: λ_{det} = 398-452 nm (**3**), red channel: λ_{det} = 463-484 nm (**1**); (b) Same conditions, green channel: λ_{det} = 516-548 nm (**4**), red channel: λ_{det} = 559-612 nm (**2**); (c) Same conditions, spectral analysis of different regions.

We were able to detect all possible products stemming from probe **1** in T84 cells by use of four different output filters. A faint fluorescence intensity in the spectral range from λ_{det} = 463-484 nm (red channel, Figure S74(a)) indicates incorporated, but non-converted **1** in some areas of the cell cluster. While strong hydrolysis of **1** to **3** seems to be dependent of the region in the cluster (green channel, Figure S74(a)), dephosphorylation activity appears to be more evenly distributed (red channel, Figure S74(b)). However it seems that compound **3** is only formed in some individual cases. Fluorescence of **4**, similarly as that of **2**, appears without preferential areas of accumulation. Although **4** can be formed *in-vitro* by two different pathways (main manuscript Figure 1(b)), the ubiquitous appearance of **4** in the cell plasma indicates that the major pathway for its formation is via the evenly spread **2** and hence suggests, that the mentioned metabolic sequence **1→2→4** is also predominant in these T84 epithelial cells. The reconstructed spectra in Figure S74(c) from dispersed detection channels

unambiguously proved also the detection of **3** in selected areas. We conclude that the presented pyrenol based platform with orthogonal reactivities is appropriate for monitoring heterogeneity in cellular metabolic activity.

Incubation of L929 cells with dye **2**

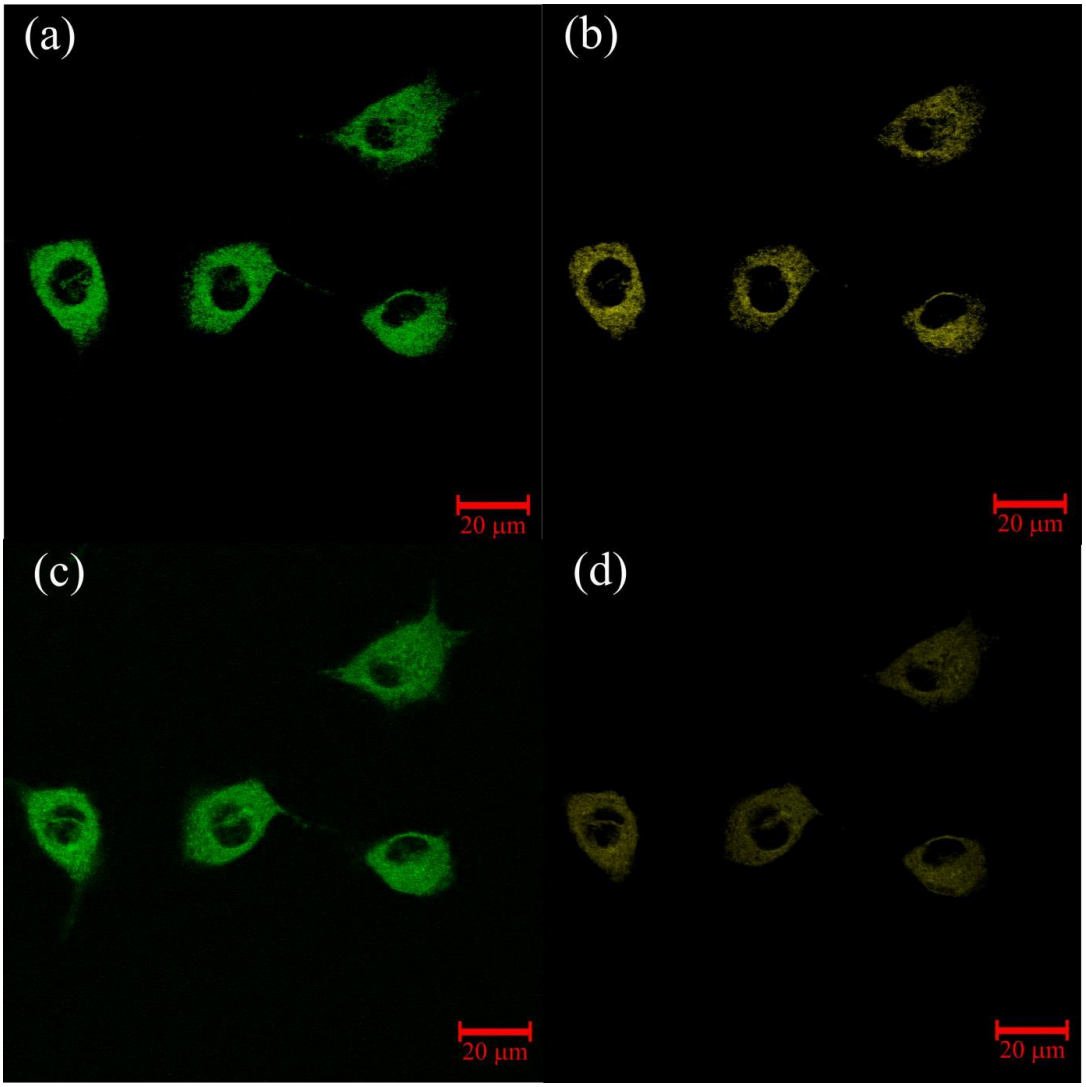

Figure S75: false colored L929 cells (a, b) 1 hour after incubation with **2**, green channel (a): λ_{det} = 516-548 nm, yellow channel (b): λ_{det} = 559-612 nm; (c, d) same conditions after 3 hours.

Esterase activity can be monitored by use of substrate **2** dissolved in DMSO to limit the esterase monitoring on a single wavelength shift. After one hour of incubation with the dye, the uptake of the substrate was complete. As the emission ratio of substrate and product was about the same (Figure S75 (a, b)), the ratio shifts towards the emission of the hydrolyzed product (Figure S75 (c, d)).

In contrast, compounds **3** and **4** are not able to permeate into the cells (Figure S76/S77). Here just staining of the medium, outside the cell, is observed.

Incubation of L929 cells with dye **3**

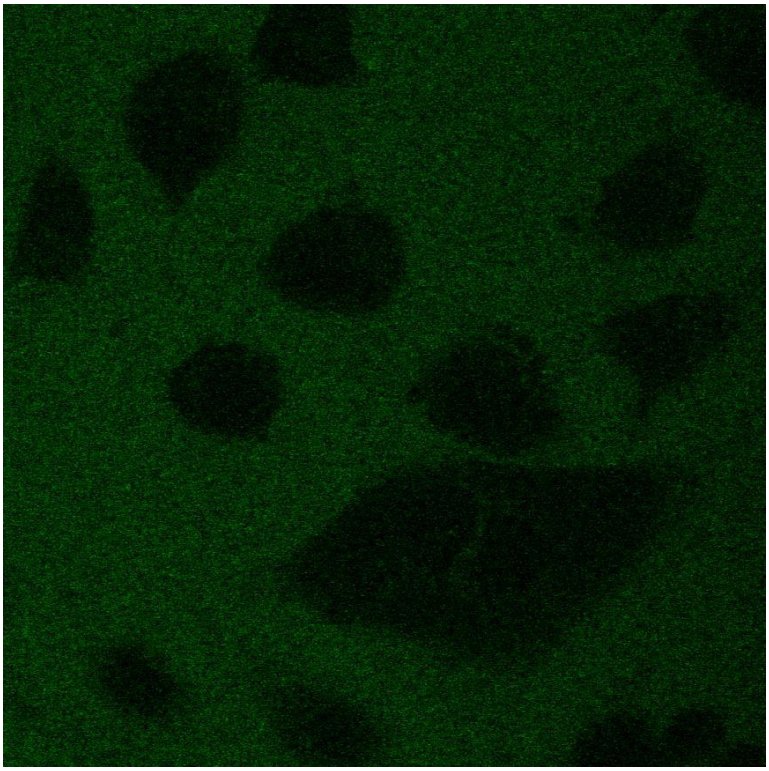

Figure S76: false colored L929 cells 24 hours after incubation with **3**.

Incubation of L929 cells with dye **4**

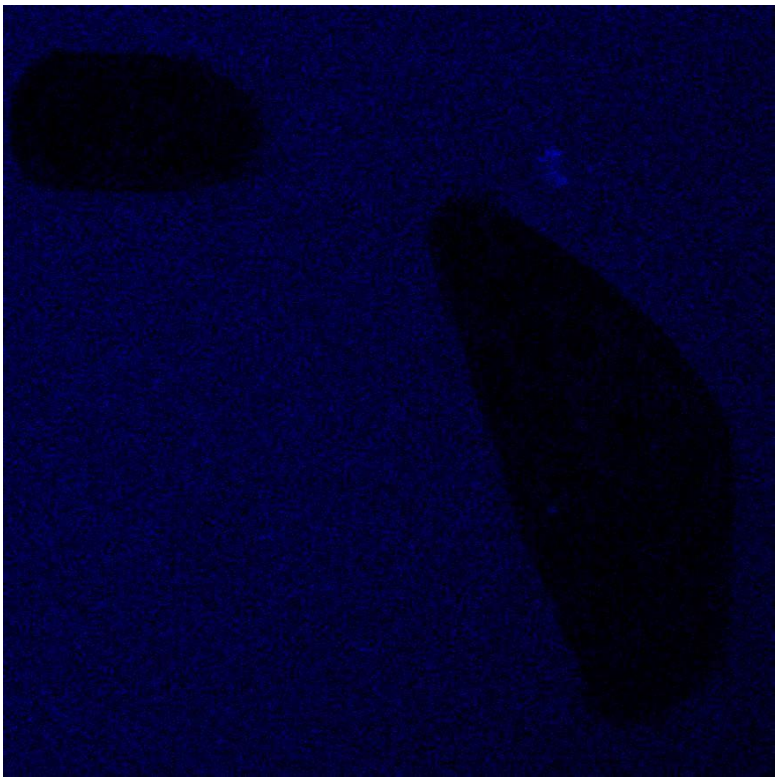

Figure S77: false colored L929 cells 24 hours after incubation with **4**.

Molecular logic

Compound 1

Excitation of the molecular logic systems with compound **1** was performed at λ_{ex} = 395 and λ_{ex} = 460 nm. The obtained spectra were summed up to give the spectra in Figure S78, S81- S92 and Figure 4 (a and b) of the main manuscript.

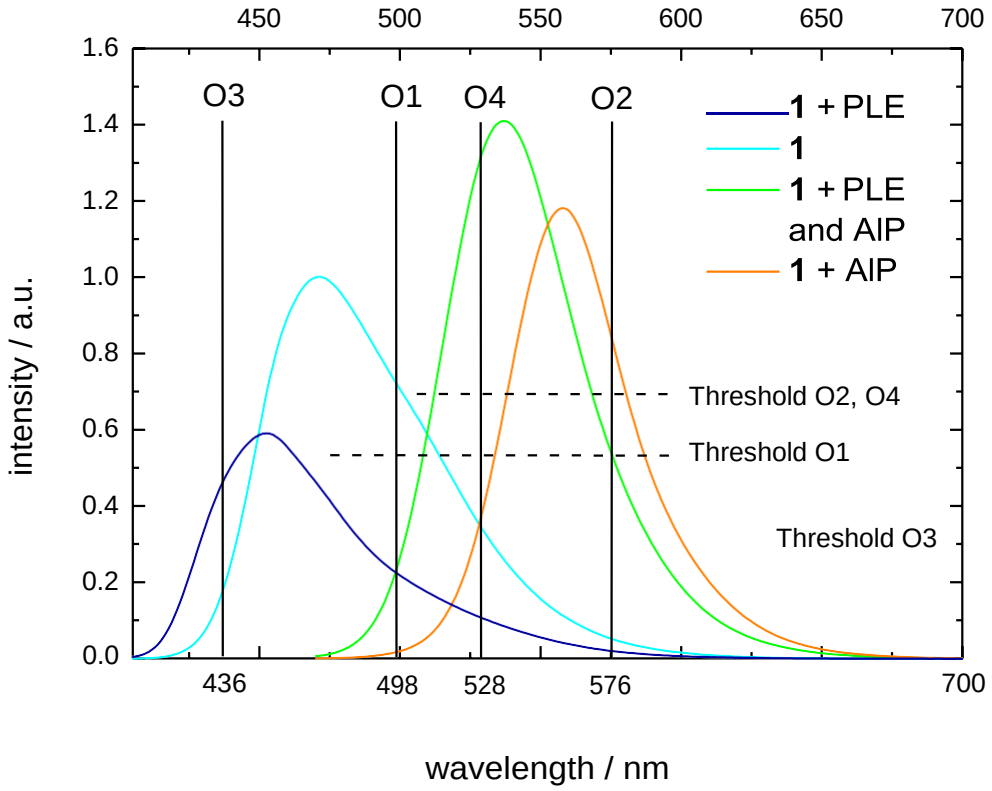

Figure S78: Fluorescence spectra (normalized to substrate fluorescence, λ_{exc} = 395 and simultaneously 460 nm, as described above).

1:2 demultiplexer

Table S7: Truth table for 1:2 demultiplexer.

In (AlP)	Ad (PLE)	O2	O4
0	0	0	0
1	0	1	0
0	1	0	0
1	1	0	1

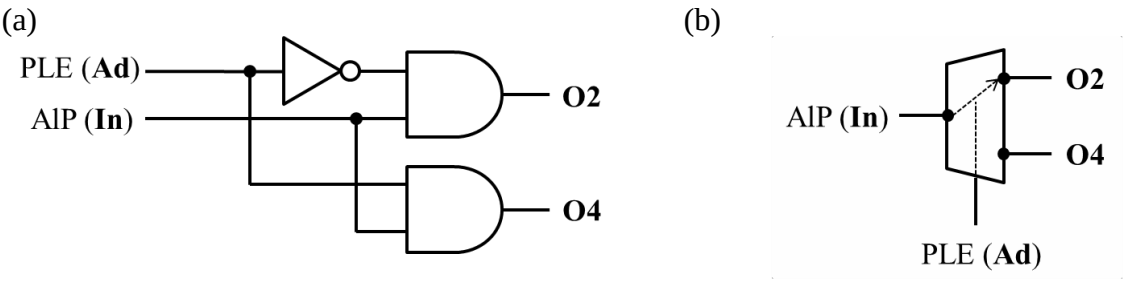

Figure S79: (a) Circuit diagram and (b) schematic switching operation of the described 1:2 demultiplexer.

2:4 decoder

Table S8: Truth table for 2:4 decoder.

In1 (AlP)	In 2 (PLE)	O1 (λ = 498 nm)	O2 (λ = 576 nm)	O3 (λ = 436 nm)	O4 (λ = 528 nm)
0	0	1	0	0	0
1	0	0	1	0	0
0	1	0	0	1	0
1	1	0	0	0	1

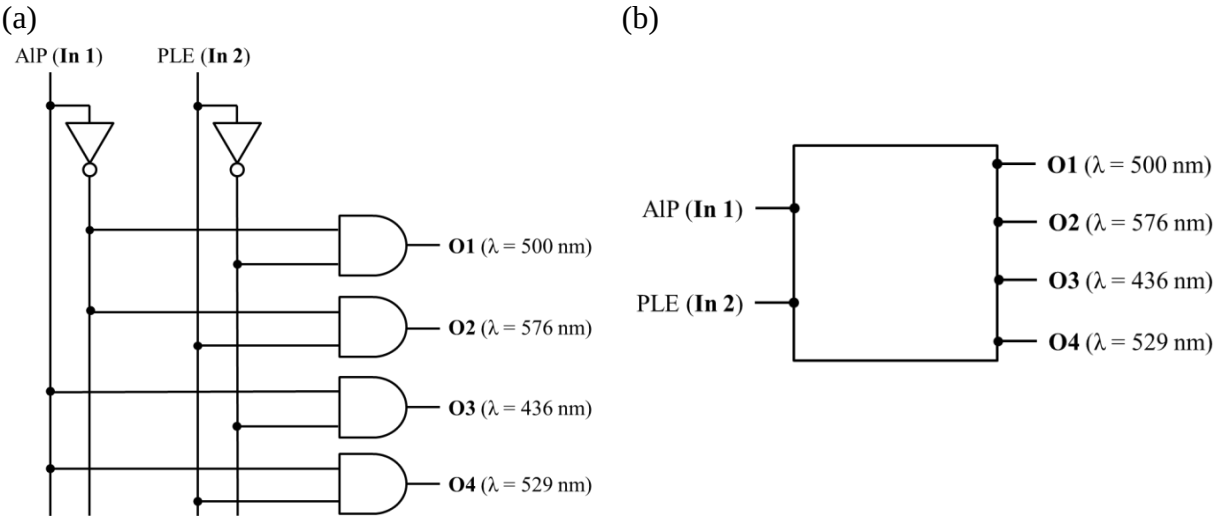

Figure S80: (a) Circuit diagram and (b) schematic switching operation of the described 2:4 decoder.

NOR gate

Table S9: Truth table for NOR-Gate.

In1 (AlP)	In 2 (PLE)	O1 (λ = 498 nm)
0	0	1
1	0	0
0	1	0
1	1	0

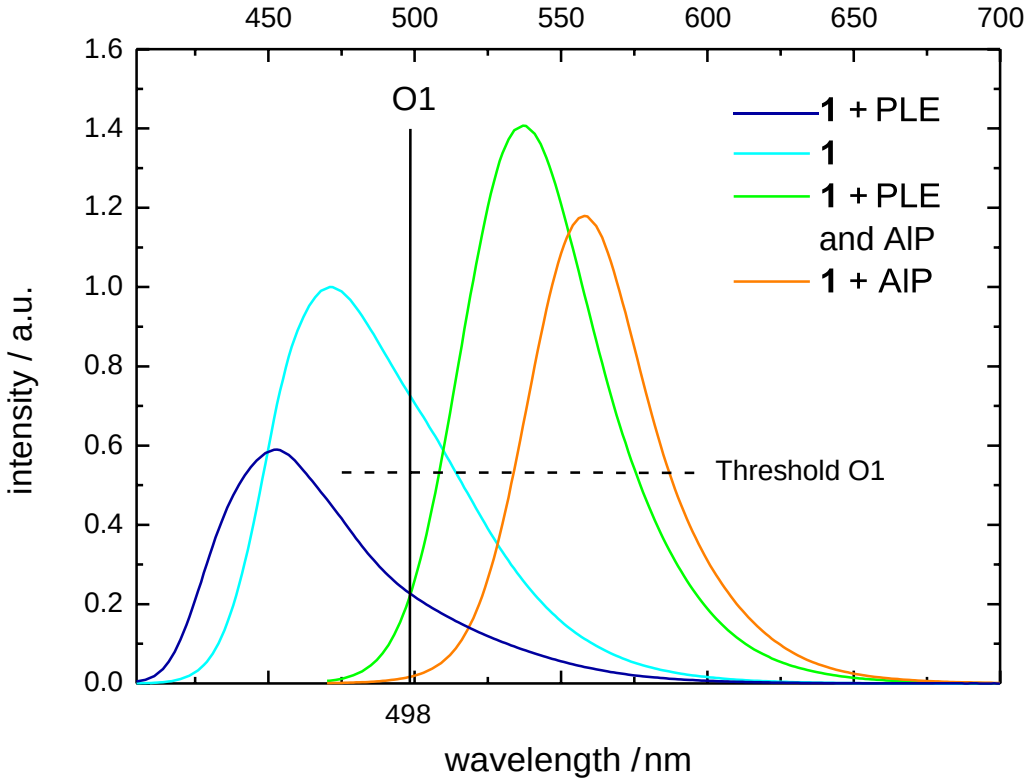

Figure S81: Fluorescence emission of **1** and its hydrolysis derivatives with corresponding output channel and threshold level for NOR gate.

OR gate

Table S10: Truth table for OR-Gate as inversion of NOR gate (negative logic).

In1 (AlP)	In 2 (PLE)	O1 (λ = 498 nm, negative logic)
0	0	0
1	0	1
0	1	1
1	1	1

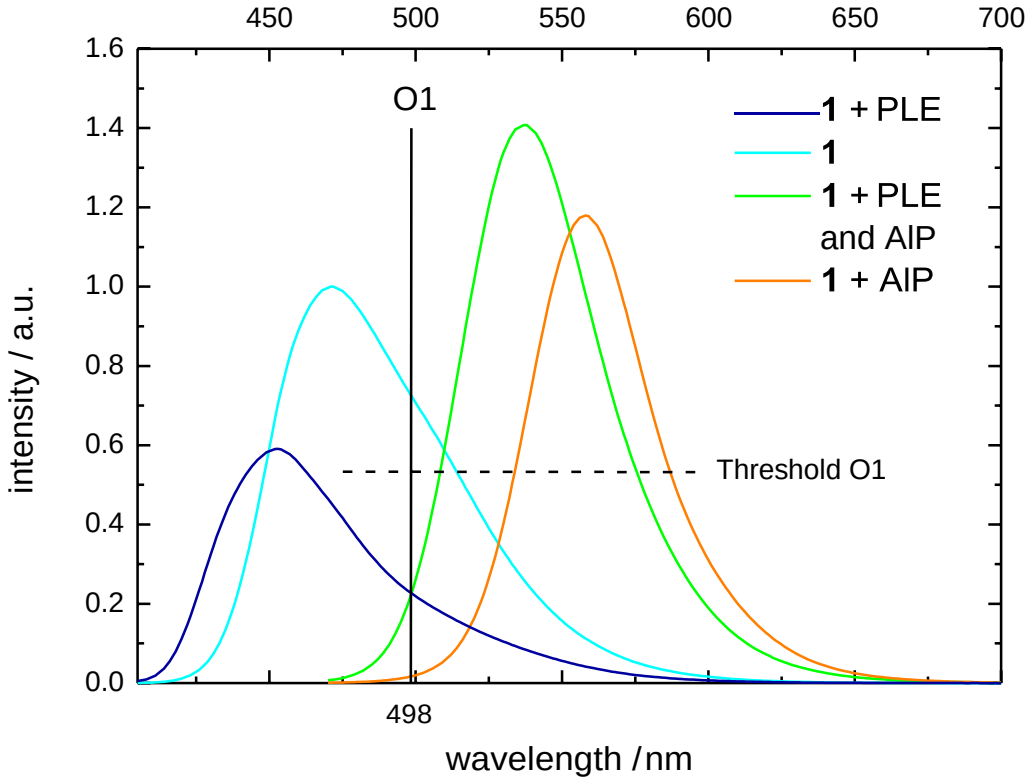

Figure S82: Fluorescence emission of **1** and its hydrolysis derivatives with corresponding output channel and threshold level for OR gate.

INHIB 1 gate

Table S11: Truth table for INHIB 1 gate.

In1 (AlP)	In 2 (PLE)	O2 (λ = 576 nm)
0	0	0
1	0	1
0	1	0
1	1	0

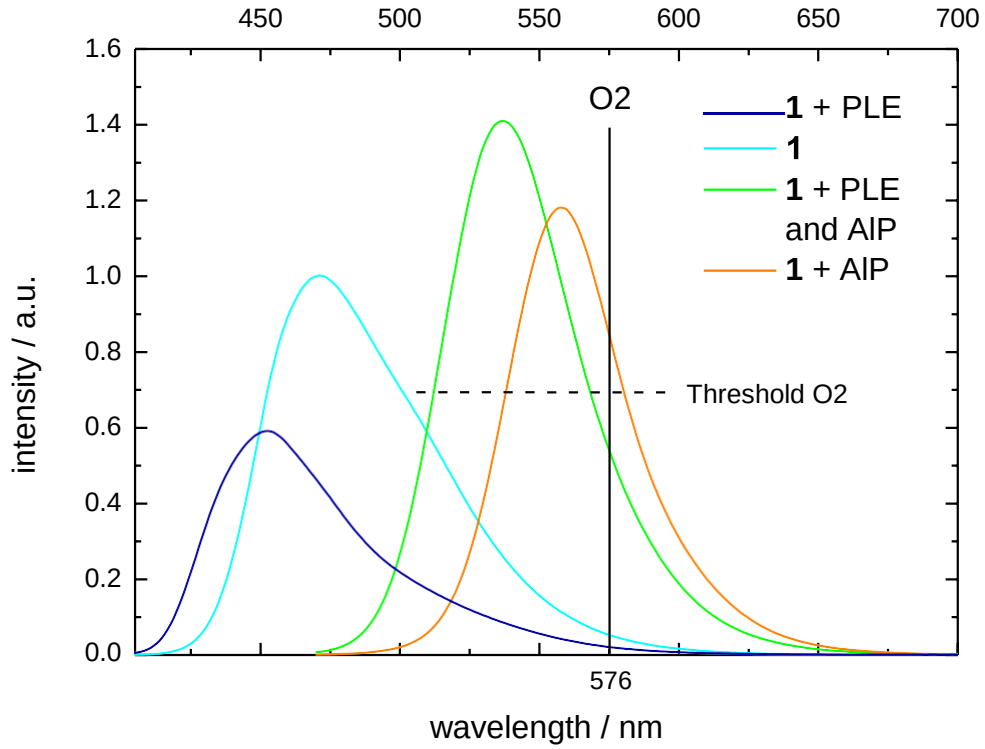

Figure S83: Fluorescence emission of **1** and its hydrolysis derivatives with corresponding output channel and threshold level for INHIB 1 gate.

INHIB 2 gate

Table S12: Truth table for INHIB 2 gate.

In1 (AlP)	In 2 (PLE)	O3 (λ = 436 nm)
0	0	0
1	0	0
0	1	1
1	1	0

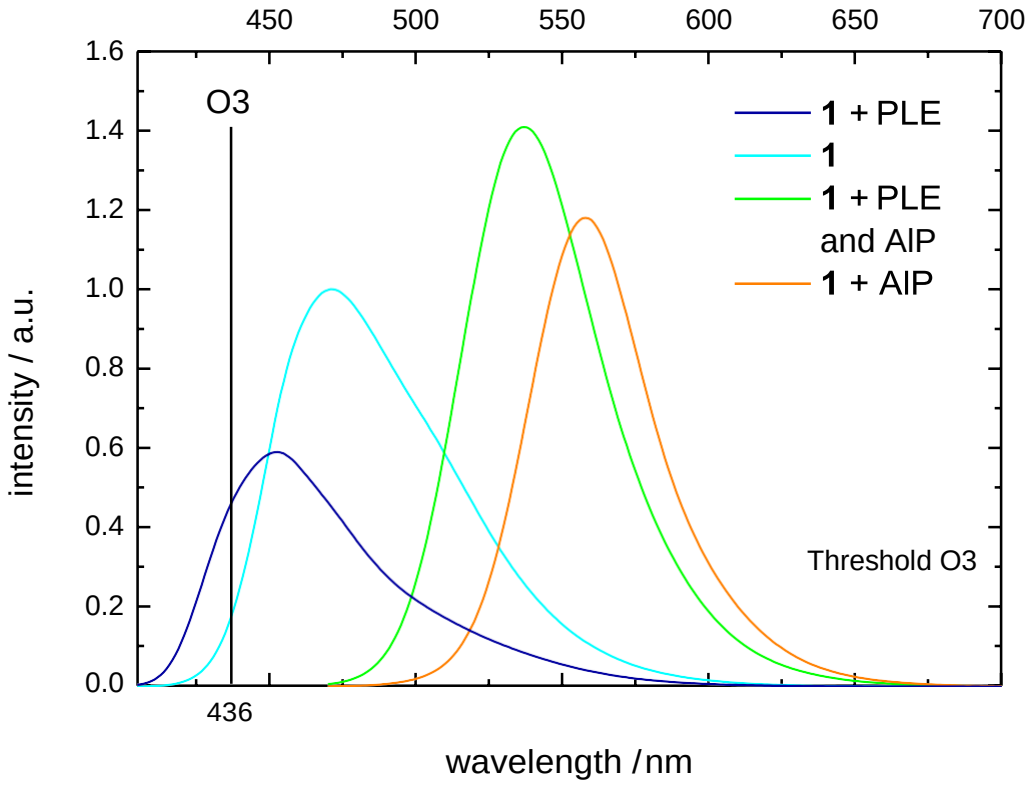

Figure S84: Fluorescence emission of **1** and its hydrolysis derivatives with corresponding output channel and threshold level for INHIB 2 gate.

AND gate

Table S13: Truth table for AND gate.

In1 (AlP)	In 2 (PLE)	O4 (λ = 528 nm)
0	0	0
1	0	0
0	1	0
1	1	1

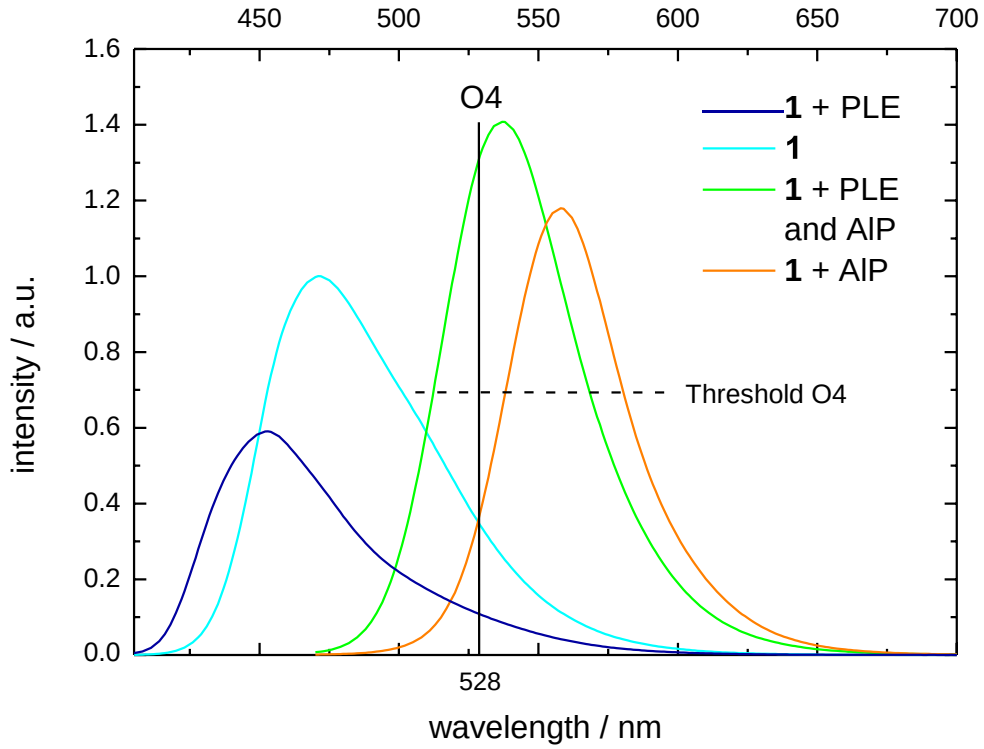

Figure S85: Fluorescence emission of **1** and its hydrolysis derivatives with corresponding output channel and threshold level for AND gate.

NAND gate

Table S14: Truth table for NAND-Gate as inversion of AND gate (negative logic).

In1 (AlP)	**In 2 (PLE)**	**O4 (λ = 528 nm, negative logic)**
0	0	1
1	0	1
0	1	1
1	1	0

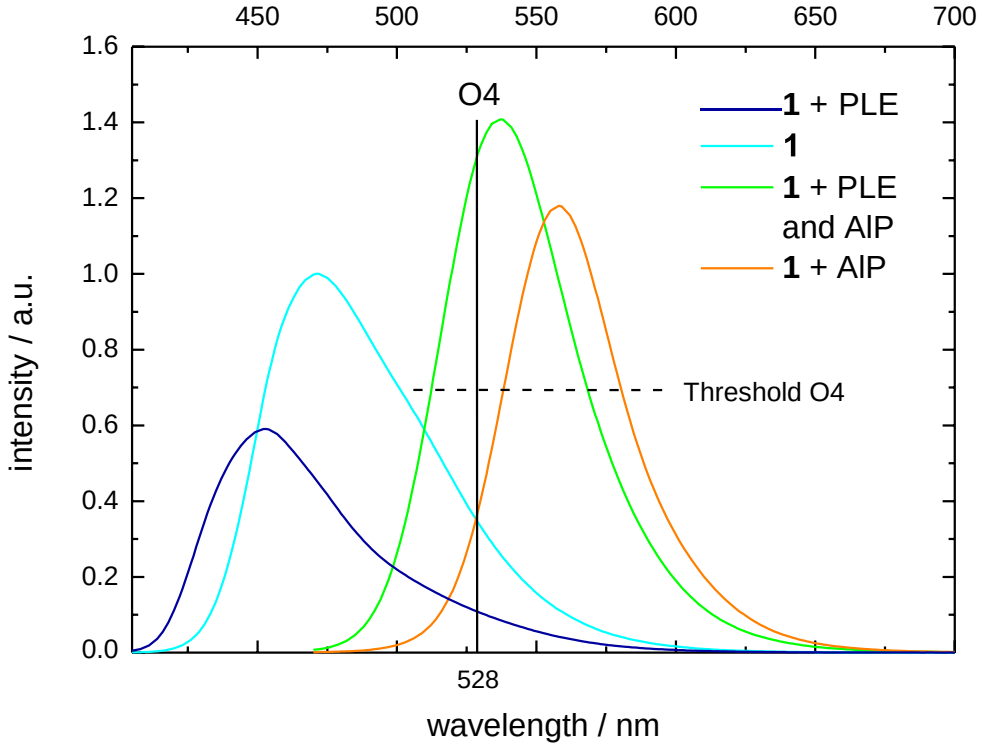

Figure S86: Fluorescence emission of **1** and its hydrolysis derivatives with corresponding output channel and threshold level for NAND gate.

TRANSFER gate

Table S15: Truth table for transfer gate.

In1 (AlP)	In 2 (PLE)	O5 (λ = 553 nm)
0	0	0
1	0	1
0	1	0
1	1	1

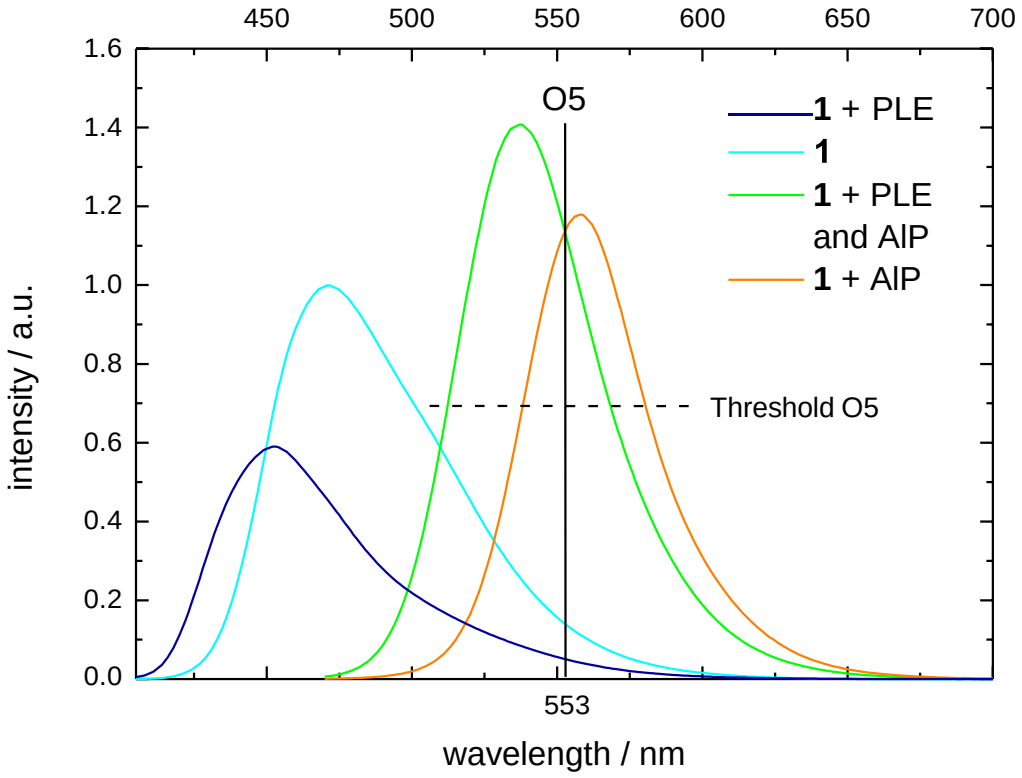

Figure S87: Fluorescence emission of **1** and its hydrolysis derivatives with corresponding output channel and threshold level for transfer gate.

- - - - - - - - - - - - - - - - -

XNOR gate

Table S16: Truth table for **XNOR** gate.

In1 (AlP)	**In 2 (PLE)**	**O6 (λ = 509 nm)**
0	0	1
1	0	0
0	1	0
1	1	1

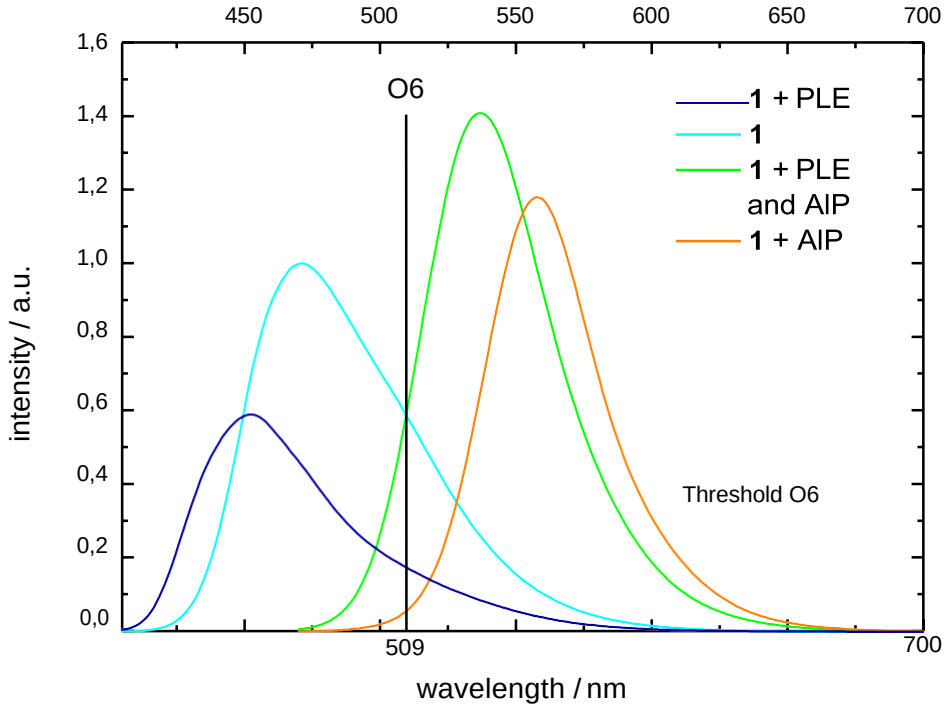

Figure S88: Fluorescence emission of **1** and its hydrolysis derivatives with corresponding output channel and threshold level for XNOR gate.

- - - - - - - - - - - - - - - - -

XOR gate

Table S17: Truth table for **XOR** gate as inversion of XNOR gate.

In1 (AlP)	**In 2 (PLE)**	**O6 (λ = 509 nm, negative logic)**
0	0	0
1	0	1
0	1	1
1	1	0

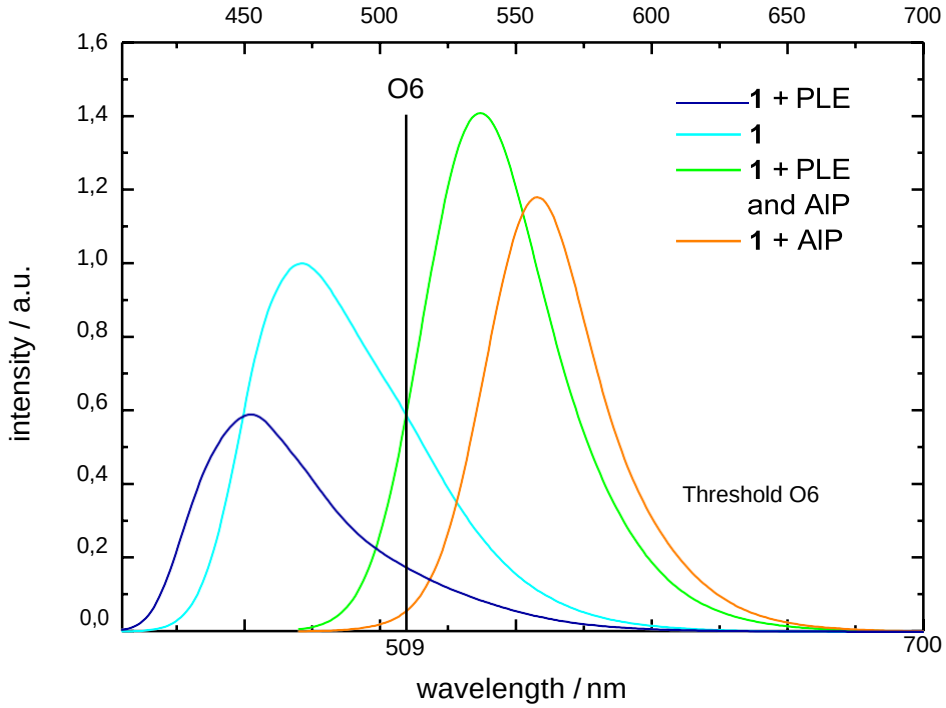

Figure S89: Fluorescence emission of **1** and its hydrolysis derivatives with corresponding output channel and threshold level for XOR gate.

Half-adder

Table S18: Truth table for half-adder.

In1 (AlP)	In2 (PLE)	O4 (λ = 528 nm)	O6 (λ = 509 nm, negative logic)
0	0	0	0
1	0	0	1
0	1	0	1
1	1	1	0

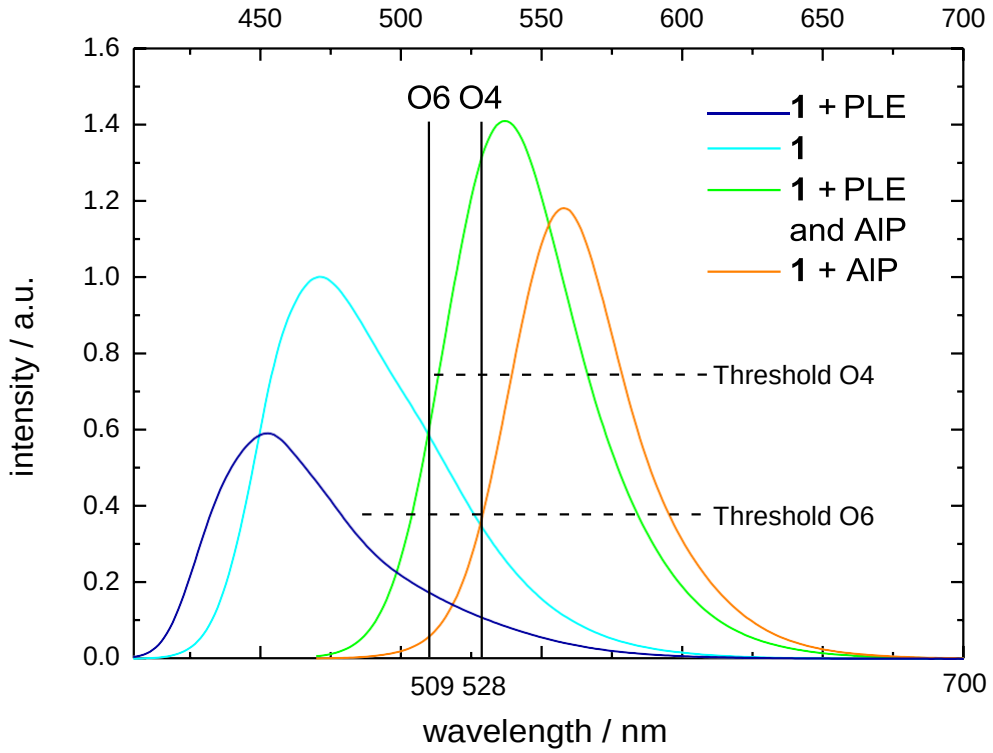

Figure S90: Fluorescence emission of **1** and its hydrolysis derivatives with corresponding output channel and threshold level for half-adder.

Half-subtractor

Table S19: Truth table for half-subtractor.

In1 (AlP)	In2 (PLE)	O3 (λ = 436 nm)	O6 (λ = 509 nm, negative logic)
0	0	0	0
1	0	0	1
0	1	1	1
1	1	0	0

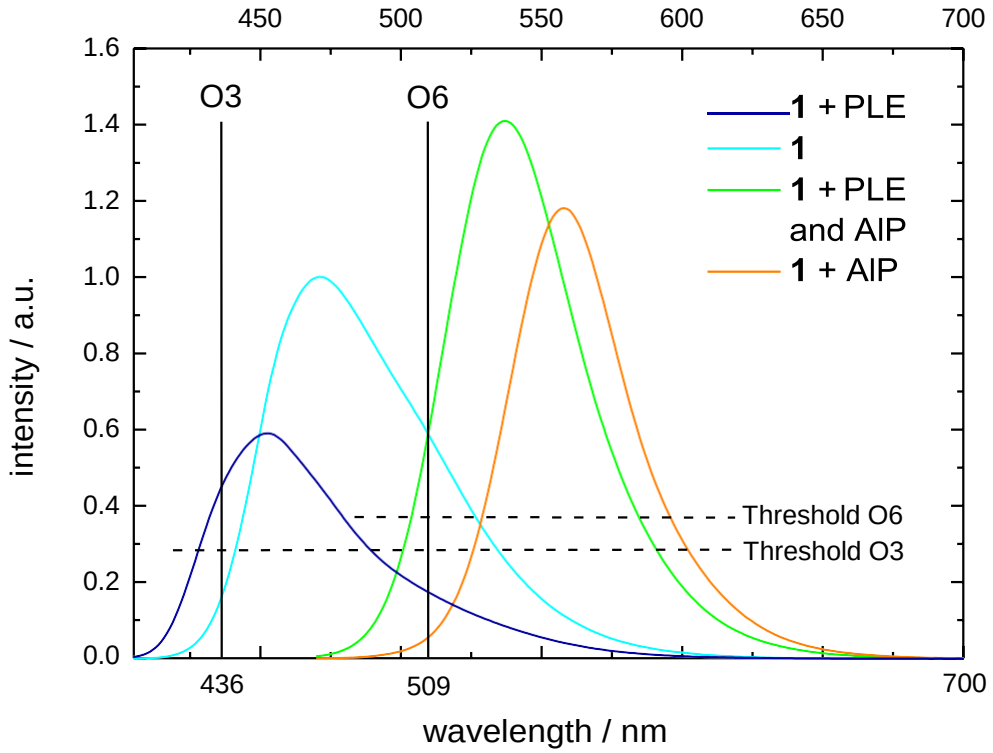

Figure S91: Fluorescence emission of **1** and its hydrolysis derivatives with corresponding output channel and threshold level for half-subtractor.

Feynman gate

Table S20: Truth table for **Feynman** gate.

In1 (AlP)	In 2 (PLE)	O5 (λ = 553 nm)	O6 (λ = 509 nm, negative logic)
0	0	0	0
1	0	1	1
0	1	0	1
1	1	1	0

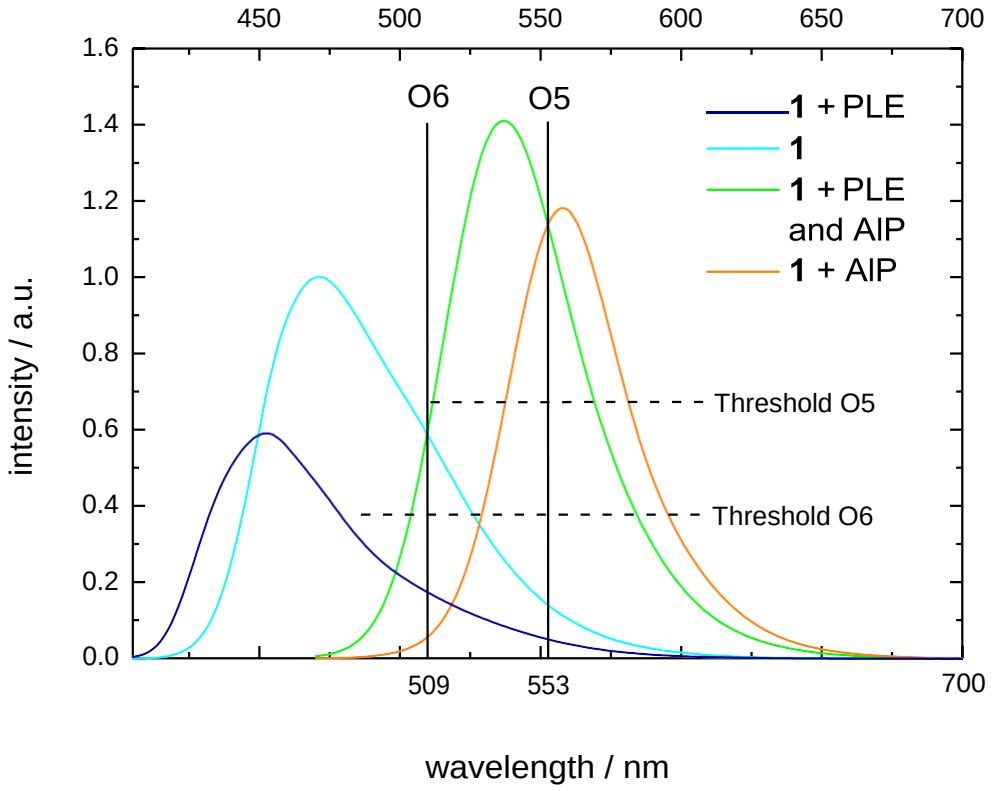

Figure S92: Fluorescence emission of **1** and its hydrolysis derivatives with corresponding output channel and threshold level for Feynman gate.

Molecular Keypad Lock

Table S21: Truth table for Molecular Keypad Lock.

1. Input	2. Input	3. Input	O7 (λ = 536 nm)
A	B	C	1
A	C	B	0
B	A	C	0
B	C	A	0
C	A	B	0
C	B	A	0

A: Acid Phosphatase (AP); B: KOH; C: λ_{ex}

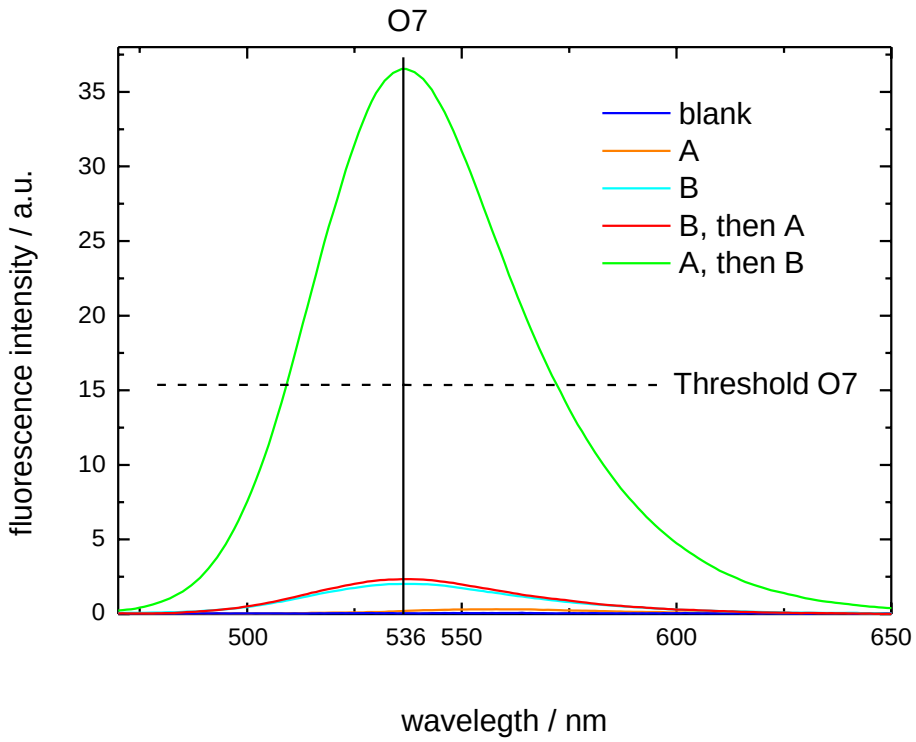

Figure S93: Fluorescence emission of **1** after several addition sequences with corresponding output channel and threshold level for molecular keypad lock.

A molecular keypad lock can be mimicked by use of acid phosphatase (A), KOH (B) and excitation light (C) as inputs (Table S21, Figure S93). In the initial state of the system, the pH is defined by the added acetic acid. At the pH of ~ 5, the activity of the acid phosphatase is high. After 6 minutes, the phosphate group is hydrolyzed by the enzyme and KOH is added to cleave the carboxylic ester to yield compound **4**. After additional 6 minutes, fluorescence at **O7** and thus a positive feedback of the keypad lock is only generated, when the excitation light is introduced into the system. Any interchange in the input sequence thus produces no signal above the corresponding threshold (Figure S93), as the KOH shifts the solution to a highly basic pH, where the enzymatic activity is very low. Furthermore, if compound **4** is not generated by the system, the excitation light at λ_{ex} = 460 nm naturally does not yield fluorescence emission at **O7**. Hence there is just one input sequence (A→B→C) that sets this device to "*on*".

Compound 4

base as Input, Initial state: pH < 0

XOR gate

Table S22: Truth table for XOR gate.

In I (OH^-)	In II (OH^-)	O III (λ = 569 nm)
0	0	0
1	0	1
0	1	1
1	1	0

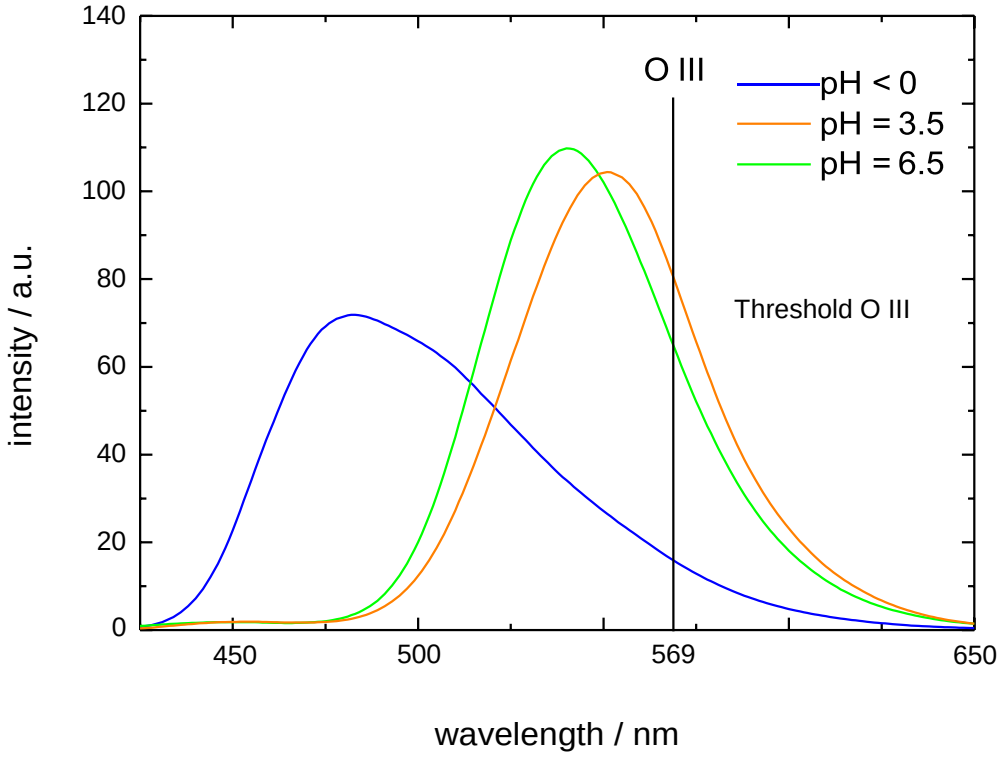

Figure S94: Fluorescence emission of **4** at different pH values with corresponding output channel and threshold level for XOR gate.

AND gate

Table S23: Truth table for AND gate.

In I (OH^-)	In I (OH^-)	O IV (λ = 524 nm)
0	0	0
1	0	0
0	1	0
1	1	1

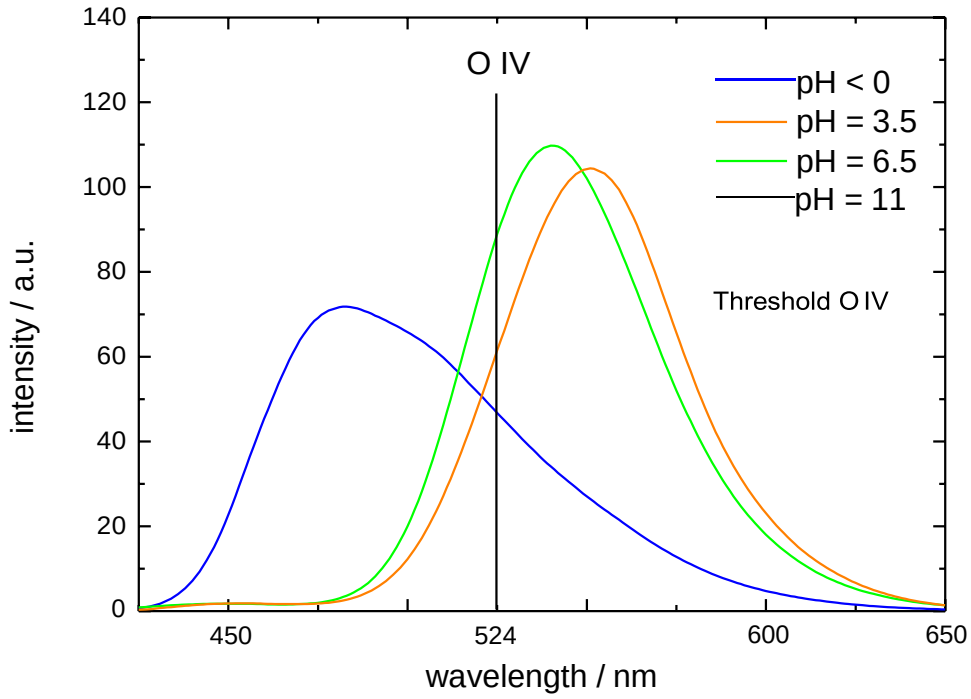

Figure S95: Fluorescence emission of **4** at different pH values with corresponding output channel and threshold level for AND gate.

OR gate

Table S24: Truth table for OR gate.

In I (OH^-)	In II (OH^-)	O II (λ = 548 nm)
0	0	0
1	0	1
0	1	1
1	1	1

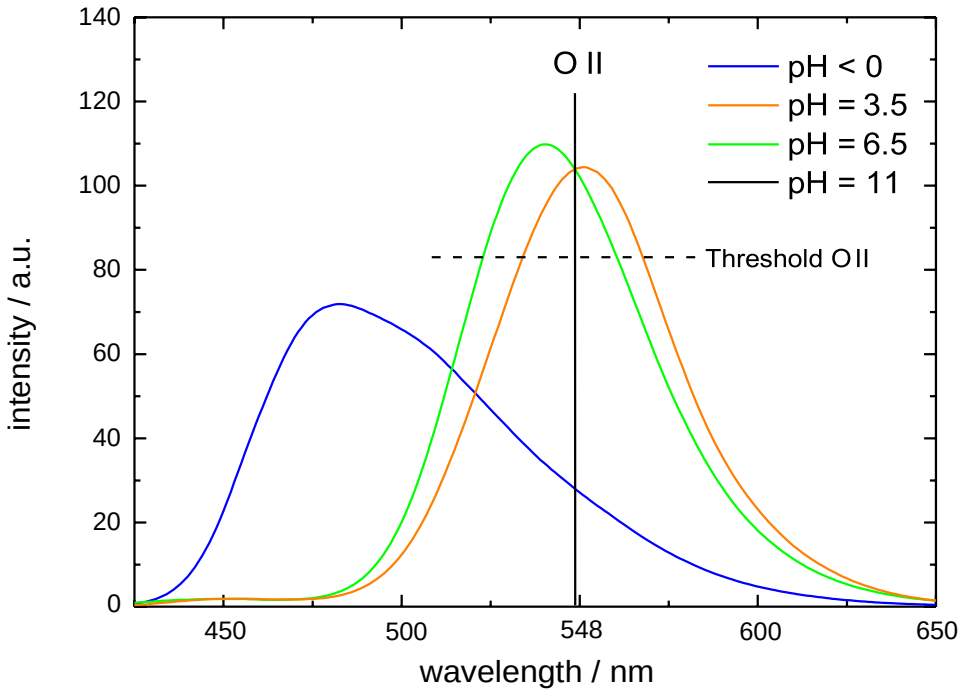

Figure S96: Fluorescence emission of **4** at different pH values with corresponding output channel and threshold level for OR gate.

base as Input, Initial state: pH = 3.5

NAND gate

Table S25: Truth table for NAND gate.

In I (OH^-)	In II (OH^-)	O II (λ = 548 nm)
0	0	1
1	0	1
0	1	1
1	1	0

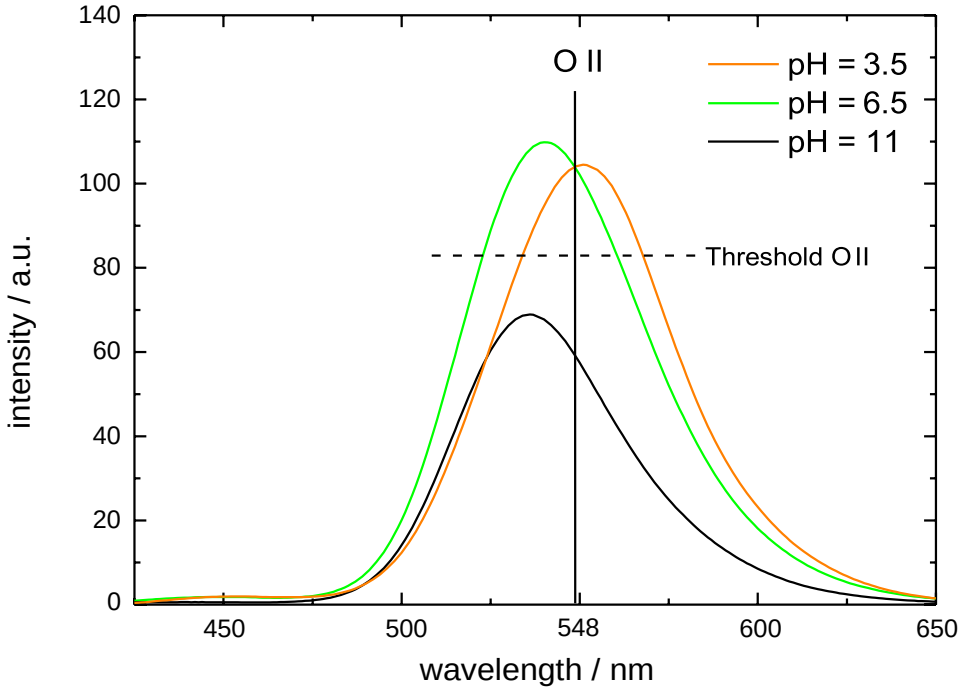

Figure S97: Fluorescence emission of **4** at different pH values with corresponding output channel and threshold level for NAND gate.

XNOR gate

Table S26: Truth table for XNOR gate as inversion of a XOR gate.

In I (OH^-)	**In II (OH^-)**	**O I (λ = 514 nm, negative logic)**
0	0	1
1	0	0
0	1	0
1	1	1

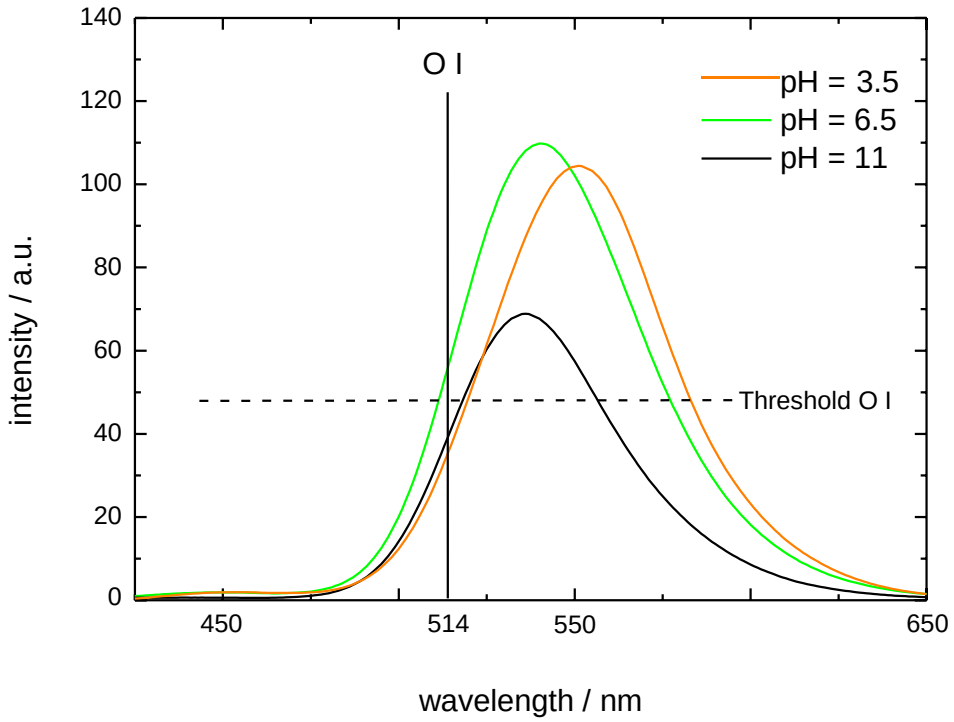

Figure S98: Fluorescence emission of **4** at different pH values with corresponding output channel and threshold level for XNOR gate.

Acid and base as input, Initial state: pH = 3.5

INHIB 1 gate

Table S27: Truth table for INHIB 1 gate.

In I (OH^-)	**In II (H^+)**	**O V (λ = 482 nm)**
0	0	0
1	0	0
0	1	1
1	1	0

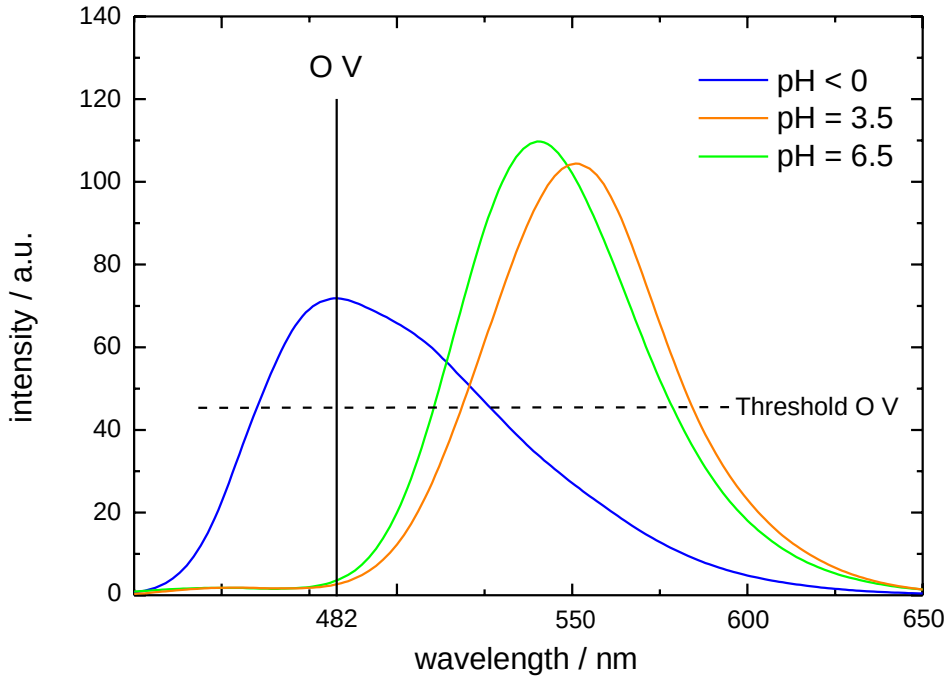

Figure S99: Fluorescence emission of **4** at different pH values with corresponding output channel and threshold level for INHIB 1 gate.

INHIB 2 gate

Table S28: Truth table for INHIB 2 gate.

In I (OH^-)	In II (H^+)	O IV (λ = 524 nm)
0	0	0
1	0	1
0	1	0
1	1	0

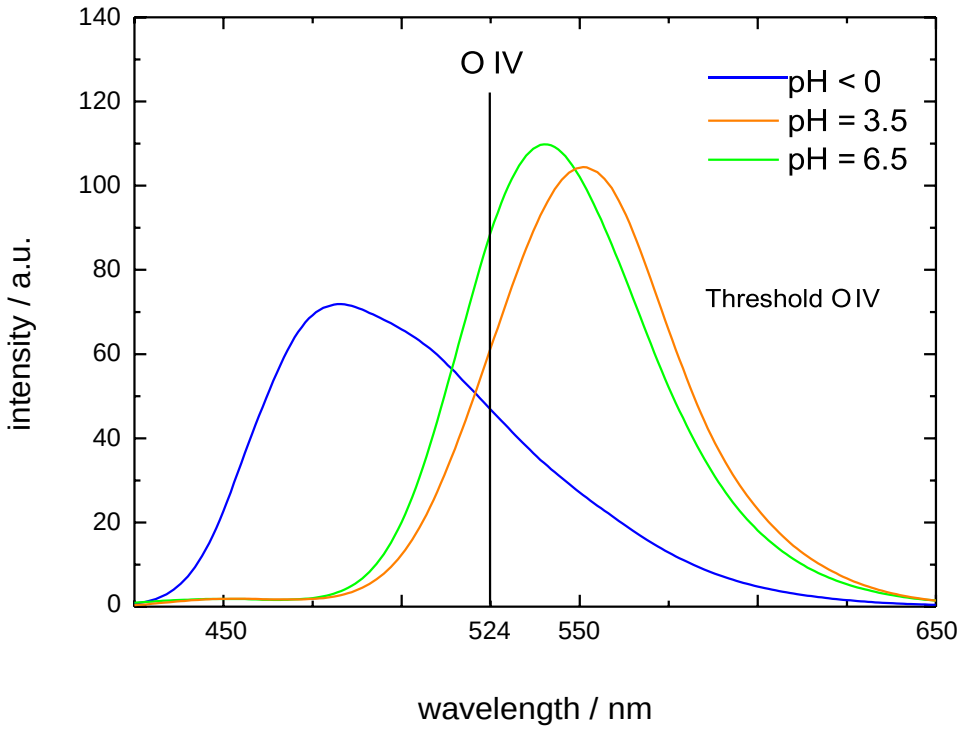

Figure S100: Fluorescence emission of **4** at different pH values with corresponding output channel and threshold level for INHIB 1 gate.

Further different INHIB gates possible by choosing different initial states and output wavelength.

Acid and base as input, Initial state: pH = 7

IMP gate

Table S29: Truth table for OH^- IMP H^+ gate.

In I (OH^-)	**In II (H^+)**	**O II (λ = 548 nm)**
0	0	1
1	0	0
0	1	1
1	1	1

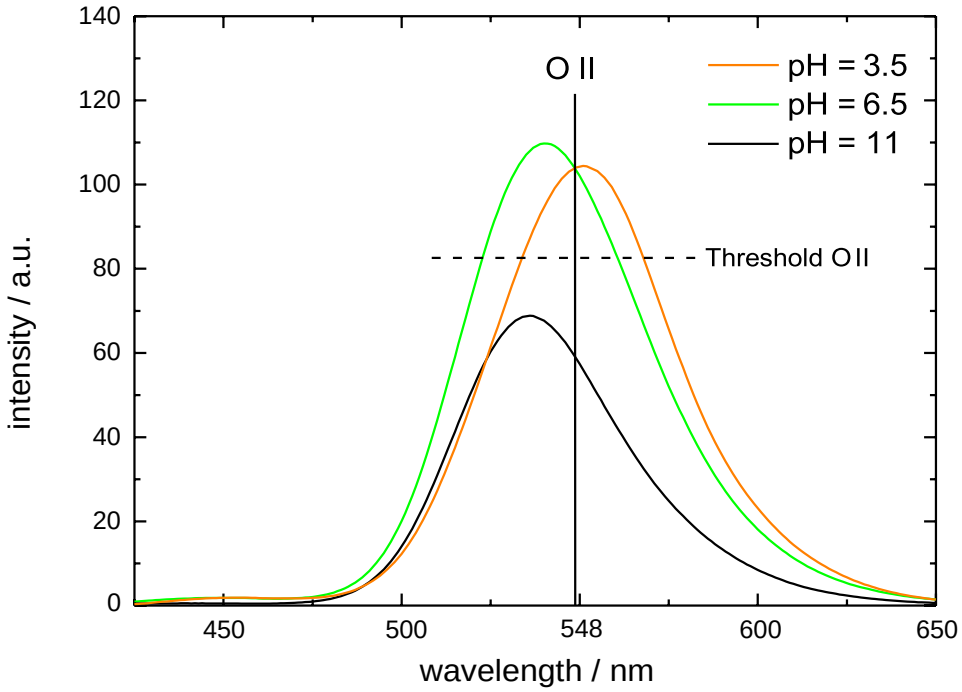

Figure S101: Fluorescence emission of **4** at different pH values with corresponding output channel and threshold level for OH^- IMP H^+ gate.

Acid and base as input, Initial state: pH = 3.5

NIMP gate

Table S30: Truth table for OH^- NIMP H^+ gate.

In I (OH^-)	**In II (H^+)**	**O IV (λ = 524 nm)**
0	0	0
1	0	1
0	1	0
1	1	0

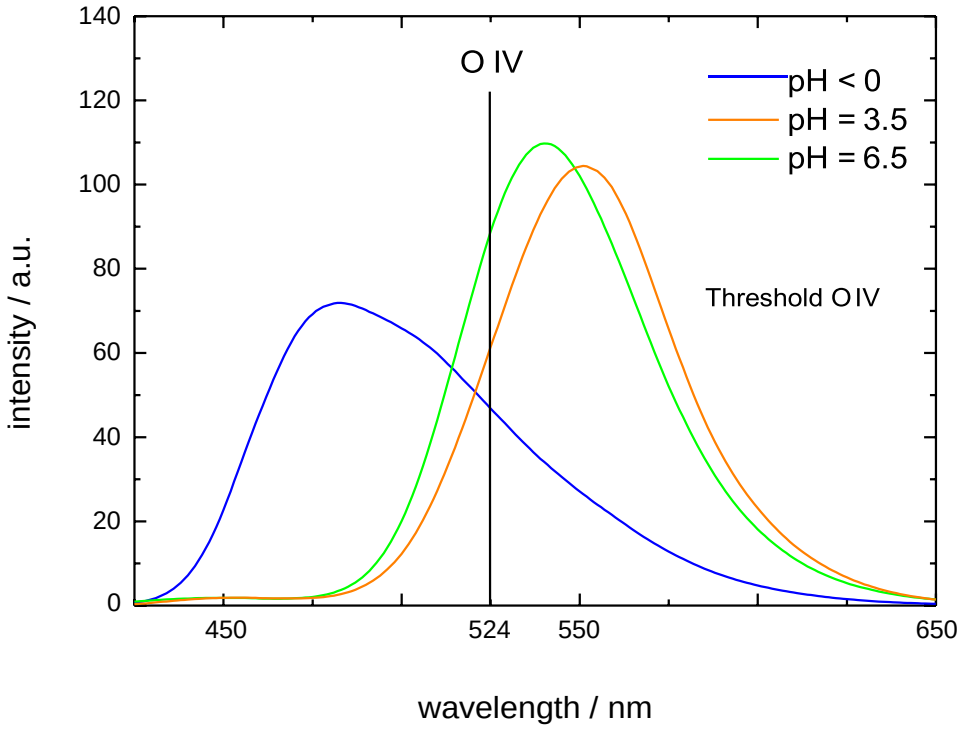

Figure S102: Fluorescence emission of **4** at different pH values with corresponding output channel and threshold level for OH^- NIMP H^+ gate.

Acid and base as input, Initial state: pH = 3.5

Comparator

Table S31: Truth table for comparator.

In I (OH^-)	In II (H^+)	O III In I = In II (λ = 569 nm)	O IV In I > In II (λ = 524 nm)	O V In I < In II (λ = 482 nm)
0	0	1	0	0
1	0	0	1	0
0	1	0	0	1
1	1	1	0	0

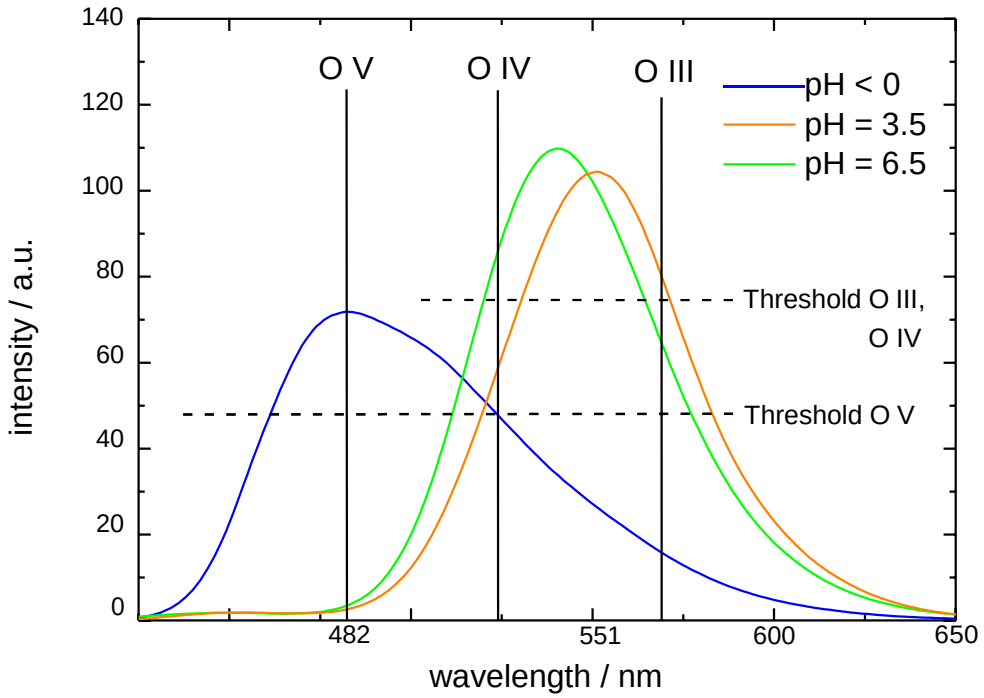

Figure S103: Fluorescence emission of **4** at different pH values with corresponding output channels and threshold levels for comparator.

base as input, Initial state: pH < 0

Half-adder

Table S32: Truth table for molecular half-adder.

In I (OH^-)	In II (OH^-)	O IV (λ = 524 nm)	O III (λ = 569 nm)
0	0	0	0
1	0	0	1
0	1	0	1
1	1	1	0

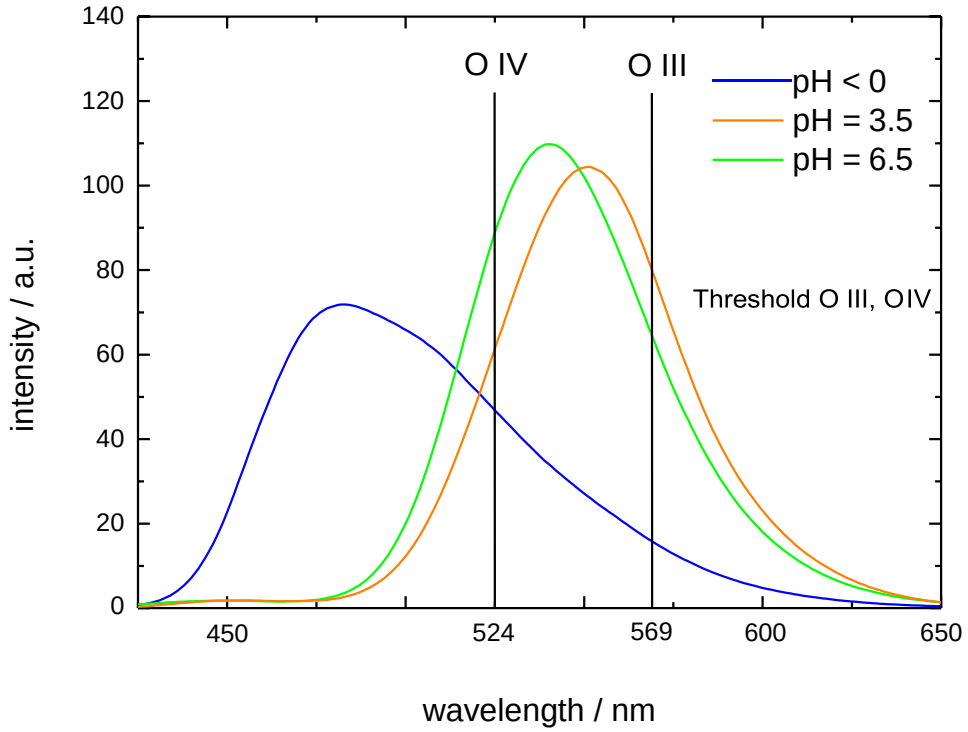

Figure S104: Fluorescence emission of **4** at different pH values with corresponding output channels and threshold levels for half-adder.

Half-subtractor

Table S33: Truth table for molecular half-subtractor.

In I (OH^-, high amount)	In II (OH^-, low amount)	O III (λ = 569 nm)	O II (λ = 548 nm)
0	0	0	0
1	0	0	1
0	1	1	1
1	1	0	0

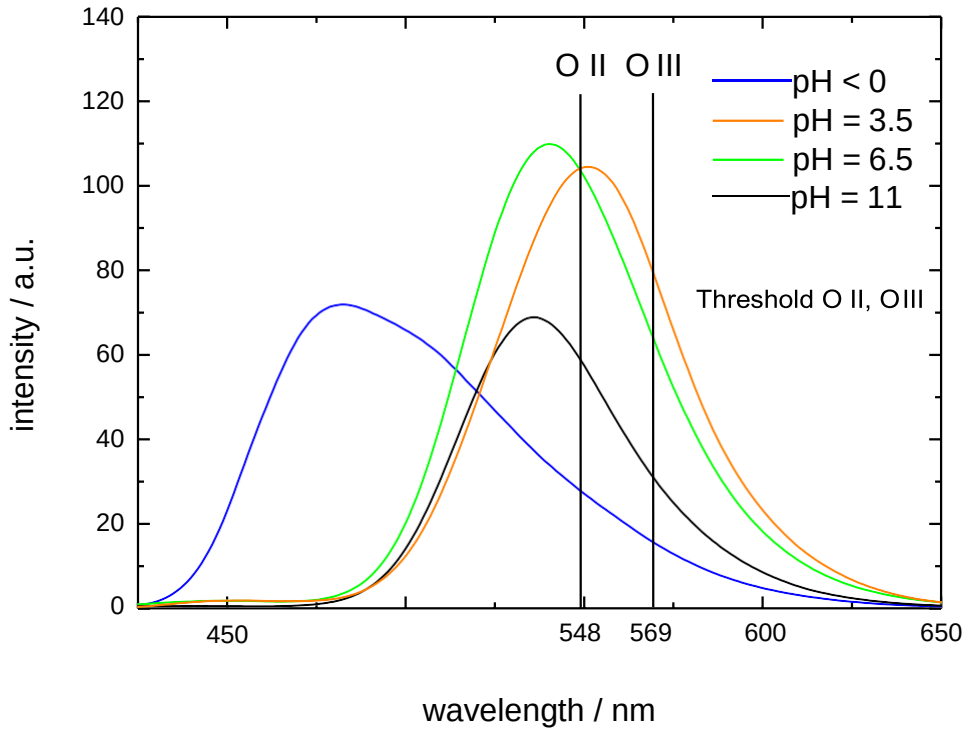

Figure S105: Fluorescence emission of **4** at different pH values with corresponding output channels and threshold levels for half-subtractor.

Supporting References

1. E. Pines, *The Chemistry of Phenols*, John Wiley & Sons Ltd, 2003.
2. B. Finkler, C. Spies, M. Vester, F. Walte, K. Omlor, I. Riemann, M. Zimmer, F. Stracke, M. Gerhards, and G. Jung, *Photochem. Photobiol. Sci.*, 2014, **13**, 548–562.
3. E. Pines, D. Pines, Y.-Z. Ma, and G. R. Fleming, *ChemPhysChem*, 2004, **5**, 1315–1327.
4. D. B. Spry and M. D. Fayer, *J. Chem. Phys.*, 2007, **127**, 204501 1–10.
5. D. B. Spry and M. D. Fayer, *J. Chem. Phys.*, 2008, **128**, 084508 1–9.
6. D. B. Spry and M. D. Fayer, *J. Phys. Chem. B*, 2009, **113**, 10210–10221.
7. A. Weller, *Discuss. Faraday Soc.*, 1959, **27**, 28–33.
8. A. Weller, *Progrogress React. Kinet.*, 1961, **1**, 187–214.
9. J. Widengren, B. Terry, and R. Rigler, *Chem. Phys.*, 1999, **249**, 259–271.
10. B. Hinkeldey, A. Schmitt, and G. Jung, *ChemPhysChem*, 2008, **9**, 2019–2027.
11. C. Hansch, A. Leo, and R. W. Taft, *Chem. Rev.*, 1991, **91**, 165–195.